Isotachophoresis Enhanced Point-of-Care Immunoassays for Clinical Diagnostics

Gary J. Kerr

A dissertation
submitted in partial fulfillment of the
requirements for the degree of
Doctor of Philosophy

University of Washington
2017

Reading Committee:
Jonathan D. Posner, Chair
François Baneyx
Walter James Pfaendtner

Program Authorized to Offer Degree:
Chemical Engineering

University of Washington

Abstract

Isotachophoresis Enhanced Point-of-Care Immunoassays for Clinical Diagnostics

Gary J. Kerr

Chair of the Supervisory Committee:
Bryan T. McMinn Endowed Associate Professor Jonathan D. Posner
Department of Mechanical Engineering

Lateral flow diagnostics are the most common and most commercially successful form of point-of-care diagnostic. The first and most prevalent lateral flow assay is the pregnancy test. Lateral flow assays are low cost, rapid, and simple to operate. However, lateral flow immunoassays have been limited in their success due to poor performance related to an inability to detect low analyte concentrations. In this thesis, we aim to create a high-performance point-of-care immunoassay by integrating sample concentration into a sandwich immunoassay. We use a method called isotachophoresis (ITP) to enhance the detection of low analyte concentrations in the lateral flow format.

We present the performance characteristics for a lateral flow enhanced with ITP diagnostic (LID) assay for the detection of strep throat and the detection of chlamydia. We additionally put forth a method for investigating parameters that are important for the performance of LID assays. Lastly, we validate the LID format in clinically relevant samples.

We show a limit-of-detection of strep throat cells in clean buffer to be 2000 CFU/mL, an improvement of more than 100-fold over a commercial lateral flow assay. This assay also demonstrates an improvement in the analytical sensitivity when compared to the commercial assay. We also present the detection of chlamydia in the LID format demonstrating a 3-fold improvement over a commercial lateral flow assay. The dramatic difference in improvement when comparing the streptococcus assay to chlamydia motivated an investigation into the parameters that are important when using isotachophoresis to enhance the performance of a lateral flow assay.

For designing the chemistry of a LID assay, it is important to investigate the ionic strength (IS), pH and lysis chemistry. Each of these parameters affect the binding of antibody to antigen, as well as the performance of the ITP. Designing with both the binding and ITP performance in mind can be difficult. We present guidelines for obtaining and utilizing these parameter effects in the chemistry design. We develop a model to calculate the limit-of-detection for lateral flow and LID assays from antibody and assay parameters. This model shows that the benefit of a LID assay can be limited by non-specific binding between label and capture antibodies. The model finds that ITP is the most beneficial to antibody pairs with low non-specific affinities.

Finally, we test the strep throat LID assay in contrived clinical samples to validate the compatibility of the format with clinical samples. Our assay is able to successfully differentiate positive from negative samples in these clinically relevant samples. Our assay identifies all positive samples in the expected clinical range.

TABLE OF CONTENTS

LIST OF FIGURES

LIST OF TABLES

ACKNOWLEDGEMENTS

I would like to acknowledge and thank Prof. Jonathan D. Posner for his help and guidance over the past thirty months. I would like to thank the members of the Posner group, past and present, that have contributed to both my research and my over-all experience in obtaining my Ph.D. I would also like to thank the members of my committee for their assistance and feedback throughout my graduate school experience.

A large thank you to Roger Peck from PATH for the insight that he has provided into the design of lateral flow assays and selection of antibodies. Also to Prof. James Lai for going out of his way to give me access to ELISA equipment as well as helping me to understand the process as well as the results that I was able to obtain. Lastly, to Bob Suchland for completing the difficult task of culturing chlamydia trachomatis for this research.

For their personal support, I would to acknowledge my friends and family. Thank you all.

DEDICATION

This dissertation is dedicated to Kimberly Englert, Aretha Kerr, and Chomsky Kerr for keeping me sane during difficult times.

Chapter 1. INTRODUCTION

In this chapter, we present the motivation and background material for isotachophoretic enhancement of infectious disease lateral flow diagnostics. We provide an introduction to clinical and laboratory diagnostics, lateral flow (LF) assays, isotachophoresis (ITP), ITP enhanced LF assays, streptococcus pyogenes, and chlamydia trachomatis. At the end this chapter, detailed objectives for this dissertation are presented.

Diagnosis is a critical step in health treatment. However, in many parts of the world, clinics and health professionals lack the tools to diagnose patients. Without diagnostic testing, health care workers have to rely on symptomatic cues to diagnose and treat illness—an ineffective method. This inability to properly treat ailing patients puts individuals and communities at risk. Incorrect diagnoses costs lives, and ineffectively treated disease can become a starting point for epidemics. The work presented in this thesis is one potential solution to diagnosing patients at the point of care when specialized equipment, trained personnel, and laboratory testing are not an option.

1.1 Laboratory and clinical diagnostics

Diagnostics are used to gain information about a patient or a sample. The goal of diagnostics is to provide high enough confidence in a particular diagnosis to act upon the information.[7] The quality of clinical and laboratory diagnostics, like the ones that compose the bulk of this work, are characterized with consistent performance metrics. The performance metrics are used to predict how well the assay can accurately diagnose an ailment in real world settings. Confusion in these terms can arise from overlap in terms or simple misuse. This section will discuss the metrics relevant for laboratory diagnostic development as well as metrics for clinical performance.

For the laboratory development of diagnostics, the most important metrics are analytical sensitivity, analytical selectivity, and limit-of-detection (LoD). Figure 1-1 shows a sample plot highlighting these laboratory metrics. Analytical sensitivity and LoD are often confused and both are often used as the lowest concentration of analyte that can be reliably detected by the diagnostic.[8] The preferred use of analytical sensitivity is the change in signal response to a change in analyte, i.e. dR/dx where R is the measured signal and x is the input variable of interest.[8,9] For a simple linear response curve, the analytical sensitivity would be the slope of the line. Often the analytical sensitivity is only used for the section of the response curve that can be fit linearly. This is referred to as the reportable range, measuring interval, or linear range.[10,11] Higher analytical sensitivity indicates more response of the test output to the loading of analyte in the sample as well as less quantitative error.[12] Ideally, the analytical sensitivity is determined using a pure substance (e.g. purified protein) or the matrix based reference (e.g. cells or pooled patient samples).[9,13]

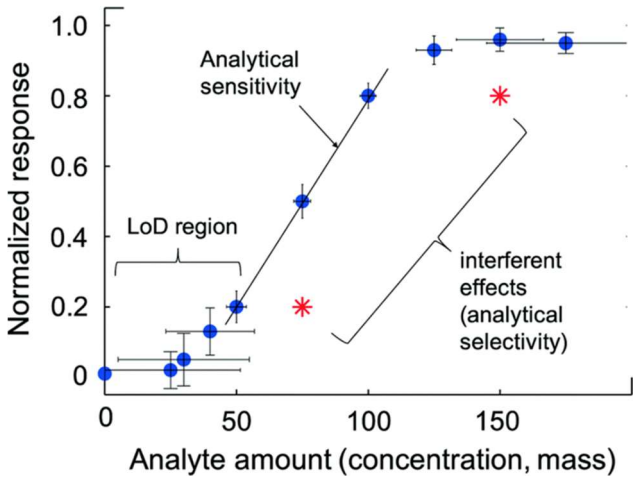

Figure 1-1: Representative data for analytical sensitivity, analytical selectivity, and limit-of-detection (LoD) for laboratory test development, from Borysiak et.al. The normalized response of the test is plotted versus the analyte amount. The analytical sensitivity of the procedure is the slope of the calibration curve. Finally, the LoD region is bracketed where blanks and multiple low level samples are measured so that the smallest analyte amount that is significantly different from the blank response can be determined.[1]

Analytical selectivity is the ability for the test to function as intended with other components present in the sample. This could include anything from a more complex matrix than purified antigen: e.g. medications, food, alcohol, and other potential antigens. The selection of which particular interferents to test should be based upon the sample source as well as the mechanisms of the assay.[8,14] The term "selectivity" is slightly different than the term "specificity," though they are often used interchangeably. A specific reaction is one that only occurs with the target, whereas a selective reaction is one that preferentially reacts with the target and can occur with other substances present.[15,16] Testing for the analytical selectivity of a test is an important step in moving a diagnostic towards clinical evaluation.

The limit of detection indicates the lower bound of detectable analyte loading. This requires that the signal generated at this low loading of analyte be reliably differentiated from a blank (analyte free) sample. Figure 1-2 shows a breakdown of the distributions of response from blank samples and samples at the limit-of-detection. There is overlap between high signal from blank samples and low signal from the low positives. When a blank sample generates a signal that is interpreted as a positive, this is known as a false positive. When a positive sample generates a signal that is interpreted as a negative, this is known as a false negative. For a binary assay, a test that generates either a positive or negative response, the normalized signal intensity at the LoD can be determined by $LoD_{NI} = LoB_{NI} + z \times \sigma_{s,NI}$, where the signal intensity the is the limit of the blank (LoB_{NI}) is $LoB_{NI} = \mu_{B,NI} + z \times \sigma_{B,NI}$. $\mu_{B,NI}$ is the average intensity from negative tests, z is the z-score matching the desired confidence (1.645 for 95% confidence), $\sigma_{B,NI}$ is the standard deviation of the blank test responses, and $\sigma_{s,NI}$ is the average standard deviation of the signal from low positive test responses. It is important to note that the subscript *NI* indicates that the value has units of normalized signal intensity.

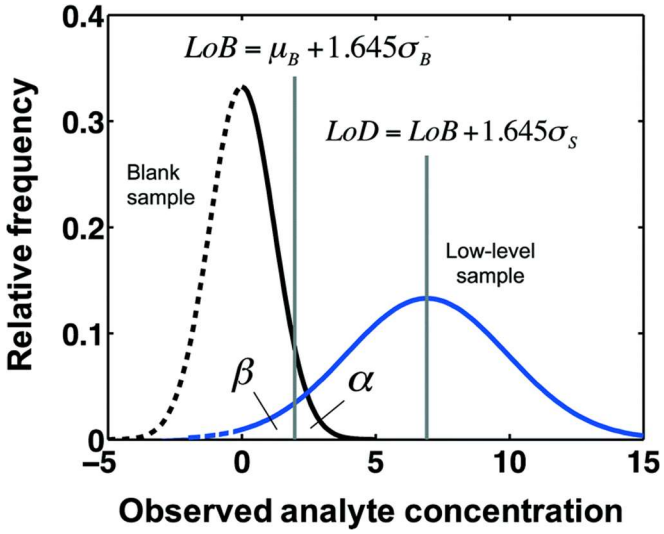

Figure 1-2: Plot showing distributions of measurement replicates for blank samples and a sample containing low-levels of analyte, from Borysiak et.al.[1,8] The overlap region due to measurement uncertainty causes some blank samples to be measured as containing analyte (false positive) and low-level samples to be measured as containing no sample (false negative). The limit-of-blank (LoB) and limit-of-detection (LoD) can be determined by setting the overlap error to a given certainty. The equations to determine the LoB and LoD for overlap error are given, with the LoB approximately equal to 2 units/L, and the LoD approximately equal to 7 units/L. The dashed line indicates that some instruments do not report measurement values less than zero, resulting in a non-normal distribution that requires non-parametric statistics to calculate the LoD.

Two important metrics for assessing a diagnostic in a clinical setting are clinical sensitivity and clinical specificity. Clinical sensitivity is a percentage of positive results that are also positive by the "gold standard" method. For example, if the new diagnostic gives a positive response from 85 out of 100 positive samples, the clinical sensitivity is 85%. The clinical specificity is a similar metric for the negative test results (i.e. percentage of negative results that are also negative by the "gold standard" method). Both the clinical sensitivity and clinical specificity are as close to 100% as possible in the ideal case.

In summary, analytical sensitivity is the response of the signal to the loading of analyte. Analytical selectivity is the ability to operate as intended with other materials present. Limit of

detection is the lowest amount of analyte that can be consistently detected. Each of these factors indicate the potential performance of a laboratory diagnostic in a clinical setting, i.e. the clinical sensitivity and clinical specificity.

1.2 Lateral flow (LF) immunoassays

The diagnostic format developed for this dissertation is closely tied to the lateral flow (LF) format. The technical basis of the lateral flow immunoassay was derived from the latex agglutination assay, the first of which was developed in 1956 by Plotz and Singer.[17] The basic technology that the lateral flow immunoassay is based upon was first described in the 1960s[18], but the first commercial application was in 1988 in Unipath's Clearview home pregnancy test.[19] This technology has since spread into areas such as clinical, veterinary, agricultural, food industry, bio-defense and environmental applications.[2] With medical care shifting toward prevention and early detection of disease, point-of-care (PoC) testing is becoming more prevalent.[20] Porous paper substrates have been used, since the late 1980s, to construct LF PoC diagnostic devices for use in rapid diagnostic tests.[21] These devices have enjoyed some commercial success because of their simplicity, low cost, and robust operation. In a conventional LF assay, the target analyte binds to a labeled detection protein, e.g. antibody conjugated to colloidal gold, and travels through the paper substrate by capillary forces. At the test zone, the target reacts and binds with a specific probe molecule immobilized on the surface which accumulates the captured label and generates a visually detectable signal.

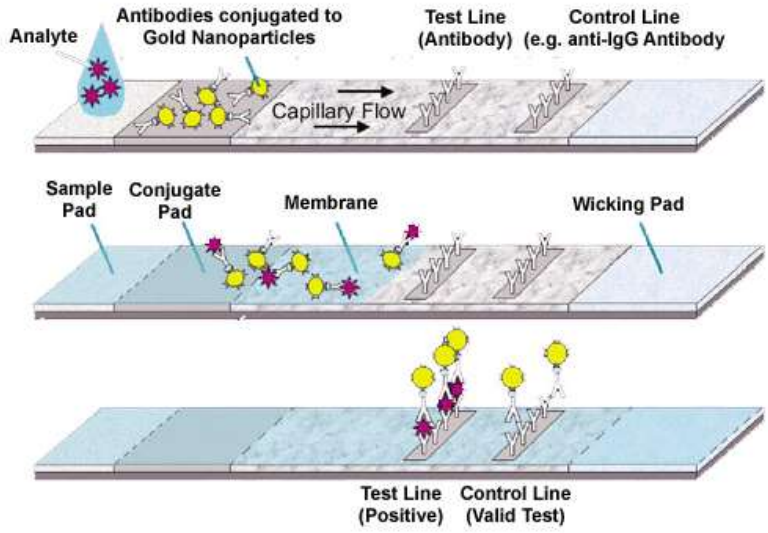

Figure 1-3: The standard design and operation of a lateral flow assay, from Cytodiagnostics.[2] Sample solution is added to the sample pad. Gold conjugate is released form the conjugate pad to bind to the analyte. Gold bound analyte binds to the test-line and free gold label binds to the control line. The wicking pad maintains flow through the membrane.

Figure 1-3 shows a schematic of a typical LF test device and how a positive signal is generated. This device consists of overlapping membranes that are mounted on a plastic backing, for handling. To run a lateral flow assay, the sample is applied to an absorbent sample pad, which is impregnated with buffers and surfactants to improve the flow of the solution onto the device for the detection system. The sample pad ensures that any analyte that may be present in the system is under favorable binding conditions for the antibodies used in the device (i.e. removing aggregated proteins and interferant molecules). The solution flows from the sample pad to the conjugate release pad, which contains antibodies (known as the label antibody) that are specific to the antigen and conjugated to a label, typically colloidal gold or fluorescent particles. The sample with the label then flows to the detection membrane. This is made from a porous membrane, typically constructed from nitrocellulose. Nitrocellulose is used because antibodies securely adsorbs to the surface, it has high surface area, and low cost. Antibodies (known as the capture

antibody) that are specific to the antigen and complimentary to the label antibodies are immobilized in a narrow line to create the test-line. A second, control-line, composed of immobilized antibodies or antigen, is designed to capture label to indicate proper flow through the strip. The lateral flow assay terminates with an absorbent pad to maintain the flow through the assay.[2,22,23]

The main advantages of LF tests over conventional laboratory-based tests are that they are easy to manufacture, low-cost, readable by eye with visible signals, instrument-free, and can use stabilized dry reagents.[24] Additionally, because there is little training or equipment required to run the test, lateral flow assays are suitable for low resource or impoverished settings.[25] Despite being inexpensive, instrument-free, and simple to use, LFs are often limited to screening applications. This limitation in the use of LFs, in their present form, is a result of the fact that these assays are not easily quantifiable and are not sensitive enough for applications with low concentration of analyte. The commercially successful LF assays are ones where the concentration of the target is high (e.g. the pregnancy test). Moreover, LF assays are generally limited to antibody-antigen interaction which limits their application when a suitable antibody is not available for an analyte. The unavailability of a suitable antibody could be a result of the type of target (e.g. DNA), low affinity of the antibody to the target, or an undesired affinity for similar molecules that may be found in samples.

Most of the effort towards improving the limit of detection of these tests has been applied to optimizing the antibody, label, or construction of the test.[26–33] The detection limit of a LF test can be improved by a factor of nearly 10-fold by using different labels and labeling techniques without an assay reader.[29,30] Optimizing the size of the nanoparticle labels can improve the visual detection by an order of magnitude or more.[34,35] Fluorescent labels and superparamagnetic

particles have been used in place of colloidal gold with a reported increase in sensitivity of 10-1,000x, but both require an assay reader.[36,37]

Recently, there has been a push to enhance the signal in LF assays by developing paper-based microfluidic devices that incorporate sophisticated functions and device designs using capillary action to drive the flow.[38–40] However, the detection limit improvement reported in these studies is limited to about 3-fold. In another example, immunomagnetic separation has been used to improve the limit-of-detection of E.coli by a factor of 10.[41] This process requires an additional step and more than doubles the length of time required to run the test. Additional work has been done in modifying the structure to create 2-D flow, resulting in a moderate improvement in limit of detection of ~4x.[33]

There are many additional approaches to improving lateral flow assays that have been published and well summarized in review articles.[26,29,32,42–44] These methods include techniques such as enzymatic labeling, electrochemical signal generation, silver enhancement of gold nanoparticles, carbon black labeling, and phosphorescence. Each of these processes provides marginal improvement, requires expensive equipment, and/or much longer assay time. Our group has previously used isotachophoresis to improve the limit of detection of a lateral flow assay by 2 orders of magnitude.[45]

1.3 Isotachophoresis (ITP)

The approach taken in this dissertation to improve the lateral flow assay is through the utilization of isotachophoresis (ITP). ITP is an electrophoretic technique that has been historically used in traditional capillary microfluidic devices to concentrate and separate a variety of ionic compounds, ranging from small metallic ions to proteins, DNA, and nucleic acids as a pre-

treatment method.[46–51] ITP uses a discontinuous electrolyte system that creates concentration and separation of ionic species based on their differential migration velocities under an applied electric field and is capable of up to a million-fold increase in concentration.[52,53] The ITP electrolyte system is formed by a leading electrolyte (LE) and trailing electrolyte (TE).

Electrophoresis techniques, like ITP, use the migration of charged particles in a fluid due to an applied electric field. At low Reynolds numbers, the electrostatic force acting on a particle is equivalent to the viscous forces acting on its surface. As a result, under constant electrophoresis, charged particles obtain a terminal velocity. For small molecules, this equilibrium can be estimated as:

$$3\pi\eta dV = zeE \qquad \text{Equation 1.1}$$

where η is the fluid's viscosity, d is the hydrated diameter, V is the velocity, z is the valence, e is a unit charge, and E is the applied electric field. Electrophoretic mobility, μ, is typically used as a convenient notation for describing the ratio of particle velocity to the applied electric field, when applied to equation 1.1 gives:

$$V = \mu E \qquad \text{Equation 1.2}$$

Isotachophoresis utilizes the constant velocity in a channel to separate ions based on their electrophoretic mobility. The system is designed in such a way that the mobility of the target is sandwiched between that of the LE and TE. The electric field generated by passing a current though the systems is much higher in the TE than the LE as a result of the high conductivity of the leading electrolyte relative to the low conductivity trailing electrolyte. This is dictated by Maxwell's current density equation: $E = \frac{J}{\sigma}$, where J is the current density. Since the current is

constant throughout the system, the current density is constant if the effective area remains constant. The ratio of the electric field generated in the TE to the LE in this case is expressed as:

$$\frac{E_{TE}}{E_{LE}} = \frac{\sigma_{LE}}{\sigma_{TE}} \qquad \text{Equation 1.3}$$

Using equation 1.2, ions move faster in the high electric field in the trailing electrolyte and slower in the low electric field generated in the leading electrolyte. This can also be stated as: $V_{target}=\mu_{target}$ x E and $E_{TE}>E_{LE}$, thus $V_{target,TE}>V_{target,LE}$. These conditions are used to concentrate the target ions in between the LE and TE.

The system requires a leading ion, trailing ion, and counter ion. A simplified schematic of an ITP system is shown in fig. 1-4. The leading ion has high mobility and controls the upper cap of mobility for the system. The trailing ion has low mobility and dictates the lower bound of mobility for the system. The counter ion balances the system by holding the opposite charge of the leading and trailing ions, as well as migrating in the opposite direction of these ions.

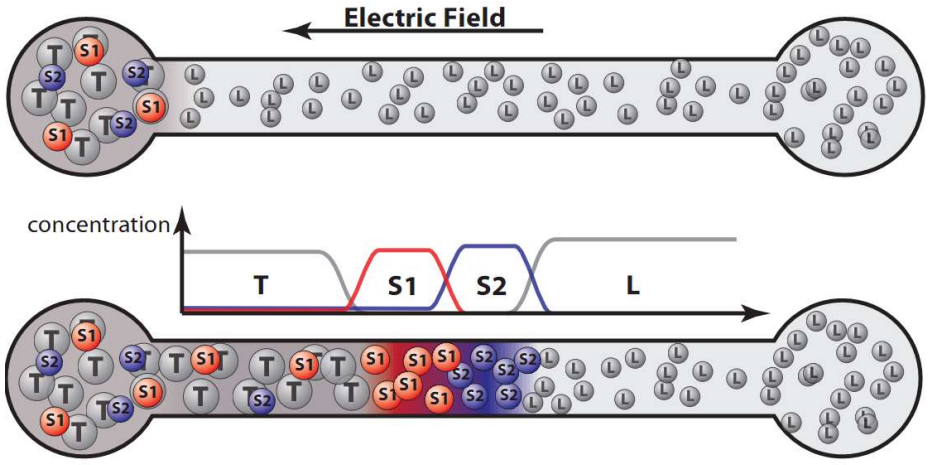

Figure 1-4**:** Schematic of negative ions involved in an anionic ITP process. S1 and S2: sample ions, T: trailing ions, L: leading ions. Obtained from Santiago group.[3]

The basic operational trend of the ion mobility (μ), conductivity (σ), and electric field (E) are shown in fig. 1-5. For the sample to stack at the interface between the LE and TE (as shown in fig. 1-4), the trends in fig. 1-5 must hold true. Since the ions are separated by mobility, the leading ion must have the highest mobility, with the target having the next highest, and the lowest mobility for the trailing ion. The conductivity and electric field trends in fig. 1-5 are dictated by equation 1.3.

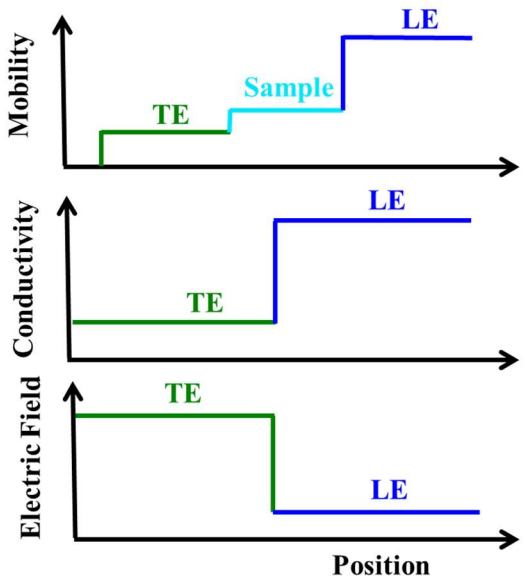

Figure 1-5: Schematic illustrating the general trends in electrophoretic mobility, conductivity, and electric field in a functional ITP system.

Electrophoretic mobility, μ, can also be defined as the rate of migration of an ion in a given system. Electrophoretic mobility is dependent on the pH and ionic strength of the solution. Thus, it is likely that the mobility of the leading ion (μ_{LI}) or mobility of the trailing ion (μ_{TI}) will be different in the LE chemistry when compared to the TE chemistry. For an ITP system to form an interface, it is necessary for $\mu_{TI} < \mu_{LI}$ under both the LE and TE conditions. For an analyte (A) to focus at the LE/TE interface, it is required that $\mu_{TI} < \mu_A$ under TE conditions and $\mu_A < \mu_{LI}$ under

LE conditions. For any given analyte with a mobility between the leading ion and trailing ion, the velocity of the analyte is higher in the TE than in the LE, resulting in a self-sharpening effect. Thus, the ions with the highest mobility will migrate toward the electrode at a higher rate than those with lower mobilities, while maintaining a constant overall velocity. This is the method by which ITP separates ions. The design of the LE and TE chemistries in traditional ITP systems has been well studied and covered in many publications.[4,52,54–58]

Isotachophoresis is accompanied with electroosmosis.[54] Electroosmosis is the result of contact of the electrolyte with the walls of the channel. Any ions adsorbed onto the wall along with ionized groups of the wall cause a net charge of the wall surface. Ions of the opposite sign accumulate near the net charge of the wall, creating an electric double layer. Electroosmosis occurs when a voltage bias is applied and drive mobile ions near the wall to move. This movement acts upon the solvent molecules, moving the solution as a whole. Figure 1-6 is a simplified schematic showing the basics of electroosmotic flow. For the negatively charged walls, the positively charged ions accumulate near the surface, neutralizing the charge of the wall. The positive ions near the wall move in the direction of the electric field from the positive electrode (anode) to the negative electrode (anode).

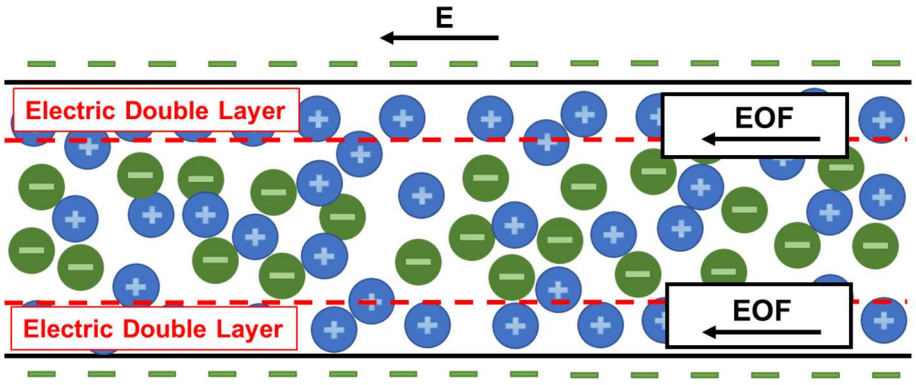

Figure 1-6: Schematic of the electric double layer and electroosmotic flow (EOF) in an electric field.

In summary, ITP is a powerful concentration and separation technique that utilizes electric fields to concentrate a target into a narrow band. Electrokinetic techniques are a strategy that has been shown to improve the limit of detection in surface reaction biosensors.[59,60] Our group has previously shown the ability of ITP to enhance a lateral flow assay by dramatically lowering the limit of detection of IgG proteins in a simple electrolyte solution as will be described in the next section.[45] This previous work will be further explained in the next section.

1.4 Lateral flow enhanced by isotachophoresis diagnostics (LID)

The work presented in this thesis is based upon previous work done in our group on the incorporation of ITP into a lateral flow assay on nitrocellulose devices.[4,5] The theory behind this prior work is that concentrating the target into a narrow plug before passing over the capture line of a lateral flow diagnostic format will increase the signal generated at low levels of analyte, as shown in figure 1-7. Signal generation in lateral flow assays is reaction rate limited, due to the relatively short exposure time of target to test-line, when compared to equilibrium assays like ELISA. When this is the case, concentrating the target in to a narrow band increases the reaction rate and thus increases the signal generation. The intent being that, by increasing this low loading signal, the limit-of-detection of the colorimetric assay is decreased.

In this proof-of-concept work, they were able to stack both a fluorescent reporter and gold nanoparticle. They were able to extract roughly 60% of the sample from a well of trailing electrolyte, stacking this sample into a plug with a concentration over 900-fold higher than the starting sample concentration. They were also able to obtain roughly 600x improvement in limit of detection over a similarly designed one-site lateral flow assay. These assays are considered one-site because the target being detected is also the label, requiring a single binding event to

generate signal. In these assays, the mobility of the leading and trailing electrolytes sandwich the mobility of the label (in this case IgG labeled gold). With the target mixed into the trailing electrolyte, the higher mobility of the target results in it accumulating at the front of the trailing electrolyte. This results in a highly-concentrated band of target (i.e. the plug) passing over immobilized capture proteins to generate a signal, similar to the performance shown in figure 1-8.

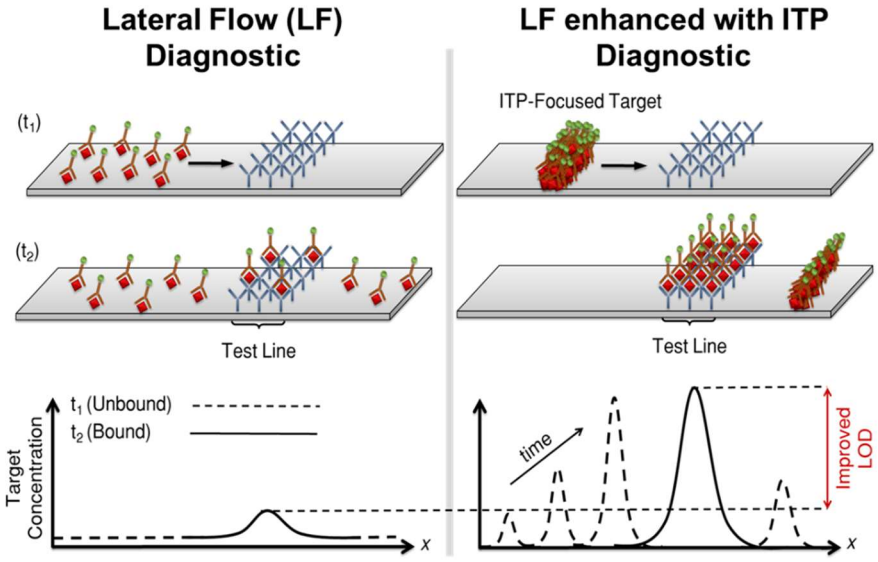

Figure 1-7: A schematic from the work of Dr. Moghadam illustrating the operation of lateral flow assays alongside the expected improvement from ITP, achieved by concentrating the target before passing over a test-line of capture antibodies, in the lateral flow format. The lateral flow diagnostic (left) generates signal by a consistent low level of target passing over the test-line. ITP (right) concentrates the target into a tight band before passing over the test-line, increasing the signal generated.[4]

This initial system consisted of a test line of mouse IgG and target/label of goat-anti-mouse antibodies conjugated to gold. The electrolyte systems consisted of a high conductivity leading electrolyte with HCl and tris (ionic strength of more than 40mM), and an extremely low conductivity trailing electrolyte consisting of glycine and bis-tris (ionic strength of less than 0.05mM). This system had an extreme ratio of conductivity of 1400 to achieve the high stacking.

This conductivity ratio is only functional in a very idealized system, like the one used for these IgG experiments. This optimized ITP setup does not account for the necessity of high ionic strength lysis chemistry and is extremely sensitive to ionic contaminants present in real-world samples.

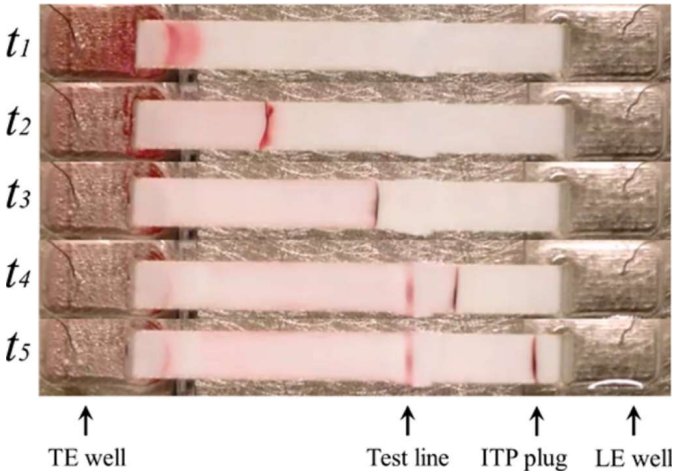

Figure 1-8: Experimental snapshots taken at 5 different times showing that ITP-focused IgG adsorbed to colloidal gold is captured at the test zone. The target is extracted from the TE well, stacked into a narrow plug, which is passes over a test-line. The label binds to the capture line as the plug passes over, with excess label continuing toward the LE well.[45]

This work transitioned the traditional use of micro-channels for ITP to an open nitrocellulose device. Similar work was completed at the soon after by Bercovici, et. al.[61] In addition to being low cost and easy to use, nitrocellulose allows processing a larger amount of sample, as well as opening up the opportunity to use antibody surface capture. One of the major difficulties that was overcome in this work is the heating and evaporation from the open surface of the nitrocellulose membrane, which is the result of Joule heating. Joule heating is generated by the passage of current through an electrolyte. This heating is the main limitation when trying to use a high electric field to speed up the process of ITP in an open system. The amount of power

dissipated into a volume unit by Joule heating (w) for an amount of current (I) passing through an electrolyte system over a cross section S is dictated by the equation:

$$w = \frac{E\,I}{S} = \frac{I^2}{\sigma\,S^2} \qquad \text{Equation 1.4}$$

Based on equation 1.4, the Joule heating increases with increased current passed through the system. This places a functional limit on the electric field applied and, as a result, the conductivity of the system. In high conductivity systems, the amount of current required to generate a sufficient electric field for effective stacking is also higher, resulting in excessive heating. When Joule heating is in excess, denaturation of proteins and evaporation/drying can occur in open systems. We have observed temperatures in excess of 50ºC on the membrane. Denaturation of proteins can occur at temperatures as low as 36.5ºC.[62] Extreme cases of drying have caused ignition of the membrane itself in our nitrocellulose system.

The Joule heating was mitigated in this previous work by limiting the overall conductivity and introducing a cross-shaped membrane to ensure rewetting to counteract any drying that occurs. The other major limitation of ITP systems is controlling the electroosmotic flow (EOF). The EOF is controlled in this case by the addition of a polar long-chain polymer. In an additional demonstration of functionality, blood serum was added to the sample in the trailing electrolyte well, where they were able to separate fluorescently labeled IgG from this complex matrix. They were also able to create a functional system powered by only a small button battery and a voltage multiplier. This is the first step to a full equipment free point-of-care device based on the LID technology.

This work demonstrated the capability of the format to improve signal response over a lateral flow assay. However, this work is not a demonstration of real world functionality. IgG-

IgG binding is well known for being robust with high binding affinity. Infectious disease antibodies are generally less robust and more sensitive to the binding conditions. In addition, the assay was optimized for ITP, but not for the lateral flow assay. Neither the pH nor the ionic strength if the lateral flow solution were optimized for binding. This is most evident in the ionic strength of the sample solution. The ionic strength of the solution used for the lateral flow assay was less than 1 mM, but a standard binding buffer has an ionic strength of >150mM.[63,64] This work was also done using a one-site system. A one-site system uses the label as the target, which circumvents the need to suppress non-specific signal generation. The target being the same as the label is rarely the case in commercial lateral flow assays. Infectious disease assays are almost exclusively sandwich assays. The target is also extracted from the low conductivity trailing electrolyte. In an infectious disease assay, the trailing electrolyte is unable to incorporate a high ionic strength lysing solution without extensive dilution (>10x). Thus, the work presented in this thesis places the target in the high conductivity leading electrolyte. In summary, the previous work did not resolve the practical issues of non-specific binding or realistic solution properties (pH, IS) that are required to address lysis chemistry and the optimal binding conditions of antibodies for specific diseases.

This prior proof-of-concept work developed a model for a one-site system. The model assumes an excess of label present for a first order reaction between the label and the capture antibody. The calculations presented in the previous work agree with the improvement in detection that was observed in that work; however, it also indicates that non-specific signal generation in sandwich assays would be increased. In a sandwich assay, the interaction between the label and capture antibody is also increased by ITP. This interaction increases the limit-of-blank intensity,

which decreases performance by increasing the limit of detection. The importance of minimizing this effect was overlooked in the previous work.

In summary, the work completed by Dr. Moghadam demonstrated the ability of ITP to concentrate traditional lateral flow labels on nitrocellulose and capture these labeled antibodies on an antibody test-line. This assay format, however, was not tested in the traditional 2-site format, did not incorporate cell lysis in the process, and did not address the issue of increased non-specific binding in LID systems.

1.5 Streptococcus pyogenes

In this section, we discuss the current testing for streptococcus pyogenes as well as the motivation for the selection of this disease for enhancement by the LID format. Streptococcus pyogenes, also known as group A streptococci (GAS) or strep throat is well known to cause throat discomfort. Sore throat is one of the top 20 most common reasons that children and adults present to primary care and is responsible for 2-4% of all visits to a family physician.[65] While the majority of sore throats are caused by viruses, a significant proportion (10% in adults and 15-35% in children) are due to the strep throat bacteria.[66,67] One study found that in the US in 2003, strep throat caused more than 10,000 cases of invasive disease with nearly 2,000 of those cases leading to death.[68] In addition, the US Centers for Disease Control and Prevention (CDC) claims that more than 10 million cases of noninvasive GAS occur annually in the US.[69] Streptococcus pyogenes is a non-motile, gram-positive bacteria that colonizes the human throat and skin. Treatment of strep is important, as there is good evidence that antibiotics have a significant beneficial effect on symptoms, reduce the risk of complications (such as peritonsillar abscess, glomerulonephritis, rheumatic fever), and can reduce the spreading of infection within schools/colleges.[70,71]

Clinical features of strep overlap with those of viral infections, therefore, current clinical practice involves use of a rapid antigen test using a throat swab, which can be performed in CLIA waivered labs. 50-80% of adults and children presenting with sore throat currently undergo strep testing.[72,73] However, current lateral flow tests have suboptimal accuracy. A 2014 systematic review of 48 studies that evaluated the 'real world' accuracy of rapid, lateral flow based, strep tests showed clinical sensitivities ranging from 59 to 96% and specificities of 90 to 95%.[74,75]

As a result of the low sensitivity, no GAS rapid test has been FDA approved for use without a backup for confirmation of negative results. The CDC, Infectious Disease Society of America (IDSA), and professional bodies such as the American Academy of Pediatrics recommend strategies to help identify patients with strep. For children, guidelines from the CDC and IDSA recommend doing a confirmatory test in a microbiology laboratory (a bacterial culture looking for beta hemolysis) because of the unacceptable number of false negatives and severity of the risk of untreated GAS in children.[76–78] There is higher occurrence of false negatives in tests for children because of the higher prevalence and lower test diagnostic sensitivity, both of which contribute to a lower probability of a negative test result being a true indicator of a lack of infection. Since nearly 80% of strep quick test results are negative, there is significant cost and potential delay in treatment for negative results when running backup cultures.[74,75]

As a result of suboptimal test accuracy, importance of treatment, and delays in obtaining definitive (laboratory) strep results, several studies have found that clinicians frequently distrust either clinical findings and/or rapid test results, which contributes to the estimated 25% of antibiotic prescriptions issuances each year in the US for adults and children which are considered inappropriate.[79,80] Newer molecular diagnostic tests offer higher sensitivity (89-95%), and specificity (97-99%) but require significant initial capital investment on equipment and thus not

yet viable as a point of care test for primary care.[74] As a result, there is a pressing need for a rapid strep test that is highly sensitive and specific, that could replace current generations of rapid strep tests, thereby improving efficiency and reducing costs related to sore throat and contribute to delivering on CDC and White House strategic goals in combating antibiotic resistance. Evidence suggests that the suboptimal clinical sensitivity of the existing GAS lateral flow assay is linked to the test's limit of detection lying above the threshold of expected bacterial loading.[81,82] The LID format focuses on improving the clinical sensitivity by achieving a LoD capable of detecting strep throat infections over the entire clinical range.

1.6 Chlamydia trachomatis

Chlamydia trachomatis (CT) was selected as the second disease for testing in the LID format. CT is the most commonly reported notifiable sexually-transmitted bacterial infectious disease in the USA, with 1.5 million cases reported in the US in 2015.[83] It is also estimated that the direct cost of chlamydia infections to Americans is greater than $200M annually.[84] CT is transmitted through sexual contact with the penis, vagina, mouth, or anus of an infected person. CT can cause cervicitis, urethritis, and proctitis.[85] CT is also responsible for the infection known as lymphogranuloma venereum, which has recently emerged as a cause of outbreaks of proctitis.[86,87]

For most, chlamydia infections are asymptomatic and thus continue to spread to others if not identified and treated.[88] Studies on chlamydia-infected people estimate that about 10% of men and 5-30% of women with laboratory-confirmed chlamydial infection develop symptoms.[15,89,90] The consequences of CT are considerable. Untreated infection can cause pelvic inflammatory disease. Complications from pelvic inflammatory disease can include infertility, ectopic pregnancy and chronic pelvic pain.[91] These infections also increase the risk of transmission of

HIV.[92] Identifying women and men with CT is critical for reducing transmission, preventing complications as well as reducing symptoms.

Chlamydia can be treated with antibiotics, but will not repair any permanent damage done by the disease.[85] Repeat infection with chlamydia is common.[93] For example, women and men whose sex partners have not been appropriately treated are at high risk for re-infection. Having multiple chlamydial infections increases a woman's risk of serious reproductive health complications, like pelvic inflammatory disease and ectopic pregnancy.[94,95] It is recommended that women and men with chlamydia should be retested about three months after treatment of an initial infection, regardless of whether they believe that their sex partners were successfully treated.[96]

Nucleic acid tests are almost exclusively used as the diagnostic for CT infections. Nucleic acid testing is highly sensitive, with clinical sensitivities reported as high as >99% with first-void urine, endocervical swabs, and urethral swab samples.[97–101] Nucleic acid tests are primarily completed in centralized laboratories with the cost of each test ranging from hundreds to nearly a thousand dollars.[97,102,103] These tests are laboratory based diagnostics and are not point-of-care. There is substantial evidence that a significant portion (approx. 20-30%) of patients attending STD clinics do not follow up for treatment even when tests are positive due to the significant turn-around time of lab-based diagnostics, thus nucleic acid tests do not meet the requirements for combatting the spread of CT. This is a major concern given that patients of these clinics are in the highest risk for transmitting infection.[104,105] Because CT is asymptomatic in many cases and easily treated, screening is an important step in reducing the spread of the infection. This is especially true for young, sexually-active people. The CDC recommends annual CT screening of all sexually

active women younger than 25 years, pregnant women, and people with higher risk lifestyles.[96] Despite these national, evidence-based recommendations, the current US screening rates are poor.

For females, vaginal swabs are the optimal specimen to screen for genital chlamydia using nucleic acid tests, with first void urine as the specimen of choice for men and commonly used for women as well.[106] Currently, LF tests for CT are poor with unacceptably low sensitivities (25-80%) and are not approved for use in clinical settings.[107] The application of lateral flow assays is limited because these samples can contain low quantities of elementary bodies (EBs) of the CT bacteria.[108–110] The average concentration of CT found by quantitative PCR was 12,000 EBs/mL for first void urine and 2,2000 EBs/swab for vaginal swabs, with other reports placing these numbers even lower.[110,111] The average loading of CT is 73 times higher in cases where the lateral flow assay diagnoses a true positive, compared to when the lateral flow assay gives a false negative.[112] As mentioned in section 1.2, the performance of lateral flow assays suffers when target loading in samples is low. This suggests that the low sensitivity of LF assays is partially due to the LoD being too high to detect low target loading.

The poor follow-up rate at STD clinics and unacceptable performance of current rapid assays, motivates the need for a point-of-care assay for the detection of chlamydia trachomatis infections. Gift et. al. suggested that a PoC test with even 63% clinical sensitivity would reduce the transmission rate and the overall cost of chlamydia trachomatis to the healthcare system.[113] The LID format allows for the detection of the low level of CT analyte present in a point-of-care format.

1.7 Goals

The goal of my dissertation is to develop ITP based immunoassays for infectious diseases with the goal of achieving higher clinical sensitivity than commercial rapid tests by lowering the

limit-of-detection. The work of Dr. Moghadam, described in section 1.4, demonstrated that ITP can be used in nitrocellulose membranes with antibody based detection. I build upon this foundation to create ITP enhanced lateral flow assays for clinical applications.

The objectives for this dissertation are:

i. Develop a paper-based infectious disease immunoassay that incorporates isotachophoresis to lower the limit-of-detection when compared to a commercial lateral flow immunoassay
ii. Identify and characterize the factors that affect signal generation in isotachophoretic immunoassays when compared to traditional lateral flow assays
iii. Validate the LID format in clinically relevant samples over the clinically relevant range

To achieve the first objective, I design a combined lysis and ITP electrolyte chemistry to extract the antigen from bacteria cells and then concentrate the antigen with ITP. In order to accomplish this, I developed a lysis chemistry that incorporates the leading electrolyte ion into the lysis. This is done in order to ensure the leading electrolyte has the appropriate properties for concentrating gold nanoparticles with ITP. I also adjust the lysis chemistry to obtain functional ITP in the presence of interferent ions from the lysis. Lastly, I characterize the performance of the optimized LID assay by measuring the limit of detection and analytical sensitivity by quantifying the colorimetric signal. These results are compared to the performance of a commercial lateral flow immunoassay to determine the amount of improvement achieved.

For the second objective, I use experimental methods to investigate antibody-antigen binding as well as a model to predict the limit-of-detection for LF and LID systems based on the assay operation and antibody parameters. The experimental methods use lateral flow and ELISA-

based approaches to investigate the specific binding between antibodies and antigen as well as the non-specific binding between antibodies with varying pH, ionic strength and chemical composition parameters. By combining these investigatory methods with modeling tools for understanding isotachophoresis and binding systems, I show the reasons that ionic strength, pH, lysis chemistry, and the non-specific binding kinetics between capture and label antibodies are the most important factors when converting a lateral flow assay into a lateral flow enhanced by isotachophoresis diagnostic (LID) assay.

For the final objective, I modify the chemistry and process of our streptococcus pyogenes assay to accommodate the interferent biological material (e.g. throat cells, saliva, and other potential infections) in clinical samples. I achieve this by filtering the sample to remove any aggregated biological material and with the addition of detergent to solubilize the proteins. I then contrive clinical samples by modifying throat swabs with bacterial loading in the clinically relevant range and obtain a contrived clinical sensitivity and specificity.

Chapter 2. EXPERIMENTAL METHODS

In this chapter, I describe the techniques and equipment used to fabricate, operate, and characterize lateral flow enhanced by isotachophoresis diagnostic (LID) assays. We also discuss the electrolyte chemistries used and the naming conventions that will be used in this dissertation.

2.1 LID assay format

The experimental setup consists of an acrylic chip used to contain the paper device and electrolyte reservoirs as shown in figure 2-1. We fabricated our paper devices from backed nitrocellulose membrane (HF-135, Millipore, Billerica, MA) cut by a CO_2 laser cutter (Universal Laser Systems, Scottsdale, AZ). LID devices are 40 mm long to allow sufficient space for ITP plug formation and preconcentration while keeping the Joule heating and evaporation at a manageable level.[5,114] As the length increases, the current required to generate the electric field increases, resulting in greater Joule heating and evaporation. The printed test line is generated by pumping antibody solution with a syringe pump (PHD 2000, Harvard Apparatus, Holliston, MA) at a rate of 80 nL/min with a translation speed of 10 cm/min (ClaremontBio, Upland, CA), resulting in a throughput of 0.8 uL/cm. After printing the test line, the devices are dried in ambient temperature for 15 minutes before further drying at 37°C in an oven for 1 hour. We then block the membranes with 1% bovine serum albumin (BSA) in aqueous solution, shaken by a rotating platform. BSA serves to minimize the non-specific interaction of the target with the membrane.[115] The devices are then washed in an aqueous solution of 5 mM tris and 0.01wt% Tween-20 for 20 minutes to remove unbound proteins. The wet devices are returned to the 37°C oven for two hours to dry. Devices are then sealed in a pouch with desiccant to ensure low humidity conditions.

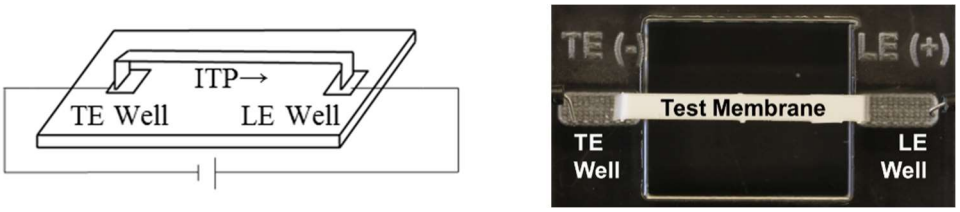

Figure 2-1: Simplified schematic of the LID format (left) and an image of the basic setup (right).

Laser cut acrylic sample holders, with 100 uL reservoirs, held the paper devices. Platinum wires, dipped in the reservoirs, conveyed the applied voltage to the paper devices with the negative electrode on the TE side and positive electrode on the LE side. The current is supplied by a programmable high voltage supply (HSV488, LabSmith, Livermore, CA).

To operate the device, we first add leading electrolyte (LE) to the LE reservoir, which wets the paper device through capillary action. Once the leading electrolyte fills ~80% of the paper, the trailing electrolyte (TE) is added to the TE reservoir. To run ITP, we set the current to 1.5 mA during plug formation, and then reduce the current to 0.5 mA over the testing area. The papers are allowed to dry for 1 hour at room temperature before the line intensity is measured.

To establish positive and negative test results, we quantify the test line intensity using a high-resolution flatbed scanner and a custom MATLAB algorithm. The dried test strips are placed on an 18% grey exposure card and scanned as a 16-bit greyscale image using a flatbed scanner (V800, Epson, Long Beach, CA). The normalized intensity is calculated as

$$NI = \frac{\langle I_b \rangle_{xy} - \langle I_t \rangle_{y,\min}}{\langle I_b \rangle_{xy} - \langle I_o \rangle_{xy}} \qquad \text{Equation 2.1}$$

where the angled brackets denote spatial averaging, the subscripts x and y denote the direction of averaging, and the subscripts b, t and o refer to the background, test line, and 18% grey card respectively. The minimum test line intensity, $\langle I_t \rangle_{y,min}$, is determined from a Gaussian fit of the

span-wise, y-direction, spatial average of the scanned image intensity. The background intensity, $\langle I_b \rangle_{xy}$, is determined as the average of the area averaged intensity regions directly adjacent (left and right) to the test line. Figure 2-2 describes the normalization procedure.

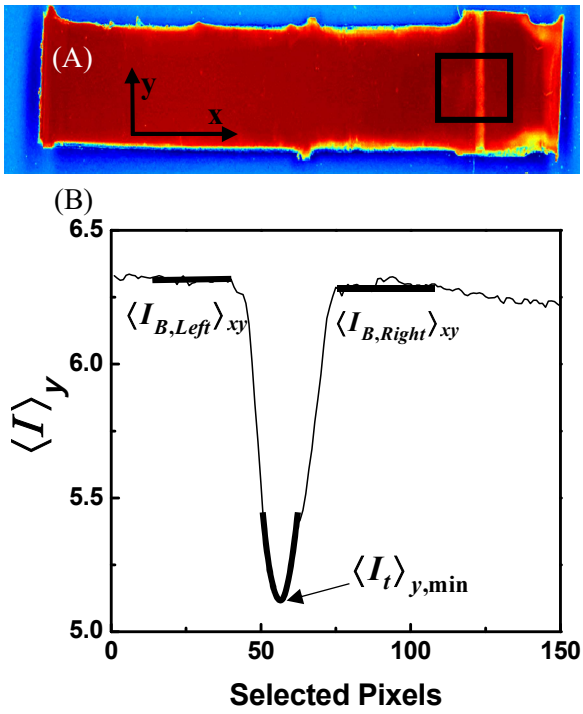

Figure 2-2: Sample scanned image of test strip (A) and extraction of values (B) used for determination of normalized intensity. A scanner was used to obtain the images and a MATLAB script was used to obtain the normalized intensity value.

We use the Clinical and Laboratory Standards Institute's (CLSI) definition to determine the assays' limits of detection.[8] We account for the sample size and adjust the z-score with the degrees of freedom when calculating the limit of detection in normalized intensity units using the equation $LoD_{NI} = LoB_{NI} + c_\beta \times \sigma_{s,NI}$, where the limit of the blank (LoB_{NI}) is $LoB_{NI} = \overline{NI}_{Blank} + 1.645 \times \sigma_{Blank,NI}$, $\overline{NI}_{Blank}$ is the average normalized intensity of the blank, $\sigma_{s,NI}$ is the sample standard deviations of low positives, $\sigma_{Blank,NI}$ is the standard deviation of the blanks,

$c_\beta = 1.645/(1-1/(4\times f))$, and f is the degrees of freedom (the number of tests done minus the number of concentrations tested).[1,8] Each measurement is repeated five times at minimum. The subscript *NI* indicates that the LoD value obtained is in unit-less normalized intensity values. For the calculation of the LoB_{NI} and LoD, we used a one-tailed 95% confidence interval (z-score of 1.645). We chose to use a one tailed test because for blank tests we are only concerned with the upper limit of NI and for positive tests, only the lower limit of NI is relevant for consistent determination of the positive result.

To test the repeatability of the measuring system, we scanned and quantified a single strip ten times. The average NI value from this strip was 0.13 and the coefficient of variation that we obtained from this testing was 0.01, which equates to 1% variability from the scanning and analysis.

2.2 Streptococcus pyogenes assay

In this work, we use a variety of electrolyte chemistries in the development of LID assays to detect strep throat and chlamydia trachomatis. Additionally, each assay target is tested using multiple antibody pairs. The chemistries and antibody pairs are described for streptococcus pyogenes in this section.

We used rabbit-anti-streptococcus pyogenes (Arista Biologicals, Allentown, PA), that targets the carbohydrate antigen as our capture antibody in this assay. In our research, we used two different antibody pairs. For the initial assay development, we used the antibody 0502 from Arista as the capture and 0801 as the label. This system will be referred to as assay "0502." For parts of this work, we used a self-pairing polyclonal antibody, 0803 from Arista Biologicals. This system will be referred to as assay "0803." This was necessitated as a result of the discontinuation

of the antibodies for the 0502 pair. The GAS carbohydrate antigen is extracted from the gram-positive streptococcus bacteria (inactivated group A streptococcus, Fitzgerald, Acton, MA) using radical reaction lysis chemistry.

For the limit-of-detection characterization in clean samples, we add a known quantity of streptococcus positive control to a 100 uL radical reaction lysis and extraction solution of 80mM HCl and 600mM sodium nitrate. Bis-tris, PVP, and additional hydrochloric acid are then added to the lysed target to form 400 uL of LE consisting of 40mM HCl, 80mM bis-tris, 1 wt% polyvinylpyrrolidone (PVP), and 150mM sodium nitrate as the final composition, resulting in a measured pH of 6.3 and conductivity of 16.5 mS/cm. The TE is an aqueous solution of bis-tris and tricine with a measured pH of 7.3 and conductivity of 392 uS/cm. Labeled gold nanoparticles (rabbit-anti-strep, Arista Biologicals, Allentown, PA) in the LE give a final optical density at 540 nm of 0.6. For the clinical validation study, we slightly lower the final sodium nitrite concentration to 125mM and add 0.075% Tween-20.

2.3 Chlamydia trachomatis assay

For the chlamydia trachomatis assay, we target the lipopolysaccharide (LPS) membrane fragment based on a lateral flow assay that was previously developed by PATH. We investigate a total of nine different antibodies for potential use in the final assay design. These antibodies are: 15174 (QED Biosciences, San Diego, CA), MAV07-743 (henceforth referred to as "MAV," Meridian Life Sciences, Memphis, TN), HM032, HM031, HM215, HM406, HM407 (EastCoast Bio, North Berwick, ME), 6709 and 6701 (Biospacific, Emeryville, CA). When describing these pairs, the assay will be named with the convention of "capture antibody/label antibody." The

lipopolysaccharide (LPS) target is extracted from the cells (serovar D/UW-3, obtained from UW Public Health) by alkaline lysing of 200mM NaOH for 2 minutes.

The initial device development for chlamydia trachomatis assay used the antibody pair 15174/MAV. The LID device LoD determination is completed with the 15174/MAV antibody pair. Unlabeled gold (Arista Biologicals, Allentown, PA) is conjugated with the MAV mouse-anti-chlamydia trachomatis antibody. The conjugation occurs at pH 9.9 under mixing for 5 minutes, and the conjugated gold is then blocked by 1% BSA (detailed in appendix 3). HCl, bis-tris, gold and PVP are added to form a final leading electrolyte chemistry consisting of 87.5mM HCl, 150mM bis-tris, 50mM NaOH, 0.5wt% PVP, and 0.1 O.D. of conjugated gold at 540nm. This chemistry has a measured pH of 6.85 and a conductivity of 11 mS/cm. The trailing electrolyte is an aqueous solution of 50mM bis-tris and 50mM tricine.

For the antibody selection around a fixed leading electrolyte chemistry, the selected chemistry consisted of 50mM NaOH, 75mM HCl, 150mM bis-tris, 1wt% PVP, and 0.25% Triton-X. The extraction chemistry of aqueous NaOH is unchanged, and the final LE pH is 6.8 and conductivity is 14 mS/cm. By using a fixed chemistry, the operability of the ITP of the LID assay is ensured. The binding of the potential antibody pairs is investigated to create a LID assay with consistent ITP with functional antibody antigen binding.

Chapter 3. PARAMETERS AFFECTING LID PERFORMANCE

In this chapter, we identify and characterize the parameters that affect the amount of improvement achievable through incorporating isotachophoresis (ITP) into lateral flow (LF) assays. The goal of optimizing both LF and lateral flow enhanced by isotachophoresis diagnostic (LID) assays is to generate high signal when the target is present, and no signal when the target is absent. Numerous parameters affect the performance of LF and LID assays, including: temperature, humidity, test-line location, membrane treatment, membrane selection, chemistry, lysis efficiency and antibody selection. Both LID and LF assays generate signal from antibody-antigen binding, however, there are additional design considerations for LID assays that result from the requirements of isotachophoresis.

Antibody-antigen binding and ITP both depend upon the solution pH and ionic strength (IS).[116–119] The solution chemistry is influenced by the lysis chemistry, which affects both the lysis efficiency and ITP performance. LID demonstrates improved performance over LF by increasing the specific signal by using ITP to concentrate the target. ITP also concentrates the label, which can lead to decreased performance by increasing the non-specific signal. The chemistry requirements for lysis, ITP, and binding are often different and at odds with each other which makes optimization of the chemistry challenging.

Experiments and discussion on the effect of the pH and IS on signal generation and ITP are presented and discussed in the first section. The effect of lysis chemistry on ITP is discussed in the second section. A model and experimental results for non-specific signal generation in LID and LF assays are presented in the third section. The final section presents the results that were obtained for strep and CT LID assays in the LID format in clean solutions.

3.1 pH and ionic strength (IS)

In this section, we will discuss the effect of the solution ionic strength and pH on the antibody binding in addition to their effect and limitations in an ITP system. Ionic strength (IS) is defined as: $IS = \frac{1}{2}\sum([i]\times v_i^2)$, where $[i]$ is the molar concentration and v_i is the valence of the ion. Molarity is not the same as ionic strength unless the system is composed of only fully dissociating chemicals, e.g. salts and strong acids and bases. Frequently, a calculator (such as CurtiPot©) is used to determine the ionic strength of weakly dissociating chemicals. We are, however, able to estimate the IS for the strep and chlamydia trachomatis (CT) LID chemistries from the concentration of a single component. When all ions are monovalent in a neutrally charged solution, the IS is equivalent to the molar concentration of positive or negative charges. In this situation, it is possible for one ion to match the overall ionic strength. For example, in the CT systems have a mixture of sodium, hydrogen and protonated buffer as the positive ions in the system, but essentially all negative charges are from chlorine. It is appropriate to estimate the IS as the concentration of chlorine ions. This method assumes full dissociation of salts and strong acids and bases, and ignores the contribution to the ionic strength of the weak acids and bases.

pH is defined as the decimal logarithm of the reciprocal of the hydrogen ion activity: $pH = \log_{10}\frac{1}{a_{H^+}}$.[120] The hydrogen ion activity can be considered the effective concentration of the hydronium ions. We measure the pH with a pH-meter (Seven Excellence, Mettler Toledo, Columbus, OH).

3.1.1. *Effect of pH and IS on specific and non-specific binding*

Antibody conformation and binding activity are sensitive to pH and IS. Previously, IS has been shown to have a smaller impact on the antibody-antigen binding than the pH.[116,117] We

determine the operational IS range before pH because IS is less impactful. Techniques such as differential scanning calorimetry, surface plasmon resonance, and circular dichroism spectroscopy can be used to investigate the binding and conformation of antibodies.[121] These techniques are expensive, so most antibody based diagnostics are developed empirically. We use this empirical approach to investigate the effect that pH and IS have on the specific and non-specific binding. This empirical testing is done through the use of positive and negative lateral flow assays to compare the performance of the system under different chemistry conditions.

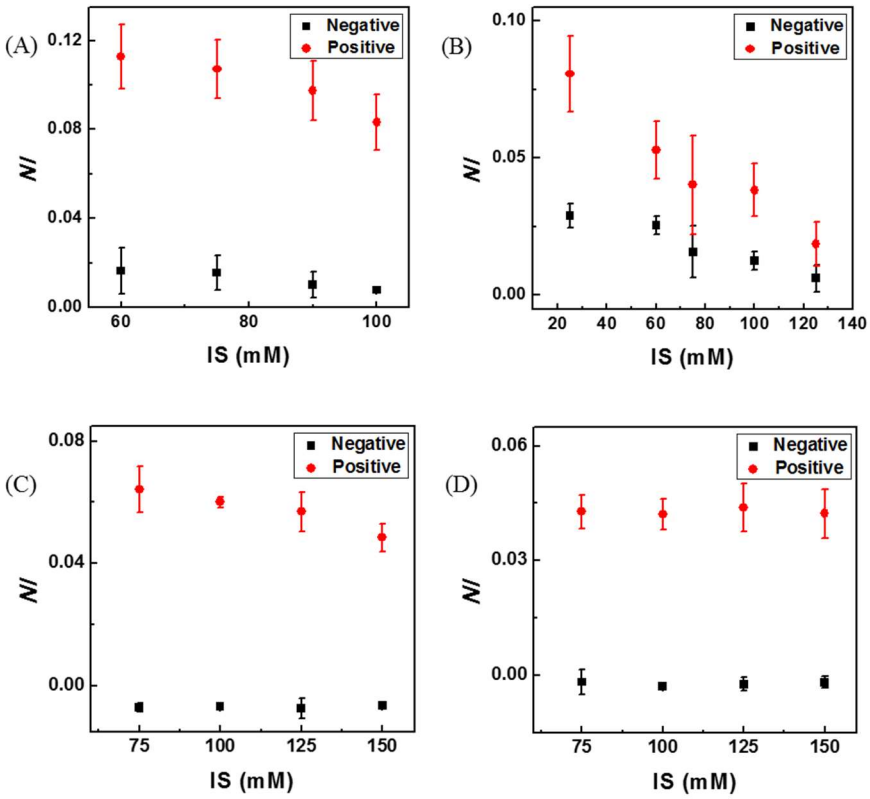

Figure 3-1: Experimental response from positive and negative lateral flow assays with varying sample solution ionic strength. The four systems investigated are 15174/MAV (A), 406/407 (B), 0502 (C), and 0803 (D). 15174/MAV and 406/407 are systems targeting the chlamydia trachomatis LPS protein with the ionic strength corresponding to the concentration of hydrochloric acid in the final solution. 0502 and 0803 are systems targeting the carbohydrate antigen of streptococcus pyogenes with the ionic strength corresponding to the amount of sodium nitrate in the final solution.

We investigate the effect of IS on 4 pairs of antibody systems, 2 for chlamydia trachomatis (CT) and 2 for group-A strep (GAS). The systems investigated are CT 15174/MAV, CT 406/407, GAS 0502, and GAS 0803. The responses from this screening are shown in figure 3-1. Each plot shows the average and standard deviation of positive and negative lateral flow results at varied ionic strength. The concentration of each chemical component is scaled to vary the ionic strength while maintaining a constant pH. The scaled components for CT 15174/MAV(A) are NaOH, HCl, and tris, with the HCl used to estimate the IS. The scaled components for CT 406/407(B) are NaOH, HCl, and bis-tris, with the HCl used to estimate the IS. The scaled components for GAS 0502 and 0803 (C,D) are $NaNO_2$, HCl, and bis-tris, with the $NaNO_2$ used to estimate the IS. The antibodies that demonstrate high positive signal generation and little or no signal for negative samples at an IS indicate good functionality at that IS. CT 15174/MAV (figure 3-1A) and GAS 0803 (C) show an insignificant decrease in positive signal from increasing ionic strength, with little to no effect on the negative signal. GAS 0803 (D) displays no change in the positive or negative signal over the IS range tested. CT 406/407 (B) shows a strong negative dependence of both the positive and negative signal on IS. The reason for this dependence is unclear, but it is problematic for the final system design for 406/407. With biological binding usually occurring around 150mM, we expect that the assay performance, as described in section 1.1, will further suffer at ISs below the range tested.

The pH is also an important factor in antibody based assay design (e.g. LF and LID). It is difficult to predict how an antibody antigen reaction will be affected by pH. The optimal binding of an antibody typically occurs within the biological range, 6-8. It has been found that electrostatic interactions and non-uniform surface-charge distributions are important near neutral pH for

antibody binding.[117] pH has a large effect on protein folding, which affects the antibody binding. In the same fashion as the IS testing, the effect of pH is investigated empirically.

The pH dependence is investigated for the same systems as the IS: CT 15174/MAV, CT 406/407, GAS 0502, and GAS 0803. The responses for each of these systems are in figure 3-2. The pH is modified by changing the amount of buffer present while the rest of the chemistry remains fixed, to keep the ionic strength as consistent as possible. Increasing the concentration of buffer increases the pH, and decreasing the concentration decreases the pH. The pH range for the buffering capacity of each buffer is the pKa ± 1 pH unit as a rule of thumb. The buffering capacity of the buffer is much higher at and above the pKa.

Figure 3-2 is the response of positive and negative signal generation to varying pH for four antibody pairs. Each plot shows the average and standard deviation of positive and negative lateral flow results. The data shown in fig. 3-2 is an example of how unpredictable the response of the binding of an antibody system can be. 15174/MAV (plot A) shows a positive correlation between pH and signal, whereas 0502 (plot C) shows a negative correlation. 406/407 (plot B) and 0803 (plot D) have little sensitivity to the pH in the range tested. Ideally, the binding of the antibody pair would demonstrate no sensitivity to changes in pH, with high positive signal generation and low negative signal generation dictating the functional range. The pH range of functional binding for an antibody pair is important for the design of the electrolyte system. The values of pH at which this functional range occurs dictates which ITP compatible buffer needs to be used. This range must be at least 1 pH wide to be compatible with the LID format, as will be discussed in section 3.1.3.

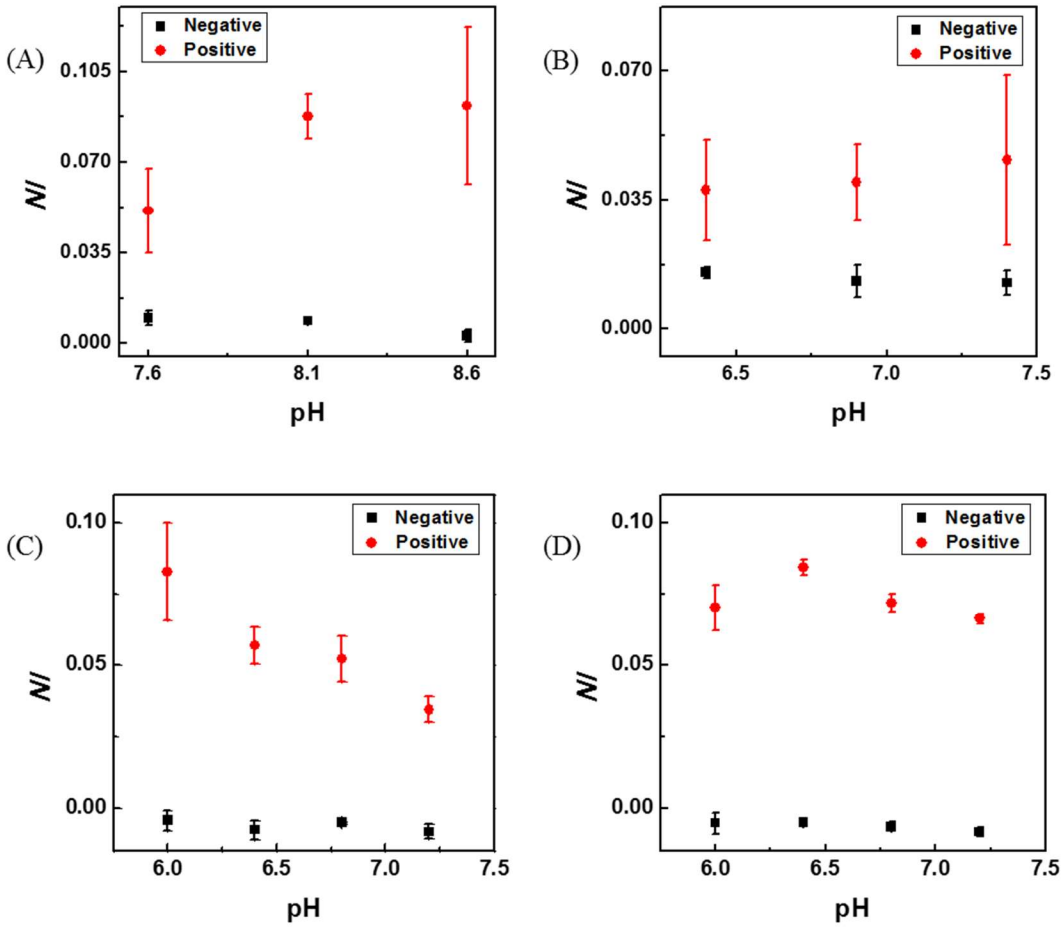

Figure 3-2: Experimental response from positive and negative lateral flow assays with varying sample solution pH. The four systems investigated are 15174/MAV (A), 406/407 (B), 0502 (C), and 0803 (D). 15174/MAV and 406/407 are systems targeting the chlamydia trachomatis LPS. 0502 and 0803 are systems targeting the carbohydrate antigen of streptococcus pyogenes. The pH for 15174/MAV is controlled by the concentration of tris, the pH in each other system is controlled by the concentration of bis-tris.

3.1.2 *Ionic strength effect on ITP*

The design of an ITP system for use in a nitrocellulose membrane has limitations on the functional range of IS. ITP requires a high IS leading electrolyte (LE) and a lower IS trailing electrolyte (TE) for stacking to occur, as discussed in section 1.3. There are additional requirements placed on the ionic strength when the supply is current limited or when the system

is open to the air, as is the case in a LID system, due to heating and evaporation off of the substrate. For a LID assay, binding occurs in the LE and the adjusted trailing electrolyte zone (ATE). The leading electrolyte chemistry is controlled and easily investigated. However, the ATE can pose challenges because it is comprised of a running mixture of the LE and the TE. Spresso, an ITP simulation tool that is a free MATLAB program created by the Santiago group from Stanford University, is an effective tool for assessing the functionality and conditional changes in a potential operating chemistry as well as investigation into the ATE conditions. From experience and ITP modeling, the IS_{ATE} is closer to the IS_{TE} than IS_{LE}. A rule of thumb for this is IS_{ATE} is approximately 30% of the IS_{LE}.

The limits for IS of a LID assay are mostly a result of a necessity to limit the Joule heating of the system, while maintaining effective stacking of the target. At IS_{LE} > 200mM, the amount of current required to generate the voltage necessary to create and move a plug also generates significant joule heating, as discussed in section 1.4. In the most extreme cases, the heat causes evaporation from the middle of the substrate causes drying leading to ignition of the nitrocellulose. The IS_{TE} is generally limited to 30mM. A standard TE is a mixture of very weak acids and bases. Even a high molarity TE, a mixture of 200mM bis-tris and 200mM tricine, has an IS of less than 25mM. This is a result of the low dissociation constant of the weak acid and weak base, meaning that the majority of the molecules remain in an associated, uncharged state. Low IS_{TE} results in a large electric field for effective stacking into a plug.

The ratio of the IS_{LE} and the IS_{TE} is another important factor. A good rule of thumb for this is $4 < \frac{IS_{LE}}{IS_{TE}} < 10$. The lower limit is a requirement to maintain effective stacking, and the upper limit is to restrict the effect of electroosmotic flow. Electroosmotic flow is counter to the direction of ITP and this flow creates dispersion of the ITP plug when the conductivity ratio of the

LE to the TE is high, leading to poor repeatability. Taking into consideration all of these rules, the IS_{LE} can range of 50-200mM and the IS_{TE} range of 1-30mM resulting in an IS_{ATE} range of roughly 20-75mM.

3.1.3 *pH in ITP systems*

pH also plays a critical role in the performance of ITP systems. It affects the charge of proteins, electroosmotic flow and conductivity, among other aspects.[56,57,122,123] The relationship between the pH and protein conformation, or ability to bind, is described by Sahin, et. al.,[117] and the relationship between pH and electroosmotic flow and conductivity by Kirby, et. al., Persat, et. al. and Lukacs, et. al.[56,57,122] For the design of LID assays, it is important to understand the limits of pH tuning in an ITP system, and the expected pH of the ATE. In a lateral flow assay, the test-line is only exposed to a single pH. In a LID assay, the test-line is exposed to the pH of the LE, TE and ATE. Binding only occurs in the LE and ATE in these assays. The pH_{TE} affects the signal generation through unbinding, in addition to the effects on the ITP plug movement and stacking. The LF screening data where we varied pH, as shown in figure 3-2, shows that the effect of pH on antibody binding depends on the antibody pair. It is important to determine the range of pH at which functional binding occurs. Functional binding, in this case, is a strong differentiation between positive and negative signals, with negative signals at or near 0 intensity. In most cases, the difference between pH_{LE} and pH_{ATE} is a least 1 pH unit, requiring a functional binding range of at least that large. The pH in the ATE is determined by simulating the ITP to investigate the effect of chemistry changes. The ITP simulation tool, Spresso, is available from Stanford Microfluidics Laboratory and is described by Bahga, et. al.[124] The pH of the ATE is higher than that of the TE as a result of protonated buffer moving counter to the plug, and uncharged buffer not moving with the plug. An example of the relative pH in each zone of ITP is shown in fig.3-3.

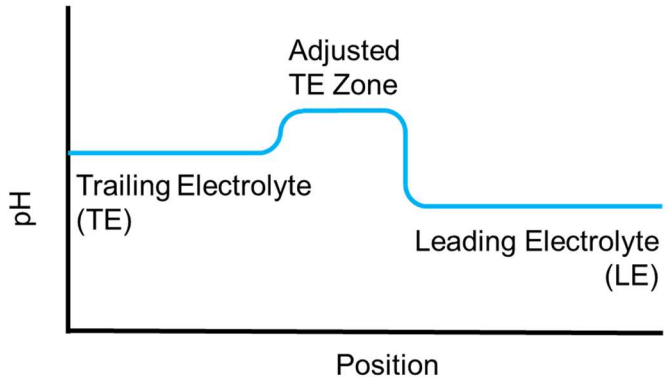

Figure 3-3: Simplified schematic of the pH trend in a high functioning anionic ITP system.

The mobility of the label, target and trailing ion have a positive correlation with pH. Figure 3-4 shows an example of the mobility trends as a function of pH. In this example, the target is IgG and two sample trailing ions, HEPES and glycine, are compared to assess functionality. For ITP, the trailing ion is required to have a lower (smaller negative number) mobility than the target (IgG in this case). From the data in fig. 3-4, ITP is possible with glycine as the trailing ion for systems with pH between 6 and 9. To simplify the process, we have created an ion table (appendix 2) that takes input of the mobility of the target at a specific pH values and suggests trailing ions that have lower mobilities than the target based upon the calculated mobility from the pKa and absolute mobility of the potential trailing ion. The functional limit of pH_{ATE} in a system with colloidal gold is 9.3. There are no trailing ions that have low enough mobilities at high pH to stack conjugated gold at the LE-TE interface.

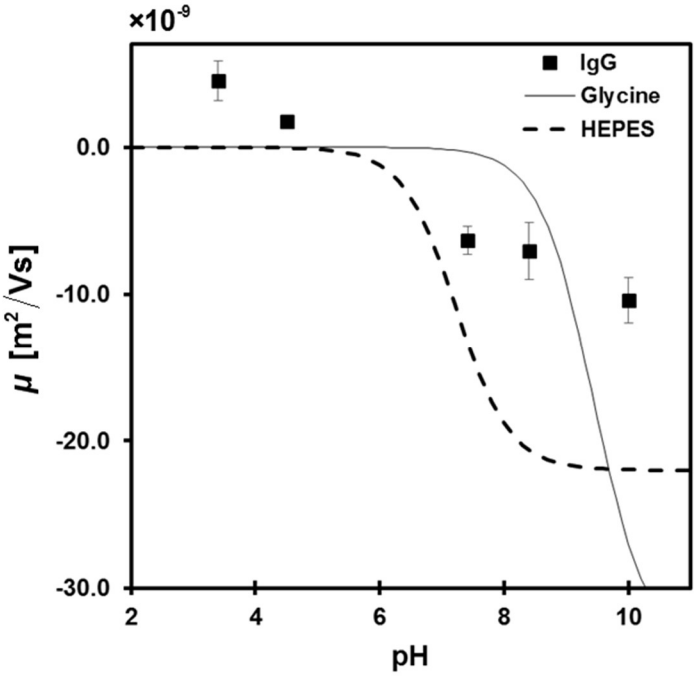

Figure 3-4: Example of experimentally determined mobility of IgG as a function of pH. These values are compared with the theoretical predictions for HEPES and glycine. The IgG will stack properly only when the mobility of the IgG is a larger negative number than the trailing ion (e.g. HEPES or glycine). Figure obtained from Dr. Moghadam's dissertation.[4]

As an example of taking all the restraints into account, the pH_{LE} selected for 15174/MAV was 8.1 with a tris buffer (pKa=8.1). The LF screening results, fig. 3-2A, indicate that this pH is in the functional range for this antibody pair, with strong positive and low negative responses of the LF test at this pH. The trailing ion of glycine, pKa of 9.78 and absolute mobility of 37.4 $m^2/V/s$, is selected by use of the ion table described earlier. Glycine has a lower mobility than conjugated gold at pH below 9.2. Perhaps the greatest challenge in adapting a lateral flow assay into a LID assay is finding antibodies that functionally bind over the range of pH and IS experienced in the LE and ATE.

3.2 Lysis chemistry

In most lateral flow immunoassays, as well as our LID assays, the target of the antibody cannot be captured effectively with whole cells. To increase this capture efficiency, the cells are typically lysed by disrupting the cell membrane, in order to release the isolated target. There are many methods available to disrupt cell membranes.[125–127] These methods are broadly separated into solution based and physical disruption methods.

The typical physical disruption methods are sonication, crushing, and freeze/thaw cycles. These methods have a long history and are capable of lysing most bacterial cells, but have many inherent disadvantages. [126,128] Many of these methods generate heat, which can cause protein denaturation and aggregation. Reproducibility is also a common problem with these techniques. These methods are sensitive to the viscosity as well as the concentration of the calls in the sample solution. These methods are not suitable for point-of-care assays, as they require equipment, such as a sonicator, French press, or freezer.

For chemical lysis, the use of surfactants/detergents, enzymes, pH and ionic strength lysis are the most common.[125–127] These methods are generally less widely applicable and usually specifically tuned for a specific purpose. Bacterial cells are separated into gram-positive and gram-negative types, based on the composition of their cell membranes, shown in figure 3-5. Gram-positive cells are more easily lysed through detergents, reactions and enzymes, and gram-negative cells are more easily lysed through pH and ionic strength lysis.[6,126] Radical reaction lysis, which is used to lyse the gram-positive group-A strep in our LID assay as well as the commercial lateral flow assay, is not a commonly used lysis strategy, but has been effective in our experience.

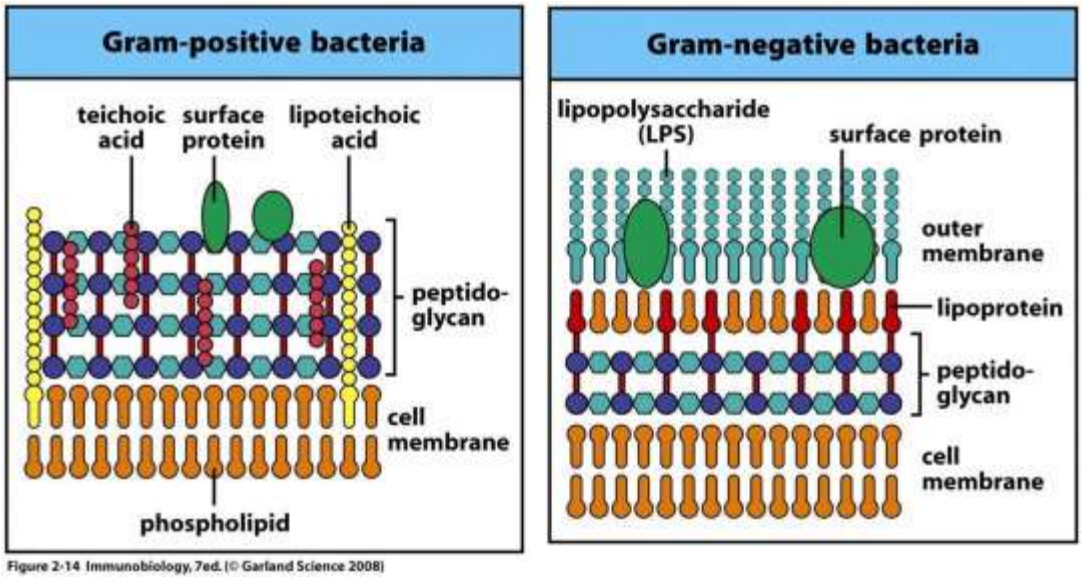

Figure 3-5: Illustration of the expected protein composition of the cell membrane of gram-positive and gram-negative bacteria.[6]

3.2.1 *Radical reaction lysis*

Group-A strep is a gram-positive bacterium, which makes it difficult to lyse with physical methods.[129] Figure 3-5 is an illustration of the compositional differences between gram-positive and gram-negative bacteria. For the commercial assay, a reaction between acetic acid and sodium nitrite is used to lyse the cells. This method is used in our assay because is it consistent and usable at the point-of-care.[130] The sample solution that results from this reaction is 1.2 M sodium nitrite and 80 mM acetic acid. The reaction between these chemicals creates nitrous acid,

$$NaNO_2 + CH_3COOH \leftrightarrow HNO_2 + NaCH_3COO$$

Nitrous acid is an unstable compound which decomposes to nitric oxide, nitrogen dioxide and water:[131]

$$2\,HNO_2 \leftrightarrow NO_2 + NO + H_2O$$

Nitric oxide is a free radical that breaks apart the cell membrane, lysing the cells. However, a solution containing 1.2 M Na^+ is not compatible with nitrocellulose based isotachophoresis. In a high conductivity system, the amount of current required to create sufficient electric field for ITP is high, resulting in increased Joule heating, drying, and burning of the substrate.

Chlorine is a common leading ion in ITP systems; this motivated us to replace the acetic acid with hydrochloric acid. The reaction to generate the radical requires the nitrate ion reacting with a proton, and is compatible with any strong acid. We are able to replace the acetic acid with hydrochloric acid with no loss is lysis efficiency.

The lysis used in the commercial assay results in a sample solution with 1.2M IS. This IS is too high for ITP in an open system, like a LID assay because it requires large currents and generates significant Joule heating. We examined the extraction efficiency with decreasing amounts of sodium nitrate and hydrochloric acid in the lateral flow format to lower the ionic strength of this lysis chemistry. We found that the extraction efficiency remained >90% with a 50% decrease in concentration based on lateral flow signal intensities when lowering the concentration of $NaNO_2$ while maintaining the concentration of strep cells. By decreasing the initial amount of $NaNO_2$ in the lysis chemistry and further diluting the lysis chemistry by 4x to form the LE chemistry, we are able to incorporate the lysis chemistry into a LID device and maintain functional ITP.

3.2.2 *Alkaline Lysis*

Unlike group-A strep, chlamydia trachomatis is a gram-negative cell. Gram-negative cells are generally more chemically robust than gram-positive, but they are less resistant to physical disruption or extreme conditions. The commercial lateral flow test uses high pH lysing to extract the proteins from the cells.[132] In a high pH solution, generated by exposing the cells to high sodium hydroxide content (200mM), the cells membranes burst open, releasing the membrane proteins.

This lysis chemistry is much lower in IS when compared to the radical reaction lysing, and we are able to use this extraction chemistry in a LID assay with a simple 4x dilution (final concentration of 50mM NaOH).

3.2.3 *LID assay design*

When transferring a lateral flow assay to a LID format, it is important to minimize the concentration of Na^+ in the final leading electrolyte. The amount of Na^+ can be important for lysis, e.g. the amount of sodium hydroxide in alkaline lysis or sodium nitrite in radical reaction lysing, but can negatively impact ITP when present in high concentrations. When an electric field is applied in ITP, anions move downstream and cations move upstream. The system must remain neutrally charged and so the amount of positively charged ions that can move upstream is limited by the charge balance.

Figure 3-6 gives an example of the positive ions moving upstream from the LE to the TE to create the adjusted TE zone. In an idealized anionic ITP system, the cation flowing upstream is protonated buffer (e.g. bis-tris$^+$, $C_8H_{20}NO_5^+$), as shown in the right column of fig. 3-6. When an excess of cations replace the protonated buffer ions, as shown in the left column of fig. 3-6, the buffer concentration in the adjusted trailing electrolyte zone (ATE) is not adequate, resulting in a high pH, beyond the preferred binding range of antibodies. Thus, it is important to limit the overall concentration of sodium cations in the electrolyte chemistry.

In summary, chemical lysis is compatible with the LID format, but with restrictions on the lysis chemistry to maintain ITP. For the streptococcus assay, we replaced the low mobility acetate anion with the commonly used chlorine leading anion to facilitate isotachophoresis. Additionally, we limit the final concentration of sodium cations in the strep and CT assays to maintain stacking and pH control.

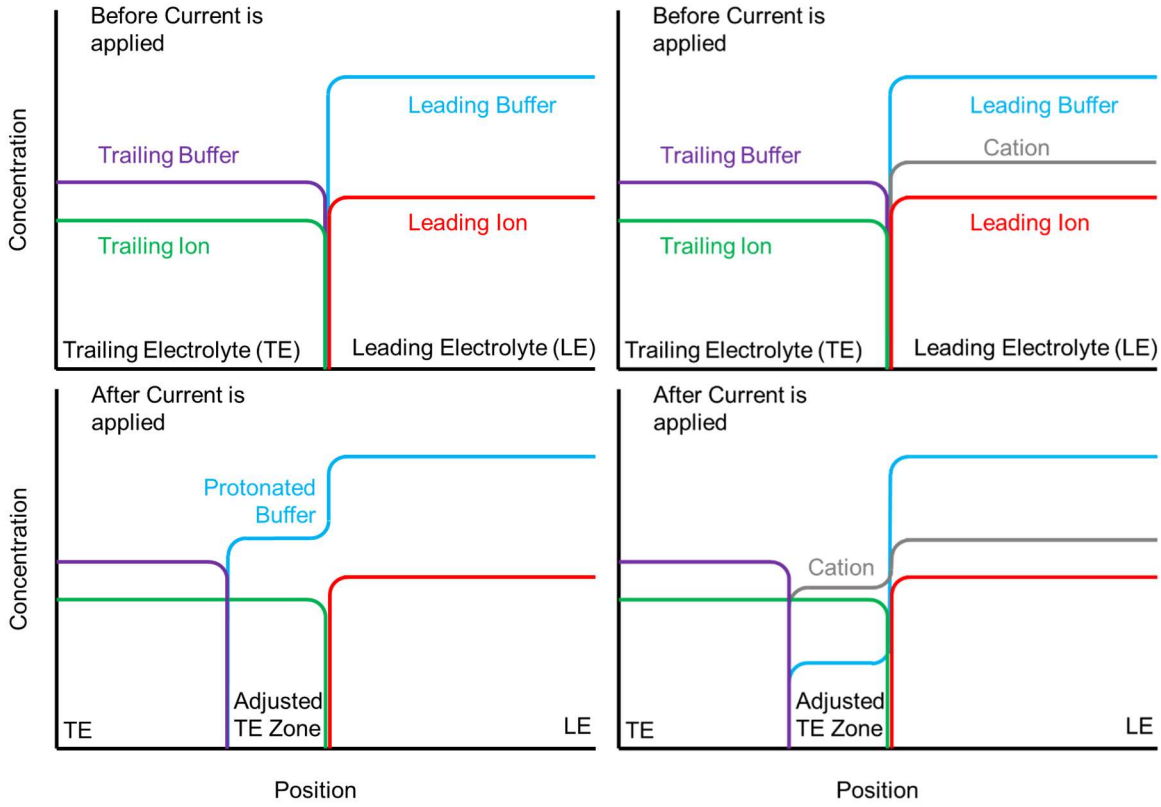

Figure 3-6: Simplified concentration trends of the leading, trailing and adjusted trailing electrolytes in an ITP system. The plots for a standard system, containing no added cation (left column), are compared to the same system with cation added to the leading electrolyte (right column). Two time points are shown: before ITP begins (top row) and during ITP (bottom row). Note that the adjusted TE zone appears only after the current is applied. In both systems, the amount of positively charged ions in the TE zone is identical, however a significant portion of the buffer ions are replaced by the cation in the system on the right. The lower concentration of buffer in the zone results in a high pH, that is not controlled by the buffer. Using the strep chemistry as an example, the leading and trailing buffers are bis-tris ($C_8H_{19}NO_5$), leading ion is chlorine (Cl-), trailing ion is deprotonated tricine ($(HOCH_2)_3CNHCH_2CO_2^-$), protonated buffer is bis-tris+ ($C_8H_{20}NO_5^+$), and the cation is sodium (Na^+).

3.3 Non-specific binding kinetics

For laboratory immunoassays in clean samples, non-specific (NS) binding in sandwich immunoassays is the result of affinity between the capture and label antibodies, or the capture antibodies and the label itself (e.g. gold nanoparticle).[133,134] This is the type of non-specific binding that will be discussed in this section. The antibody-antibody interaction is most frequently

attributed to the Fc region of the antibody, the stem of the "Y" shape.[135] The factors that affect the non-specific binding of the antibodies are: the binding conditions, the concentration of label, the detergent, the blocking agent, the presence of any confounding factors, and the washing step (if used).

3.3.1 *Model investigating the effect of ITP on non-specific binding*

ITP is a powerful technique because it concentrates the label and target before exposure to the capture line. This can result in a dramatic increase in the signal generated with low levels of analyte leading to a much lower limit-of-detection (LoD). Concentrating the label also leads to an increase in the non-specific binding interaction between the label and capture line. Increasing the non-specific binding increases the signal from negative samples, i.e. blanks. Since the limit of detection is related to the limit of blank (LoB_{NI}), increasing the signal from the blanks negatively impact the improvement of the LoD generated by ITP.

The effective concentration of the label that the test line experiences is much higher in the ITP system when compared to LF because ITP concentrates the label before exposure to the test-line. Paper-based ITP is capable of extracting a fluorescent target from the trailing electrolyte and concentrating the target by nearly 1000-fold.[5,45] The modeling of the binding in one-site LID assays that was used in the previous works published by Dr. Moghadam is not applicable for the sandwich assay format. This model also assumes an excess of target for the reaction. This model is applicable to the non-specific reaction in sandwich lateral flow assays, which acts as a one-site system with an excess of the reactant. We develop a new model for the specific signal generation, when the target is limited. We combine the one-site non-specific model with the new specific signal model to create a model for limit-of-detection.

We begin the development of the model with the rate reaction for specific and non-specific signal generation. We assume that the reactions are first order. This is a common assumption for antibody antigen reactions, and is representative of most antibody systems.[136] By assuming the first order reaction, the reaction rates can be written as:

$$\frac{dC_{LAC}}{dt} = k_{on,S}C_L C_C - k_{off,S}C_{LAC} \qquad \text{Equation 3.1}$$

$$\frac{dC_{LC}}{dt} = k_{on,NS}C_L C_c - k_{off,NS}C_{LC} \qquad \text{Equation 3.2}$$

Where k is the kinetic rate reaction and C is a concentration. The subscript L is for the label antibody, subscript A is the antigen, and subscript C is the capture antibody, with any combination of these subscripts indicating a complex of the components. The subscripts *S* and *NS* note the rate constants for specific and non-specific reactions respectively. The subscripts *on* and *off* are the rate constants for the association and dissociation reactions respectively Equation 3.1 is the rate reaction for the formation of the specific signal generating complex, LAC. Equation 3.2 is the rate reaction for the formation of the non-specific signal generating complex, LC. The reverse specific reaction rate, $k_{off,S}$, is a combination of $LAC \xrightarrow[k_{off}]{} L + AC$ and $LAC \xrightarrow[k_{off}]{} LA + C$. To solve these rate equations for concentrations, we assume perfect mixing and that the concentration of the label-antigen complex is only lost to test-line binding. We assume perfect mixing, ignoring the potential for diffusion limitations because the small capillary size of the nitrocellulose, thus the mixing requires a short diffusion length. The dissociation of this LA complex can be approximated as zero because the label-antigen reaction has time to reach equilibrium in our system and antibody antigen interactions typically have low kinetic off rates, ~$10^{-6}s^{-1}$.[121,137] We also do not consider adsorption of label or antigen onto the nitrocellulose surface. We ignore this factor because the effect of adsorption onto the nitrocellulose is consistent between LF and LID formats.

Equation 3.2 for non-specific signal generation (LC) has been solved analytically in previous work with the assumption that the consumption of L is negligible. In nearly all lateral flow assays, the label is in excess.[5,45] The non-specific signal equations using these assumptions are,

$$\frac{C_{LC}}{C_{C0}} = h_{NS,LF} = \frac{L_0^*}{L_0^*+1}\left(1 - \exp\left(-(L_0^* + 1)k_{off,NS}t_{LF}\right)\right) \quad \text{Equation 3.3}$$

$$\frac{C_{LC}}{C_{C0}} = h_{NS,ITP} = \frac{pL_0^*}{pL_0^*+1}\left(1 - \exp\left(-(pL_0^* + 1)k_{off,NS}t_{ITP}\right)\right), \quad \text{Equation 3.4}$$

where C_{C0} is the initial concentration of binding sites, h is the ratio of occupied to initial sites, C_{L0} is the initial label concentration, $L_0^*=C_{L0}k_{on,NS}/k_{off,NS}$, p is the ITP preconcentration factor, t_{LF} is the amount of time that the solution flows over the test-line in LF, and t_{ITP} is the residence time of the plug over the test-line. L_0^* is the non-specific reactant concentration combined with the reaction kinetic on rate, resulting in the rate of formation, which is then non-dimensionalized by dividing by the kinetic off rate. L_0^* can also be defined as $C_{L0}K_{A,NS}$, where $K_{A,NS}$ is the non-specific binding affinity, which is equal to $k_{on,NS}/k_{off,NS}$. The subscript *0* will continue to be used for the initial concentration of a component or complex.

The difference in non-specific signal between the LF and ITP assays is sensitive to p, t_{ITP}, t_{LF}, C_{L0}, and $K_{A,NS}$. For the systems tested in this dissertation, the p and t_{ITP} are consistently near the values of t_{ITP}=60s, and p=100. The t_{LF} affects the non-specific signal of the LF assay, but does not affect any of the trends observed from the model. The remaining 2 factors of C_{L0} and $K_{A,NS}$ are combined into the single non-dimensional factor of L_0^*.

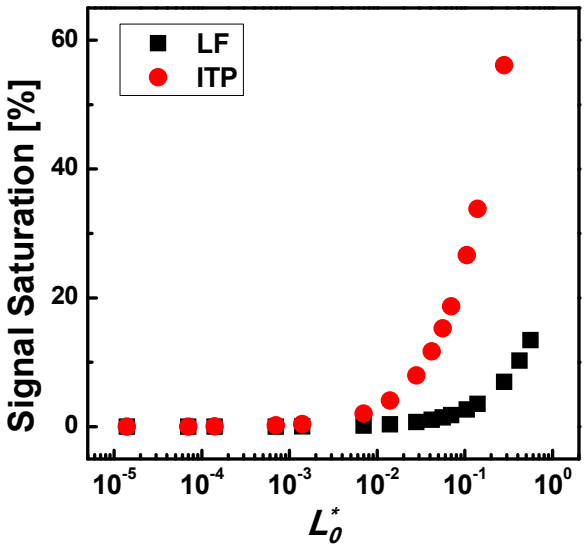

Figure 3-7: Modeled non-specific test-line signal saturation generated by varying amounts of label or varying non-specific affinities ($L_0^*=C_{L0}K_A$) for LF and ITP formats. The difference is negligible below $L_0^*= 10^{-3}$, with a dramatic increase in NS signal at higher L_0^*. The other parameters are set to: $k_{off,NS}$ =5E-5s^{-1}, p =100, t_{ITP} =60s, and t_{LF} =600s.

To investigate how the application of ITP affects the non-specific signal generation in terms of values of L_0^*, the NS signal generation for the ITP format as well as the LF format is plotted in figure 3-7. For all values of the non-dimensional factor of L_0^*, the NS signal generation is higher in the ITP format than in LF as a result of the concentrating effect of ITP on the label. However, the additional NS signal generation is negligible for L_0^* values of 0.001 or lower. For an initial concentration of label around 0.1 O.D., $K_{A,NS}$ above ~10^3M^{-1} leads to a dramatic increase in non-specific signal in ITP assays when compared to LF assays. The value of 10^3M^{-1} is for an ITP system that has a concentration factor, p, of 100 and a plug residence time, t_{ITP}, of 60s. Increasing these two factors would cause the dramatic increase in non-specific binding to increase at a lower value of $K_{A,NS}$. p=100 and t_{ITP}=60s are appropriate values for the systems described in this dissertation.

When solving for the specific signal generation (*LAC*), it is not appropriate to assume that negligible mass of *LA* is consumed. This is especially true when operating near the LoD, where we are most interested in the assay's performance. We solve equation 3.1 at the LoD with the approximation of constant concentration of available binding sites ($C_C = C_{C0}$). We use this approximation at the LoD, when less than 10% of the binding sites are expected to be occupied. By incorporating this approximation and substituting C_{LA0}-C_{LAC} for C_{LA}, we arrive at,

$$\frac{dC_{LAC}}{dt} = k_{on,S}(C_{LA0} - C_{LAC})C_{C0} - k_{off,S}C_{LAC} \qquad \text{Equation 3.5}$$

or $$\frac{dh_S}{dt} = k_{on,S}(C_{LA0} - C_{C0}h_S) - k_{off,S}h_S \qquad \text{Equation 3.6}$$

which, after separating variables and integrating for dh_s on the left and dt on the right yields:

$$h_{S,LF} = \frac{C_{LA0}K_{A,S}}{K_{A,S}C_{C0}+1}\left(1 - \exp\left(-\left(K_{A,S}C_{C0} + 1\right)k_{off,S}t_{LF}\right)\right) \qquad \text{Equation 3.7}$$

For ITP, which concentrates C_{LA0} into pC_{LA0}, the integration yields:

$$h_{S,ITP} = \frac{pC_{LA0}K_{A,S}}{K_{A,S}C_{C0}+1}\left(1 - \exp\left(-\left(K_{A,S}C_{C0} + 1\right)k_{off,S}t_{ITP}\right)\right) \qquad \text{Equation 3.8}$$

The equations for low positive specific binding (3.7 and 3.8) can easily be algebraically manipulated to find the amount of antigen required to generate a given level of signal saturation,

$$C_{LA0,LF} = \frac{h_{S,LF}(K_{A,S}C_{C0}+1)}{K_{A,S}\left(1-\exp\left(-\left(K_{A,S}C_{C0}+1\right)k_{off,S}t_{LF}\right)\right)} \qquad \text{Equation 3.9}$$

$$C_{LA0,ITP} = \frac{h_{S,ITP}(K_{A,S}C_{C0}+1)}{pK_{A,S}\left(1-\exp\left(-\left(K_{A,S}C_{C0}+1\right)k_{off,S}t_{ITP}\right)\right)} \qquad \text{Equation 3.10}$$

These equations are used to calculate the concentration at the LoD from the signal saturation.

Modeling the LoD of a system based on antibody parameters is difficult, because the definition of LoD in a real system is strongly dependent upon variance of both the blanks and the low positives, which is not captured by this model. We compensate for this with an assumed degree of variance of the blanks and with a specified saturation difference between the LoB_{NI} and LoD_{NI}. The non-specific binding equations return a value of fractional saturation, h, generated by non-specific binding, which we interpret as the average expected non-specific signal normalized intensity. This value is doubled (as shown in equation 3.11 and 3-12) to estimate the LoB_{NI}. This estimation is based upon the results that we have obtained for LF and LID assays that we have tested.

$$LoB_{NI,LF} = 2\times\left(\frac{L_0^*}{L_0^*+1}\left(1-\exp\left(-(L_0^*+1)k_{off,NS}t_{LF}\right)\right)\right) \quad \text{Equation 3.11}$$

$$LoB_{NI,ITP} = 2\times\left(\frac{pL_0^*}{pL_0^*+1}\left(1-\exp\left(-(pL_0^*+1)k_{off,NS}t_{ITP}\right)\right)\right) \quad \text{Equation 3.12}$$

We then estimate that the signal difference between the LoB_{NI} and LoD_{NI} is 5% of the saturated, or maximum, signal. The 5% used here is approximately the difference measured for many experiments the strep 0502 and CT 15174/MAV systems. We can then calculate the concentration at the LoD by substituting LoD_{NI}, which is equal to LoB_{NI}+0.05, in for h_S in equations 3.9 and 3.10. The resulting equations for the LoD or concentration at the LoD ($C_{LA0,LoD}$) for the LF and ITP systems are:

$$LoD_{LF} = C_{LA0,LoD,LF} = \frac{\left(LoB_{NI,LF}+0.05\right)\left(K_{A,S}C_{C0}+1\right)}{K_{A,S}\left(1-\exp\left(-\left(K_{A,S}C_{C0}+1\right)k_{off,S}t_{LF}\right)\right)} \quad \text{Equation 3.13}$$

$$LoD_{ITP} = C_{LA\ ,LoD,ITP} = \frac{\left(LoB_{NI,ITP}+0.05\right)\left(K_{A,S}C_{C0}+1\right)}{pK_{A,S}\left(1-\exp\left(-\left(K_{A,S}C_{C0}+1\right)k_{off,S}t_{IT}\ \right)\right)} \quad \text{Equation 3.14}$$

We investigate the factor of LoD improvement that ITP provides (LoD_{LF}/LoD_{ITP}) in the expected ranges of each variable for general antibody based lateral flow and LID assays. Table 3-1 lists the parameters and the expected range for typical LID and LF assays. These values are selected as realistic parameters that are representative of previously tested systems.

Table 3-1: Dependent parameters for the LoD improvement model and the expected ranges of those parameters.

Parameter	Lower Bound	Upper Bound	Range Selection	Description
C_{C0}	10^{-11} [sites/L]	10^{-7} [sites/L]	High: calculated amount deposited Low: 99.99% washed off or unavailable to bind	Initial binding site concentration
$K_{A,S}$	10^{4} [1/M]	10^{9} [1/M]	High: in the range of igG/igG binding[121,137] Low: poor binding	Specific binding affinity
$K_{A,NS}$	10^{2} [1/M]	10^{6} [1/M]	High: in the range of specific binding[121,137] Low: negligible binding	Non-specific binding affinity
$k_{off,S}$	10^{-6} [1/s]	10^{-3} [1/s]	Expected range for k_{off} values[121,137]	Specific off rate
$k_{off,NS}$	10^{-6} [1/s]	10^{-3} [1/s]	Expected range for k_{off} values[121,137]	Non-specific off rate
C_{L0}	10^{-6} [M]	10^{-5} [M]	Typical loading of 40nm gold label (~0.01-0.1 OD_{540})[138]	Initial label concentration
t_{LF}	300	900	Typical lateral flow time (e.g. QuickVue CT)[139]	LF time over test-line
t_{ITP}	60	600	Expected plug residence time in LID assays	ITP time over test-line
p	100	1000	Observed concentrations factors in previous works[5,45]	ITP concentration factor

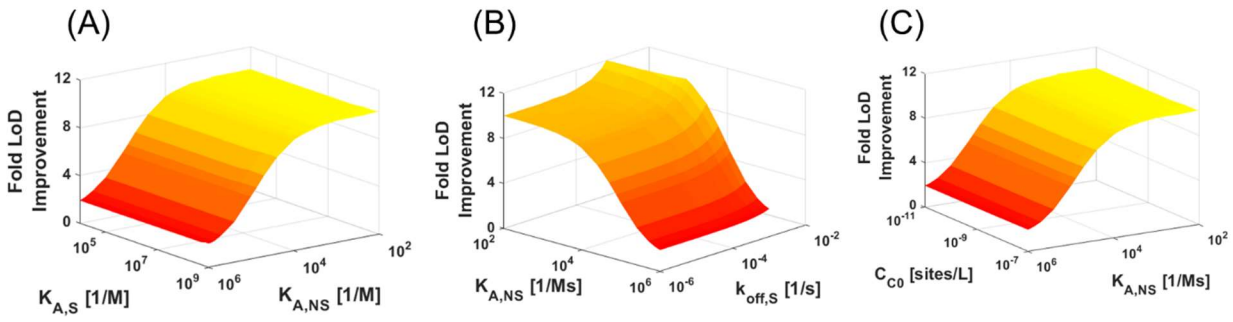

Figure 3-8: Modeled LoD improvement from ITP from $K_{A,NS}$ and factors $K_{A,S}$ (A), $k_{off,S}$ (B), and C_{C0} (C). The model shows no sensitivity to $K_{A,S}$ and C_{C0}. The highest values of $k_{off,S}$ increases the improvement from ITP, due to the shorter time scale of the ITP assay. The other factors are set to: p=100, t_{ITP}=60s, t_{LF}=600s, C_{C0} =10^{-9} sites/L, $K_{A,S}$ =10^7M^{-1}, C_{L0} =10^{-6}M, $k_{off,NS}$ =5x10^{-5}s^{-1}, and $k_{off,S}$ =5x10^{-5}s^{-1}.

The fold LoD improvement from incorporating ITP as a function of $K_{A,NS}$ with $K_{A,S}$ (A), $k_{off,S}$ (B) and C_{C0} (C) are shown in fig. 3-8. Each plot shows a significant drop in improvement at high values of $K_{A,NS}$, and little or no change in improvement with changes in $K_{A,S}$ (A), $k_{off,S}$ (B) and C_{C0} (C). It is somewhat surprising that the $K_{A,S}$ has no impact on the amount of improvement that ITP provides in lowering the LoD. The impact of $K_{A,S}$ is present in the calculated value of LoD for both the LF and ITP systems, but the ratio of these LoDs remains constant. In comparison, $K_{A,NS}$ has a dramatic effect on the improvement gained from ITP. At higher values of $K_{A,NS}$, the improvement from the ITP assay is limited because ITP increases the non-specific signal dramatically, as shown in fig. 3-7. ITP increases the exposure concentration of the label to the test-line, increasing signal resulting from the undesired reaction between the label and capture. The non-specific signal in the ITP assay is sensitive to p, t_{ITP}, C_{L0}, and $K_{A,NS}$. p and t_{ITP} are treated as constant, with values of t_{ITP}=60s and p=100 adequately describing the assays developed for this dissertation. The effect of C_{L0} will be explored later in the section. When the $K_{A,NS}$ of the antibody pair is high, greater than 10^3M^{-1}, there is a non-negligible increase in the non-specific binding in

the ITP assay when compared to the LF assay, with a typical label concentration of 10^{-6}M, as was observed from fig. 3-7. This threshold remains in the full LoD model as systems with a $K_{A,NS}$ of greater than $10^{3}M^{-1}$ sees diminished improvement from ITP because the increase in non-specific signal at high values of $K_{A,NS}$ significantly increases the LoB_{NI}, increasing the LoD_{ITP}, resulting in less improvement. In this analysis, $K_{A,NS}$ is used as the x-axis throughout the simulations presented here.

Figure 3-9 shows the LoD fold improvement as a function of the non-specific binding kinetics: $K_{A,NS}$, $k_{on,NS}$ and $k_{off,NS}$. The non-specific binding parameters of $k_{off,NS}$ and $K_{A,NS}$ appear separately in the model. The effect of these parameters on the LoD improvement are plotted together in fig. 3-9A. When the two factors are high, ITP provides no improvement to the LoD. When either the non-specific affinity ($K_{A,NS}$), or the non-specific off rate ($k_{off,NS}$) are low, the improvement from ITP remains at, or near, the maximum. This plot shows a strong tie between the two factors with high $k_{off,NS}$ and high $K_{A,NS}$ greatly limiting the amount of improvement ITP can provide. Since $K_{A,NS}=k_{on,NS}/k_{off,NS}$, it is possible to isolate each of these factors and remove the interdependence. Figure 3-9B shows how $k_{on,NS}$ and $k_{off,NS}$ each affect the LoD improvement. This plot shows that the LoD improvement does not vary with the $k_{off,NS}$ parameter, but shows a sharp decrease in improvement for $k_{on,NS}$ values greater than $0.5M^{-1}s^{-1}$ When the effect of $k_{off,NS}$ on $K_{A,NS}$ is taken into account, $k_{off,NS}$ has no effect on the LoD. Thus, the sensitivity of the model to non-specific binding kinetics can be isolated to $k_{on,NS}$.

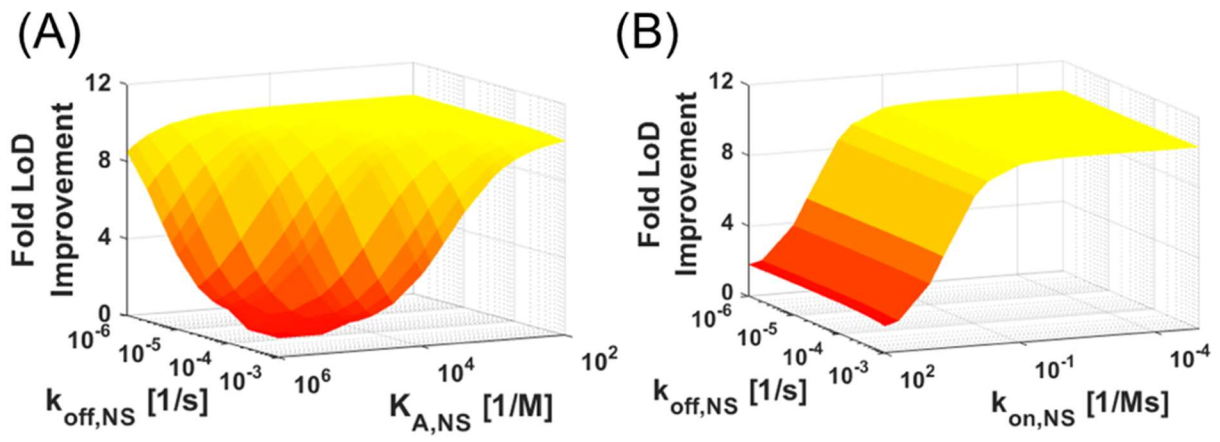

Figure 3-9: Modeled LoD improvement from ITP with varying $K_{A,NS}$ and $k_{off,NS}$ (A) and varying $k_{off,NS}$ and $k_{on,NS}$ (B). The maximum improvement occurs with low NS binding kinetics. The other parameters are set to: p=100, t_{ITP}=60s, t_{LF}=600s, C_{C0} =10^{-9} sites/L, $K_{A,S}$ =$10^{7}M^{-1}$, C_{L0} =10^{-6}M, and $k_{off,S}$ =$5x10^{-5}s^{-1}$.

A secondary and easily controlled factor in the non-specific binding is the loading of label, C_{L0}. We model the effect of the initial concentration of the label, C_{L0}, and the non-specific binding affinity, $K_{A,NS}$, on the LoD improvement from ITP in figure 3-10A. Increasing C_{L0} has a negative effect on the LoD improvement with a stronger negative impact at higher values of $K_{A,NS}$. The label is a reactant in the nonspecific binding reaction and thus increasing the concentration increases the equilibrium nonspecific binding in both the LF and LID assays. Higher label loading increases the LID signal more than the LF one, resulting in lower fold improvement, because of the concentrating effect of ITP. If we combine label concentration, C_{L0}, and the nonspecific reaction rate, $k_{on,NS}$, into a single variable, $L_{on,NS} = C_{L0} \times k_{on,NS}$ we can collapse the dependence of the fold improvement into a single independent variable as shown in fig. 3-10B. The fold improvement shows sigmoidal like behavior with maximum improvement when $L_{on,NS}$<10^{-7} and negative improvement for $L_{on,NS}$>10^{-5} due to the increase in non-specific signal in the ITP system being so severe that the limit of blank is above the signal saturation.

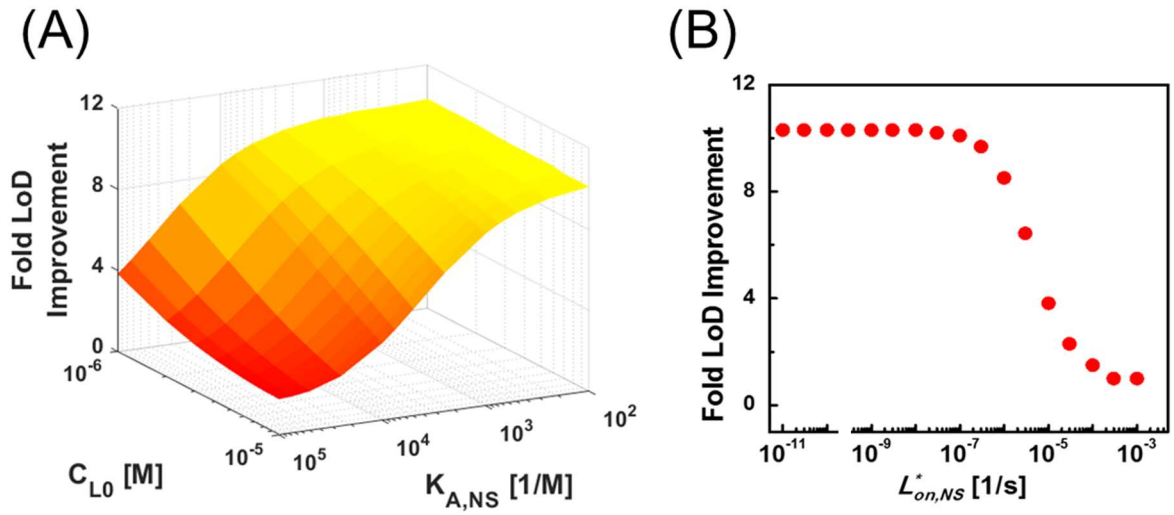

Figure 3-10: Modeled LoD improvement from ITP with varying $K_{A,NS}$ and C_{L0} (A). Increasing the initial label concentration negatively impacts the LoD improvement when $K_{A,NS}$ is not negligible. The factors of C_{L0} and $k_{on,NS}$ can be multiplied to give $L_{on,NS}$ (B). For the maximum improvement from ITP is obtained with an $L_{on,NS}$ of less than 10^{-7}. The other parameters are set to: p=100, t_{ITP}=60s, t_{LF}=600s, C_{C0} =10^{-9} sites/L, $K_{A,S}$ =$10^{7}M^{-1}$, $k_{off,NS}$ =$5x10^{-5}s^{-1}$, and $k_{off,S}$ =$5x10^{-5}s^{-1}$.

It is possible to increase the amount of improvement from a system from the ~10-fold improvement shown in the previous figures. In order to do so, the residence time of the plug, t_{ITP}, or amount of concentration achieved by ITP, p, must be increased. The effect of these two factors on the maximum improvement within the expected antibody parameter ranges, listed in table 3-1, is shown in fig. 3-11. The maximum improvement from ITP scales linearly with increases in p and t_{ITP} reaching 300-fold maximum improvement for p=1,000 and t_{ITP}=180s. These parameters can be increased in real systems by manipulating the other specified values. For example, the concentration factor, p, can be increased by increasing the volume of the petal shape without increasing the test-line width. The residence time of the plug can be increased by decreasing the applied current when the plug is on the test-line. Each of these factors affects the operability of the LID assay as well as increases the sensitivity to non-specific binding, and thus cannot be scaled to infinity in a real system.

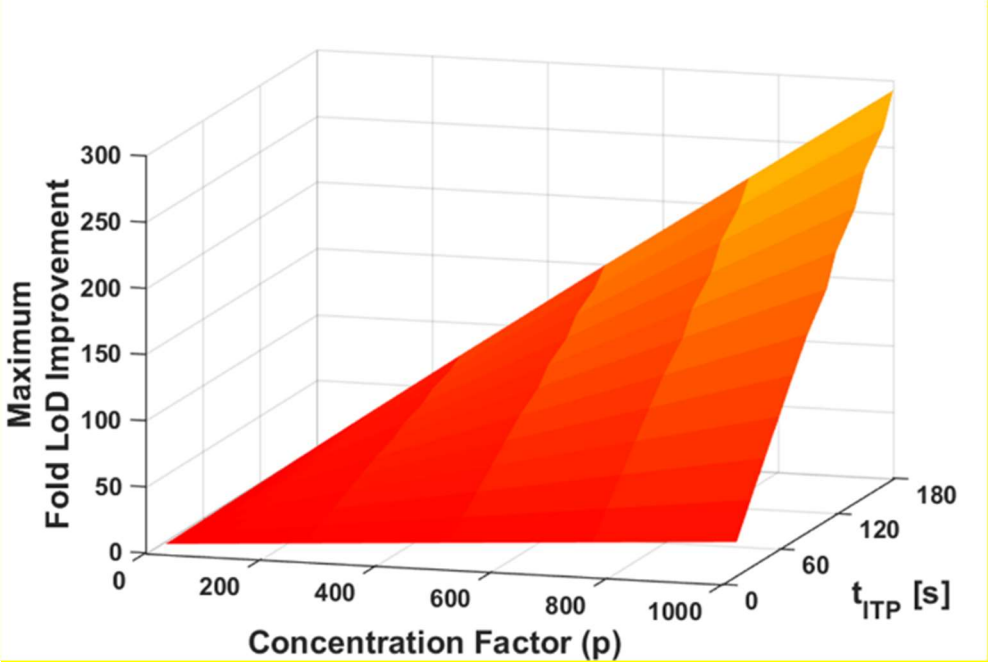

Figure 3-11: Modeled maximum LoD improvement achievable through ITP when compared to a 10-minute lateral flow assay with varying concentration factor (p) and residence time of the ITP plug (t_{ITP}). Because the z-axis is the maximum improvement, this plot is independent of the other factors.

In conclusion, the amount of improvement provided by ITP in comparison to standard lateral flow assays is independent of the specific binding kinetics. Manipulating the operating parameters, t_{ITP}, t_{LF}, p, and C_{L0}, affect the overall improvement generated by ITP. The only antibody parameter that has an effect on LoD improvement is $k_{on,NS}$. This model indicates that within normal operating ranges, ITP provides the maximum improvement for our LID systems when $K_{A,NS}<10^3 M^{-1}$. This value is sensitive to the p and t_{ITP} of the ITP system. This analysis shows the importance of the non-specific reaction in the LID assay. The parameters that most strongly impact the fold improvement by LID are the concentration of the label, the concentration factor, the reaction times, and the nonspecific reaction rate. C_{L0} and p are the parameters that dictate the concentration of the label, the reactant in the non-specific reaction. t_{ITP} controls the amount of time that the non-specific reaction has to occur, and $k_{on,NS}$ is the rate at which this undesirable

reaction occurs. Each of these parameters affect the non-specific reaction, and thus the non-specific signal generation. Non-specific signal generation increases the LoB_{NI}, which increases the LoD. When determining if ITP is appropriate for improving a lateral flow system, it is important to investigate the non-specific binding of the antibody pair.

3.3.2 *Experimental determination of non-specific binding*

There are many available methods for investigating antibody binding. The most sensitive techniques are oblique-incidence reflectivity difference and surface plasmon resonance.[121,140,141] These techniques use antibodies bound to gold plated flow cells and are capable of determining the kinetics of antibody binding. We have enzyme-linked immunosorbent assays (ELISA) which is able determine the equilibrium binding coefficient for the non-specific binding, $K_{A,NS}$. The $k_{on,NS}$ and $k_{off,NS}$ are determined through lateral flow assays.[142,143]

We determine the non-specific equilibrium affinity constant with ELISA assays with varying capture and label antibody concentrations. The equation for determining $K_{A,NS}$ via this method is: $K_{A,NS} = \frac{\frac{C_1}{C_2}-1}{\frac{C_1}{C_2}(L_2-L_1)}$, where C_1 is the higher capture antibody concentration immobilized in the ELISA well, C_2 is the lesser capture antibody concentration, L_1 is the label concentration that generates 50% saturation in C_1 capture wells, and L_2 is the label concentration that generates 50% saturation in C_2 capture wells.[144,145] C_1 and C_2 are arbitrary, but should be disparate enough to generate differentiable signal. We use 2 ug/mL for C_1 and 1 ug/mL for C_2. Figure 3-12 shows the non-specific ELISA results from 3 different antibody pairs: the high performing 0803 strep pair, the 15174/MAV CT pair that demonstrated moderate improvement, and the 6701/6709 that had low performance in the LID format. The $K_{A,NS}$ for 6701/6709 extracted from these results is

$K_{A,NS} = \frac{\frac{2}{1}-1}{\frac{2}{1}(2.3\times10^{-6}-1.3\times10^{-6})} = 5\times10^{5}[1/\mathrm{M}]$. Unfortunately, the 50% saturation point for the 0803 and 15174/MAV systems is above the range achievable with the initial label concentration, thus needs to be estimated. The 50% saturation value, or half max, for the 15174/MAV system can be extrapolated from the available data to give a rough value for the $K_{A,NS}$, and by assuming the same saturation point (absorbance of ~0.6) we determine that the $K_{A,NS}$ for the 15174/MAV system is on the order of magnitude of 10^4[1/M]. The self-pairing 0803 strep system does not show any increase in signal from increasing label concentration over the range tested, thus, it is appropriate to assume that the $K_{A,NS}$ for this system is less than 10^3[1/M], placing it in the range where the increase in non-specific signal from ITP is negligible based upon the model, with a concentration factor of ~100 and plug residence time of ~60s, as shown in figs. 3.7 and 3.8.

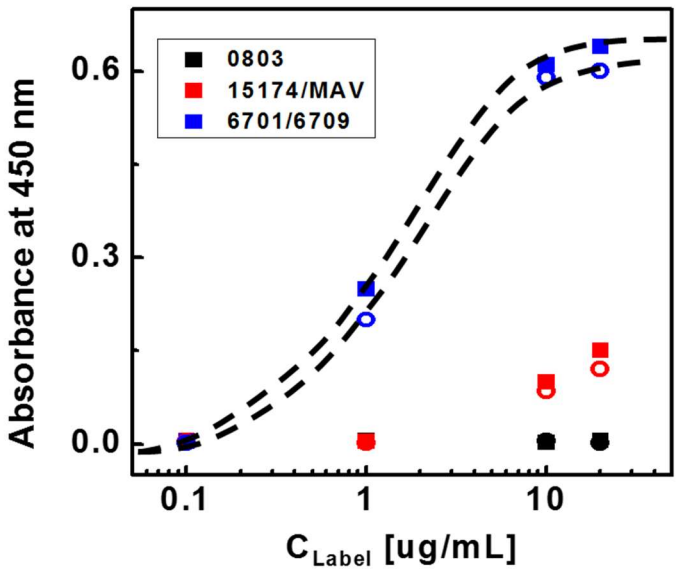

Figure 3-12: Experimental non-specific signal generation ELISA results for 3 different antibody pairs. Each system is tested using wells coated with 1 ug/mL of capture antibody (open circles) and 2 ug/mL of capture antibody (filled squares). The dashed lines are guides for the eye for the results from the 6701/6709 pair.

For the typical values of the parameters of t_{ITP}, p, and C_{L0} of the LID assays in this dissertation, the model predicts that the kinetic rates, $k_{on,NS}$ and $k_{off,NS}$, affect the fold improvement for systems with $K_{A,NS}$ of $10^3 M^{-1}$ or greater (fig. 3-9A). In this case, it is valuable to investigate the binding kinetic values, $k_{on,NS}$ and $k_{off,NS}$, in addition to the equilibrium value, $K_{A,NS}$. We use the model to extract $k_{off,NS}$ from lateral flow assays with varied label concentrations. Figure 3-13 shows the dependence of non-specific signal generation on flow time in a lateral flow assay at two different concentrations for 6701/6709. The $k_{off,NS}$ obtained from fitting fig. 3-13 with equation 3.3 for is $\sim 10^{-6}$ [1/s]. Multiplying $K_{A,NS}$ by $k_{off,NS}$ gives a $k_{on,NS}$ of 0.5 [1/Ms]. This places the 6701/6709 system in the range where the improvement provided by ITP is limited as shown in fig. 3.9B.

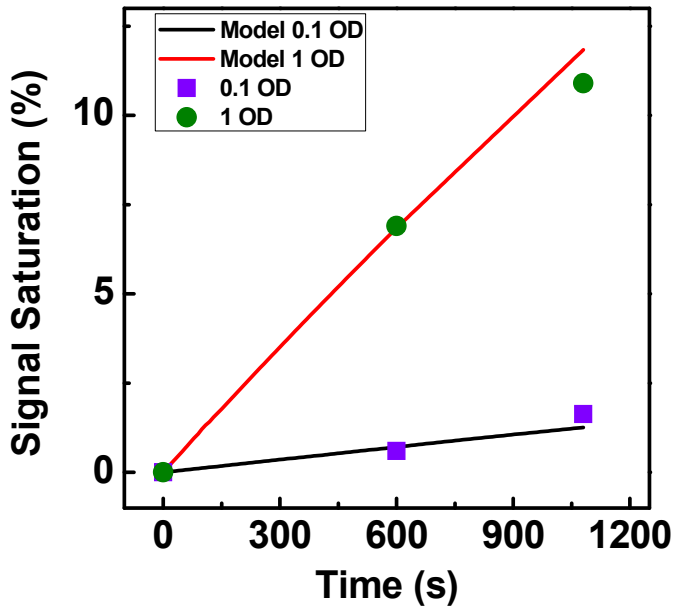

Figure 3-13: Experimental lateral flow non-specific signal generation for 6701/6709. The results are fit to equation 3.3. Data is obtained at 0, 5 and 10 minutes with conjugated gold loading of 0.1 and 1 O.D ($\approx 10^5$ and 10^4 M).

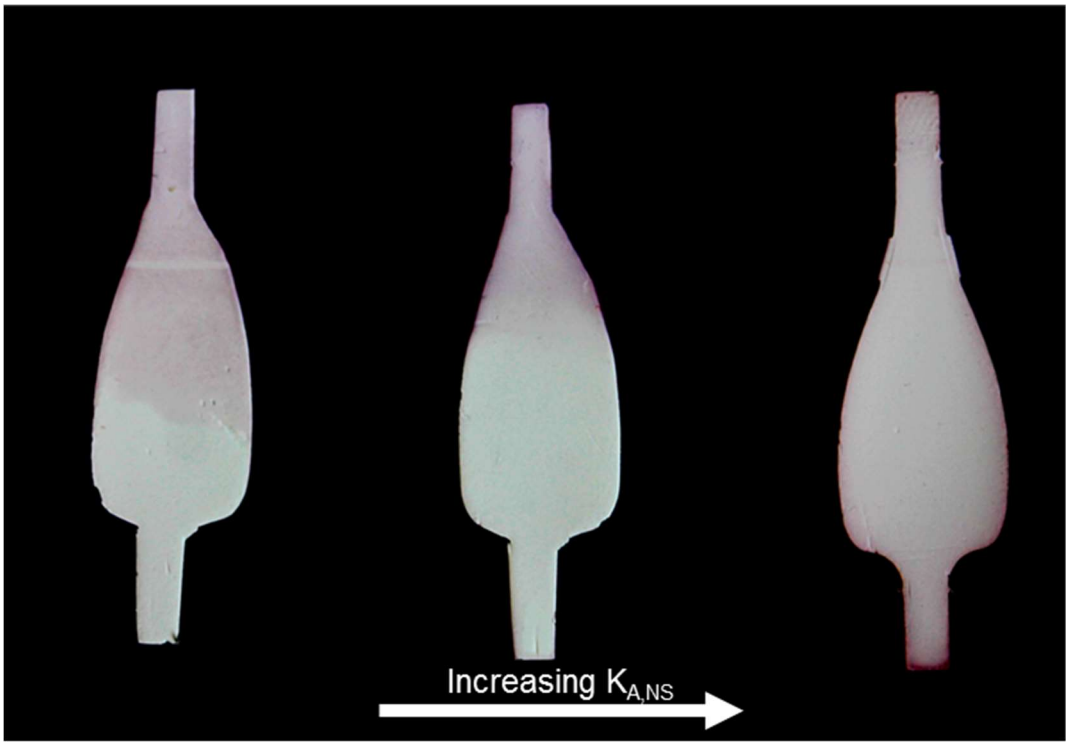

Figure 3-14: Increased contrast image of high label loading antigen-free lateral flow assays. The left-most strip is the 0803 strep system, the center strip is the 15174/MAV chlamydia system, and the right-most strip is the 6701/6709 chlamydia system. The left strip has an inverted signal indicating a stronger affinity for adsorption of the label onto the nitrocellulose than for non-specific binding onto the test-line. The center strip shows no test-line indicating a similar affinity for adsorption to the nitrocellulose and non-specific binding to the test-line. The right strip has signal indicating a stronger affinity for non-specific binding of the label to the test-line than adsorption onto the nitrocellulose.

For quick screening, or early indication of NS signal generation, blank tests with high label loading in the lateral flow format can be used. Figure 3-14 is an image of lateral flow assays run for 10 minutes with 1 O.D. of conjugated gold added to the system, with no target. The strep antibody pair 0803 with low $K_{A,NS}$ (left) shows an inverted signal on the test-line due to stronger adsorption onto the nitrocellulose membrane when compared to the binding to the test-line. As the $K_{A,NS}$ increases, the inverted signal disappears, as in the middle image for 15174/MAV, and a positive signal is generated, as shown in the right-most image of fig.3-14 for the 6701/6709

antibody pair. Based on experience, any pair that creates this inverted signal is a good candidate for ITP improvement. As the signal generated in this blank test increases, it becomes less likely that ITP will provide significant improvement in LoD.

3.4 Optimizing assay performance in clean solutions

In this section, we present the performance results obtained for the streptococcus pyogenes and chlamydia trachomatis lateral flow enhanced by isotachophoresis diagnostic (LID) assays. These results are obtained in buffer with purified bacteria cells and are compared to commercial lateral flow tests under the same conditions.

3.4.1 *Streptococcus pyogenes*

For the final optimized chemistry testing of the streptococcus pyogenes assay, we use both the rectangular shaped devices and a novel, petal-shape in the LID device. The analytical sensitivity and LoD of these assays are compared to a commercially available strep assay, BD Chek. The petal-shaped devices enable a larger mass of target to be focused to the test line. Figure 3-15 shows the development of an ITP plug on a petal-shaped device. The visible ITP plug is a dark line of focused gold nanoparticles conjugated to rabbit-anti-strep antibodies. The ITP plug forms at the interface of the TE, on the left-hand side of the plug, and the LE on the right-hand side of the plug. The focused plug initially forms with a strong curvature in the widest part of the paper, as shown in figure 3-15i. The curvature is due to the expansion of the electric field lines that results from the paper geometry. The plug curvature is tangential to the electric field lines, resulting in a curved shape.[146] As the plug moves downstream, it accumulates more labeled target, increasing in concentration and darkness, visible in figures 3-15ii-iii. The plug straightens as it moves downstream from the TE reservoir as the width of the paper decreases and the electric field

lines become parallel. When the plug reaches the test line, we decrease the current to slow the plug and increase the time for the target to bind to the patterned capture line, as shown in figure 3-15iv. A significant fraction of the labeled target binds to the test line and the remaining uncaptured gold migrates past the test line toward the LE reservoir.

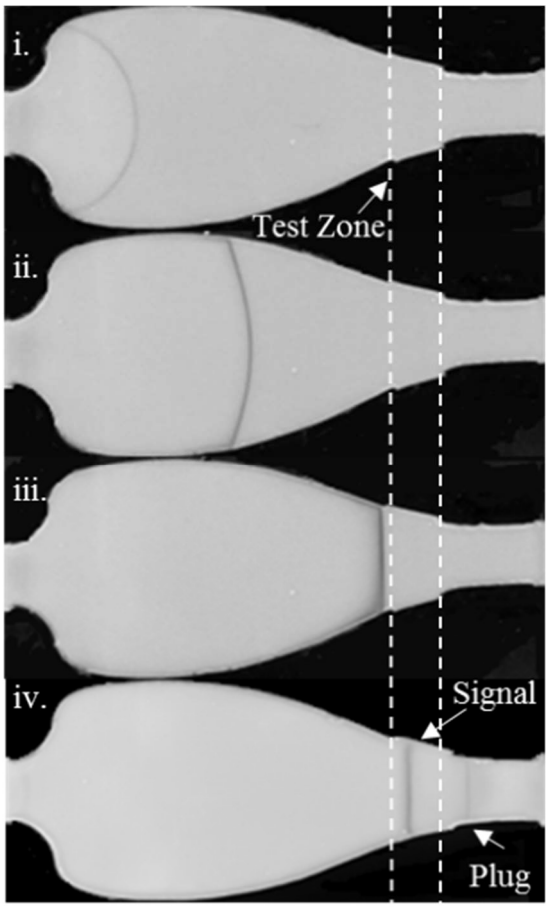

Figure 3-15: Experimental snapshots taken at 4 different times showing ITP-focused gold nanoparticles. The plug increases in concentration of gold and decreases in curvature as the plug moves downstream (i-iii). The labeled nanoparticles that are bound to the target proteins which then bind to the test line showing a positive result (iv).

Figure 3-16 shows the test lines for the commercial lateral flow assay as well as the strip and petal-shaped LID tests for three concentrations: $6x10^3$, $6.8x10^5$, and $2.5x10^6$ CFU/mL. At the highest concentration shown ($2.5x10^6$ CFU/mL), all three tests show dark lines that are clearly

positive. At $6.8x10^5$ CFU/mL, the commercial test line is just barely visible with both of the ITP assays showing strong positives. The bottom row of images, at $6x10^3$ CFU/mL, is conducted at concentrations below the commercial test's published LoD. The commercial test and the standard shaped LID assay do not show any visible line, but the petal shaped LID assay did show a positive result that can easily be seen by the naked eye. These images provide qualitative evidence that ITP improves the analytical sensitivity and LoD compared to standard lateral flow technology.

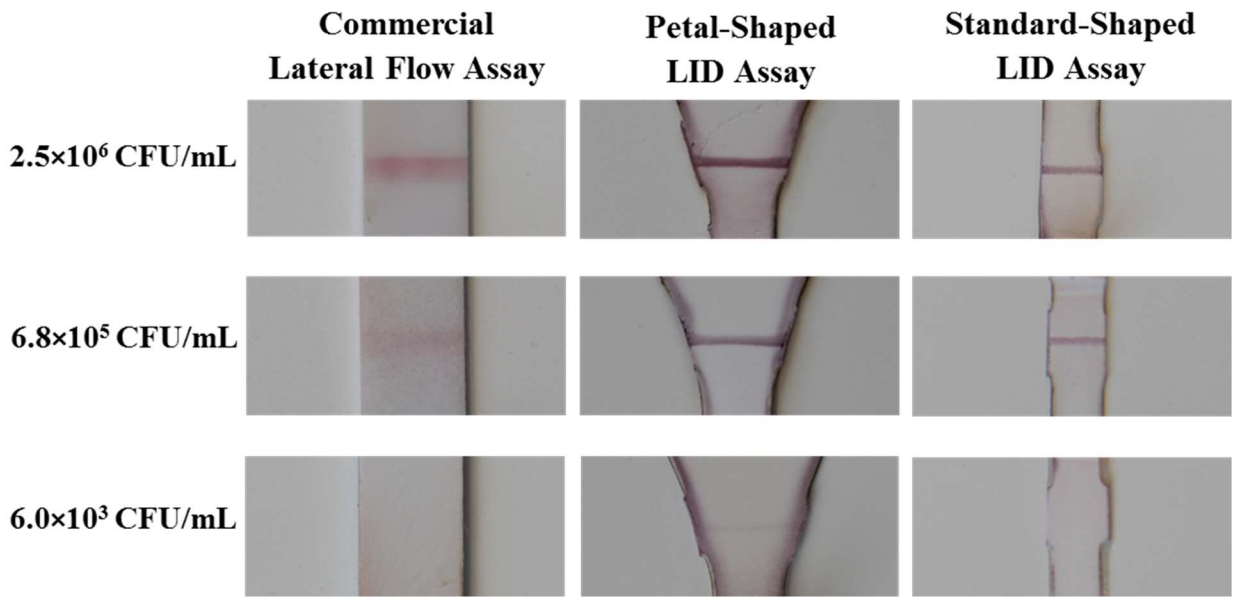

Figure 3-16: Qualitative detection of commercial LF assay (left) compared to petal-shaped LID assay (middle) and standard-shaped LID assay (right). Initial concentrations, from top to bottom, are: 2.5E6, 6E5, and 6E3 CFU/mL. At the highest concentration (2,500,000 CFU/mL) all tests show a strong positive. And at the middle concentration (680,000 CFU/mL), the commercial test gives a faint positive, as opposed to the strong positive seen with both the LID tests. At the lowest concentration (6,000 CFU/mL), only the signal from the petal-shaped LID assay is above the LoD, with a line visible to the naked eye.

Figure 3-17 shows a plot of the normalized intensity as a function of the streptococcus cell concentration for the commercial lateral flow assay as well as the strip and petal shaped LID tests. Figure 3-17's inset shows the same data, but for a larger range of concentrations, up to $75x10^4$.

The error bars show $c_\beta \times \sigma$, which represents the 95% one-tailed confidence interval. For each assay, the NI increases linearly with GAS cell concentration. The slope of the line represents the analytical sensitivity. In the concentration range that we tested, each assay exhibited linear response with adjusted R^2 values >0.98. The petal-shaped devices exhibit the greatest sensitivity of $3x10^{-6}$ NI/C_{strep} compared to $9x10^{-7}$ NI/C_{strep} and $4x10^{-8}$ NI/C_{strep} for the straight LID and commercial tests, respectively. This data shows that the straight and tear-drop LID devices have a respective increase in analytical sensitivity of 22.5x and 75x when compared to the commercial test. The range for the confidence interval of the commercial lateral flow devices is larger and increases more rapidly than the LID devices suggesting that the LID devices exhibit less variability.

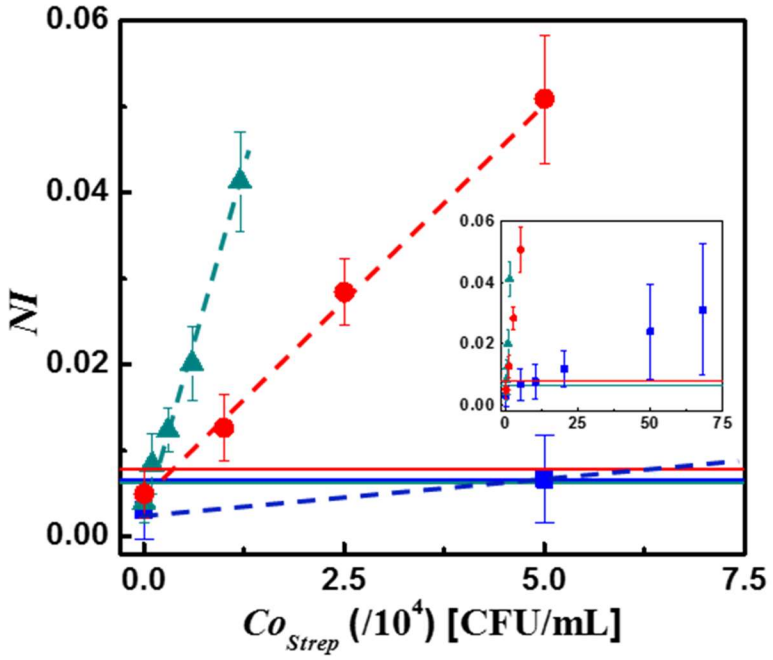

Figure 3-17: Experimental data showing quantitative detection of strep A proteins using ITP. The petal-shape (green triangles) shows a significant improvement over the ITP on standard strips (red circles) which is significantly better than the commercial test (blue squares). The solid lines are the calculated LoB_{NI} values corresponding to a 95% confidence interval. The inset shows a larger range of concentrations past the limit of detection for the commercial assay.

Table 3-2 shows the NI values associated with the LoB_{NI} and the LoD_{NI} for the commercial LFA as well as the strip and petal-shaped LID devices. The blank commercial devices are consistent, with low standard deviation. However, the positive sample standard deviation is large and grows dramatically as the concentration increases. This results in the largest LoD_{NI} for the commercial assay in comparison to the LID assays. The standard-shaped devices have the highest LoB_{NI} but lower sample standard deviation than the commercial test, giving a LoD_{NI} that is slightly lower than the commercial devices. The petal-shaped devices are the most consistent (lowest standard deviations of blank and samples) and, as a result, have the lowest values of LoD_{NI} and LoB_{NI}. The LoB_{NI} for each assay are plotted as horizontal lines in figure 3-17.

Table 3-2. Experimentally measured LoD in normalized intensity and concentration. The LID assays have significantly higher analytical sensitivity, resulting in a lower LoD.

Assay Type	LoB_{NI}	σ_s	c_β	LoD_{NI}	Analytical Sensitivity [NI/C_{Strep}]	LoD [CFU/mL]	Fold Improvement of Detection Limit
LF-Commercial	0.0066	0.0033	1.662	0.012	$4x10^{-8}$	$2.0x10^5$	—
LID-Standard	0.0078	0.0023	1.671	0.0116	$9x10^{-7}$	$9.1x10^3$	22
LID-Petal	0.0063	0.0021	1.662	0.0098	$3x10^{-6}$	$1.9x10^3$	105

We used a linear fit through the averages to obtain estimates for NI values for untested concentrations within our data. Using these fits, we calculate the LoD for each assay and provide the values in table 3-2. This data shows that the commercial test LoD is $2.1x10^5$ CFU/mL, which is in agreement with the value of LoD published by the FDA of $2.5 x10^5$ CFU/mL.[81] Since the slope of the petal shaped LID assay's linear fit is significantly greater than that of the commercial assay, the relatively close values of line intensity at the LoD for the LID and LF assays result in

orders of magnitude difference in LoD concentration. The straight and petal-shaped LID assays show LoDs of $9.1x10^3$ and $1.9x10^3$ CFU/mL respectively. This data shows that integration of ITP in petal-shaped devices improves the LoD when compared to the commercially available device. We attribute the improvement in signal strength from LID devices to the preconcentration provided by ITP in addition to the increased exposure of the test-line to the target due to the initial flow over the test-line followed by ITP creating a second pass over the test-line. The straight shaped device shows a 20x lower LoD than the commercial device because of this electrokinetic preconcentration. In addition, by modifying the device shape to increase the amount of target that passes over the test line, we lower the LoD by an additional ~5x, resulting in a 105x overall improvement in LoD.

3.4.2 *Chlamydia trachomatis*

We demonstrated that the LID format is capable of improving the limit-of-detection over a commercial lateral flow assay for an infectious disease, i.e. streptococcus pyogenes. In this work, we modify the chemistry of the LID assay that we developed for streptococcus to detect chlamydia trachomatis (CT). Utilizing the same definition and process as the assessment for the streptococcus assay, we compared our assay to a commercially available lateral flow assay (QuickVue by Quidel, San Diego, CA). QuickVue is one of the few commercial lateral flow assays for CT exist. However, this assay has been reported to have a sensitivity as low as 25%.[147]

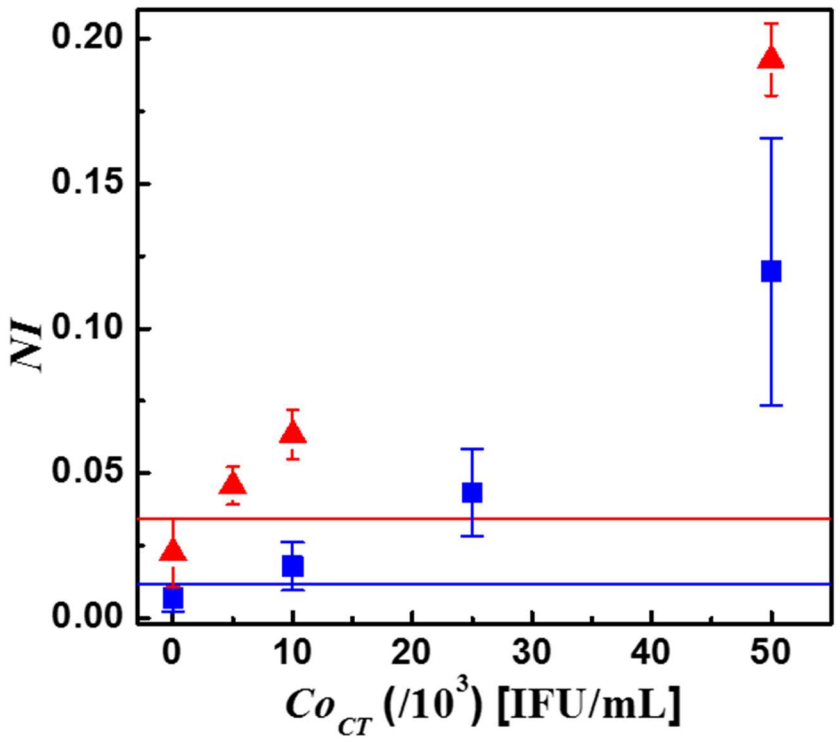

Figure 3-18: Experimental results of the normalized signal response (NI) from the 15174/MAV LID system (red triangles) and the commercial lateral flow assay (black squares). The error bars are the 95% one-tailed confidence interval of the 5 or more replicates. The horizontal lines indicate the LoB_{NI} for each assay.

We obtain the test response of our 15174/MAV LID assay and the commercial LF assay to CT bacterial loading, shown in fig. 3-18. The error bars show $c_\beta \times \sigma$, which represents the 95% one-tailed confidence interval. For each assay, the NI increases roughly linearly with CT cell concentration. The slope of the line represents the analytical sensitivity. The solid horizontal lines mark the LoB_{NI} for the commercial (blue) and LID (red) assays. The data shows that the LID assay results in stronger test line signals, including the blank. The blank signal should ideally be as low as possible, which is a problem for our assay. When working with antibody pairs that demonstrate an affinity for each other in the absence of antigen, isotachophoresis increases the intensity of the non-specific signal, when compared to lateral flow. The limit of detection was

established for the LID assay as well as the commercial assay, which target the LPS membrane fragment. We found the limit of detection of the commercial lateral flow assay to be 12,100 IFU/mL. This is in agreement with the reported value of 13,000 IFU/mL.[139] However, our assay still demonstrates roughly a 3-fold improvement in limit-of-detection over the commercial assay, with an LoD of 4,200 IFU/mL.

As a result of the limited improvement of the LoD for the CT assay, we were motivated to find a new pair of antibodies to use in the LID assay. The data shows strong non-specific binding that we hope to reduce using an antibody screening. Seven additional antibodies were screened (HM032, HM031, HM215, 6709, 6701, HM 406, and HM407), all of which target the chlamydia trachomatis LPS. The first step in analyzing the potential of an antibody pair in a LID assay is to ensure that the antibodies target complimentary sites on the antigen with limited non-specific binding between the two antibodies. We designed an ELISA screening survey that investigates the affinity of the antibodies in the direct ELISA format, as well as the signal generation of potential antibody pairs in the sandwich ELISA format. Direct ELISA uses wells coated with the antigen, lysed CT cells in this case, with label antibodies added to investigate the binding between the label antibody and the antigen. It is possible to obtain the equilibrium affinity for the label-antigen reaction through this method. Sandwich ELISA uses wells coated with a capture antibody with antigen, lysed CT, added to the well then label antibody added after. The sandwich ELISA format is used to investigate the formation of the specific signal generating complex of capture antibody-antigen-label antibody as well as the non-specific signal generating complex of capture antibody-label antibody. This method gives information about the compatibility in the sandwich format of the capture and label antibody pair as well as non-specific binding affinities of the antibody pair.

We assess the potential of the binding of the antibodies in the LID format by using a fixed LE ITP chemistry with 50mM NaOH, 100mM bis-tris, 100mM HCl, 0.5wt% PVP, and 0.025wt% Triton-X at pH 6.9. This chemistry is functional as an LE on nitrocellulose and has a pH and IS in the biological range. This chemistry is the result of diluting the NaOH extraction solution by 4x in order to create the final sample buffer.

For the direct ELISA, the negative wells are blocked overnight at 4°C with the blocking solution, 1% bovine serum albumin (BSA) in phosphate buffered saline with 0.05% tween-20 (PBST). The positive wells were coated overnight at 4°C with a solution of $1x10^7$ CFU/mL chlamydia trachomatis in 50mM Na_2CO_3. The carbonate increases the pH above 9.5, which is able to lyse the chlamydia cells, releasing the LPS. The wells coated in CT are blocked for 30 minutes with the blocking solution the following morning.

To test the binding of the direct ELISA, a 2 ug/mL solution of horse radish peroxidase (HRP)-labeled antibody in the sample buffer is added to the BSA blocked wells and CT coated wells and allowed to equilibrate for one hour. After washing, the substrate, 3,3',5,5'-tetramethylbenzidine (TMB), is added to the well and allowed to react with the HRP until there is strong differentiation between the CT coated and antigen-free wells. This typically takes less than 10 minutes. If no differentiation appears, the plate is considered invalid, and requires retesting. The reaction is stopped with the addition of a strong acid (0.4N H_2SO_4) before the absorbance at 450nm of each well is measured using a plate reader.

For the sandwich ELISA format, a 2 ug/mL solution of the capture antibody in 100mM Na_2CO_3 is left at 4°C overnight to coat the well. The next day, the wells are blocked using the same blocking formulation as the direct wells before adding the sample solution with 50,000 CFU/mL CT for the positive, and sample solution with no CT for the negative wells. The antigen

(or clean solution for the negatives) is allowed to react with the immobilized antibody on the surface for one hour. After washing with PBST, a 2 ug/mL solution of HRP-labeled antibody in the sample buffer is added and reacted for 45 minutes. Then, the substrate and stop solution are added to match the direct wells. Again, the results are obtained by a plate reader.

Capture Antibody \ Label Antibody	1. QED	2. HM032	3. HM031	4. HM215	5. MAV	6. 6709	7. 6701	8. HM406	9. HM407
1. QED		1.08	**1.35**	1.18	1.11	1.07	1.07	0.62	1.06
2. HM032	1.05		0.98	1.17	**1.48**	1.12	0.71	1.08	1
3. HM031	1.17	0.85		1.08	1.2	1.14	**1.93**	1.22	1.08
4. HM215	1.01	1.05	0.98		1.03	0.93	0.97	1.2	1.08
5. MAV	1.04	1.23	0.61	**1.64**		0.86	0.63	0.61	1.13
6. 6709	1.1	0.93	**1.38**	0.92	0.42		0.56	1.23	1.05
7. 6701	1.04	0.65	1.15	0.96	**1.31**	**1.39**		1.29	**1.38**
8. HM406	0.95	0.99	0.85	1.1	**1.29**	1.18	**1.64**		1.15
9. HM407	1.2	1.09	0.72	**1.7**	1.21	1.05	0.73	0.84	

Figure 3-19: Experimental positive/negative ELISA results of different capture and label pairs. The result displayed is the average absorbance of 4 constant loading positive wells divided by the average absorbance of 4 negative wells. The numbers in bold are potential candidates that have an absorbance ratio of at least 1.3.

For each ELISA plate, results were obtained for a single label antibody, with each potential capture pairing tested. To investigate the relative affinity of the label for the antigen, direct ELISA wells are included in each plate. Direct ELISA for the MAV antibody are included on each plate as a point of comparison and are used to standardize the results between plates. This allows us to determine the best capture antibody to pair with the label based on equilibrium binding, as well as some indication of performance when comparing different labels.

We analyze the results in three different ways: the ratio of positive to negative sandwich wells, the difference between positive and negative wells, and the difference between the negative

signal of sandwich assays and the direct standard negative well. This was done to only find pairs that generate high positive signal and low negative signal. Pairs that have low positive signal and extremely low negative signal are undesirable, but may show high signal ratios. On the other hand, a system with a high negative and extremely high positive is also undesirable, but may show high signal difference. By looking at the signals in different ways, we are able to isolate the pairs that demonstrate the desired performance. We also analyze the negative direct wells to ensure that the improvement from ITP will not be limited by non-specific binding of the antibody pair, as discussed in section 3.3.

Capture Antibody \ Label Antibody	1. QED	2. HM032	3. HM031	4. HM215	5. MAV	6. 6709	7. 6701	8. HM406	9. HM407
1. QED		7.5	**46.4**	20.6	17.7	11.5	5.1	-52.8	10.2
2. HM032	12.7		-3.6	19.3	**67.9**	16.7	-18	6.9	0.58
3. HM031	**49.5**	-18.8		9.5	28.7	18	35.8	18	10.4
4. HM215	3.6	5.1	-2.3		4.3	-10	-2	18.8	11.6
5. MAV	15.5	22.6	-71.8	**85.1**		-36.6	-67.8	-124	24.3
6. 6709	34.3	-8.5	**65.8**	-13.6	-151		-53.7	30.2	6.6
7. 6701	14.8	-61.8	16.8	-5.7	**47**	**60.2**		**57.1**	**41.5**
8. HM406	-18.5	-1	-25.7	13.2	**44.6**	23.9	**43**		17.5
9. HM407	**44.9**	7.9	-51.3	**76**	26.7	6.7	-23.3	-32	

Figure 3-20: Experimental positive-negative ELISA results of different capture and label pairs. The result displayed is the average absorbance of 4 constant loading positive wells minus the average absorbance of 4 negative wells. The numbers in bold are potential candidates that have an absorbance difference of at least 40. The absorbance numbers are scaled by a factor of 100.

Figure 3-19 shows the ratio of positive to negative wells for each of the sandwich ELISA pairs. Any values that are below 1 indicate incompatibility of capture and label antibody. Either the non-specific binding between the capture and label binding is more significant than the specific binding in the presence of antigen, or the antibodies are incompatible as a result of competition for

the same binding site on the antigen. These pairs are eliminated from consideration. Figure 3-20 shows the difference in intensity of the positive and negative wells, with the results scaled to the response of the direct standard ELISA. Although the information gained from reformatting the response is similar, the response difference is less sensitive to slight changes in low negative signal. Figure 3-21 shows the negative wells of each sandwich ELISA minus the negative signal generated by the direct standard for the respective plate. This is important because, even if a pair generates a much stronger positive signal that negative signal, the LID assay will have poor performance if high negative signal generation occurs. Using the information obtained from the ELISA screening, four antibodies were selected to be tested as a label in the lateral flow format: HM215, HM407, 6709, and MAV.

Capture Antibody \ Label Antibody	1. QED	2. HM032	3. HM031	4. HM215	5. MAV	6. 6709	7. 6701	8. HM406	9. HM407
1. QED		0.112	0.218	0.115	0.252	0.304	0.0206	0.119	0.245
2. HM032	0.304		0.356	0.11	0.2	0.256	0.0119	0.0175	0.192
3. HM031	0.327	0.162		0.126	0.206	0.224	-0.0394	0.0056	0.18
4. HM215	0.334	0.116	0.264		0.248	0.247	0.0187	0.031	0.203
5. MAV	**0.413**	0.112	0.348	0.156		**0.594**	0.0372	**0.486**	0.286
6. 6709	0.386	0.164	0.282	0.219	**0.469**		0.0225	0.106	0.167
7. 6701	0.393	0.255	0.22	0.164	0.222	0.292		0.232	0.125
8. HM406	**0.404**	0.176	0.292	0.146	0.227	0.24	-0.0363		0.149
9. HM407	0.256	0.0784	0.338	0.107	0.163	0.239	-0.0024	0.239	

Figure 3-21: Experimental negative well ELISA results of different capture and label pairs. The result displayed is the average absorbance of the average absorbance of 4 negative wells minus to the average absorbance of the standardizing direct ELISA negative wells. The numbers in bold are removed as potential candidates because have an increased negative absorbance of at least 0.4, indicating significant non-specific binding.

Next, the potential pairs are tested in the lateral flow format. Each label antibody was tested with each capture antibody that displayed functionality as a pair in the ELISA screening.

The four label antibodies were linked to Alexafluor 488 using a Pierce labeling kit. In a similar fashion to the pH and IS screenings, the tests were completed by wetting the petal-shaped strips until the nitrocellulose was completely filled. To quantify the results, the test line and surrounding area is y-averaged (similar to the gold quantification, section 2.1, with a positive peak value as opposed to a negative peak) then the average intensity of the test-line is subtracted from the background to obtain the signal intensity. The chemistry used in this testing matches the sample chemistry used in the ELISA screening. Each pair was tested at CT cell loadings of 0, 50,000, and 100,000 IFU/mL with three replicates. Figure 3-22 displays the average fluorescent intensity of the lateral flow test line for the given pair at each concentration. The expected result for a promising pair is that the signal will increase with increasing concentration, with the response from the negative test as close to 0 as possible. Most pairs show an increase in signal with increasing loading, with the exception of the pairs 407/215 and 406/215. These 2 pairs were eliminated from consideration. Of the remaining pairs, HM406/HM407 and 6701/6709 were selected to test in the LID format. HM406/HM407 was selected based upon the low signal generated by the blank tests, and 6701/6709 was selected for the strong differentiation between positive and negative. The two selected pairs were tested in the LID format using the sample chemistry of 50mM NaOH, 100mM bis-tris, 100mM HCl, 0.5wt% PVP, and 0.025wt% Triton-X as the LE and a TE of 40mM bis-tris, 40mM tricine, and 0.025wt% detergent.

The 6701/6709 system generated significant non-specific signal when the highly-concentrated plug passes over the test-line. We attempted to limit this non-specific binding by minimizing the quantity of label present in the sample, C_{L0}. However, the non-specific binding could not be sufficiently limited to consistently differentiate between blanks and positives with a loading of 10,000 IFU/mL. 10,000 IFU/mL was selected as the loading for positive tests as it is

below the limit of detection for the commercial lateral flow test, and this loading showed strong differentiation from the negative with the 15174/MAV pair. We found that this pair has a LoB_{NI} of 15-20% of the saturated signal, which is significantly higher than the LoB_{NI} of <1% of the saturated signal for the high performance strep assay. We estimate that the LoD of this antibody pair in the LID format is on the order of magnitude of 100,000 IFU/mL.

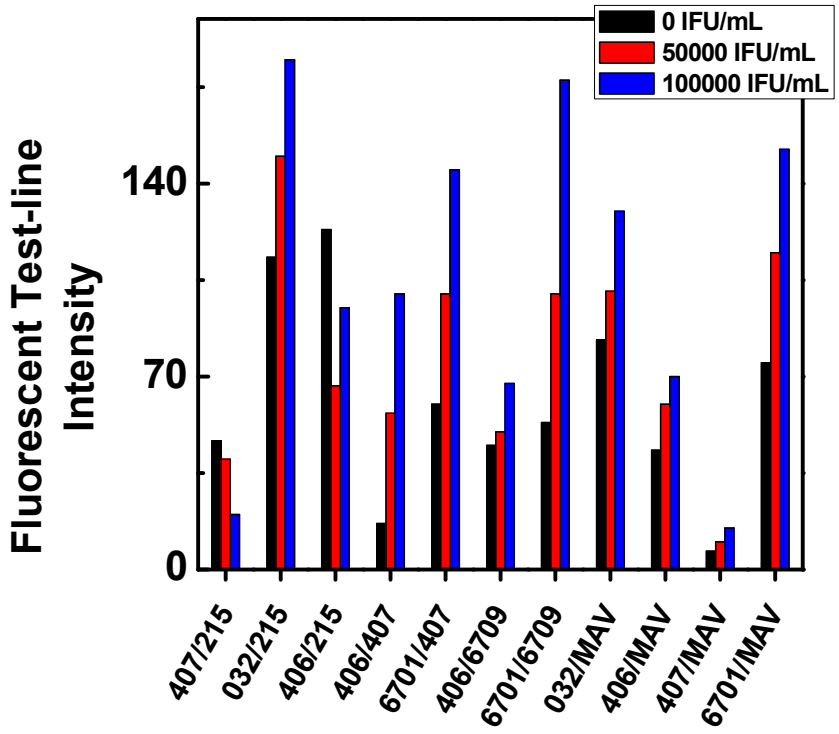

Figure 3-22: Experimental test-line intensities of a fluorescent probe obtained by subtracting the background fluorescent intensity from the average intensity of the test-line. Each bar is the average of two fixed volume lateral flow assays from two identically prepared solutions.

The 406/407 system appeared promising, with the low response from the blank lateral flow assay transferring to the LID assay as expected. Further testing of this system revealed that the positive response in the LID format of this pair is inconsistent (e.g. lower response from 10,000 than 2,500 IFU/mL). The cause of this inconsistency is not readily evident, but is also apparent in

the pH and IS screenings (figs. 3-1 and 3-2). We believe this variance is linked to the lower binding rate of the antibodies to the antigen (based on the lower response from the lateral flow tests) causing more sensitivity to factors such as residence time or heating. It could also be a result of observed sensitivity to slight changes in the pH or ionic strength during the binding. The response of this assay varied so strongly from day to day that we are unable to estimate the LoD of this pair in the LID format.

It is my assessment that none of these pairs are well suited for enhancement from ITP, due to the high non-specific signal generation of the 6701/6709 pair and the inconsistency of the 406/407 pair. In order to achieve a greater than 3-fold improvement in LoD, a robust and sensitive antibody pair needs to be found. This would require a new antibody screening. It is possible that shifting the target from LPS (perhaps to the major outer membrane protein) could be advantageous.

A challenge for the development of LID assays is the inability of matching standard antibody binding conditions (e.g. phosphate buffered saline) in the plug of the ITP system on nitrocellulose. The specific affinity of the antibody in the plug can several times lower in the plug than in the optimum binding solution. This is primarily a result of the low ionic strength in the plug, and to a lesser degree pH. To develop a high-performance LID assay, like the one designed for group A strep, the antibody pair must maintain a high specific binding at low ionic strength, as shown in fig. 3-1. It is challenging to design a high performing ITP chemistry that also results in plug (ATE) conditions (IS and pH) that demonstrates high specific affinity binding and low non-specific binding of the antibodies. These requirements make the antibody selection process and ITP chemistry design difficult.

Chapter 4. CLINICAL VALIDATION OF THE LID FORMAT

Point-of-care assays require functionality in a clinical sample. Many diagnostics fail in the process of incorporating clinical samples due to the complexity, interferents, or the sample changing the chemistry. An important step in assessing the viability of an assay format is validation with clinically relevant samples. The success of the group A streptococcus (GAS) assay in clean samples motivated the use of this assay in a clinical validation study. For the GAS assay, the relevant clinical sample is a throat swab.

With the incorporation of the clinical samples, additional requirements are placed on the system. The added biological material can coat the gold nanoparticles and block the flow in the capillaries in addition to affecting the binding to the test-line. To deal with these factors, commercial lateral flow assays filter the sample through a sample pad. This sample pad typically has detergent embedded inside to maximize the flow of the antigen onto the test strip. To mimic the purpose of the sample pad and detergent, we filter the clinical sample through a 0.45 uM pore cellulose syringe filter (MicroSolv, Leland, NC) and add a small amount of detergent to our sample solution.

To test the lateral flow enhanced with isotachophoresis diagnostic (LID) format in a clinically relevant sample, we collect numerous throat swabs and elute each sample into a 200uL volume. These volumes are combined to form a pooled throat swab sample. This pooled throat swab sample is then filtered through the syringe filter to mimic the effect of the sample pad. For this clinical format validation, 25 throat swabs were collected from 5 different people, and the volume of the pooled sample is divided into 25 equivalent volumes.

The overall chemistry from the limit-of-detection (LoD) determination for GAS was slightly modified to incorporate the throat samples. For extraction, the initial sodium nitrite concentration for lysis is decreased slightly. The HCl concentration is unchanged for the lysis, and the lysis is allowed to react for 5 minutes. 0.0075wt% of Tween-20 is added to the LE solution to prevent adsorption of the sample onto the nitrocellulose membrane. We fix the amount at slightly below the critical micellular concentration. The sample solution is finalized with the addition of conjugated gold to a final O.D. of 0.5 at 540nm.

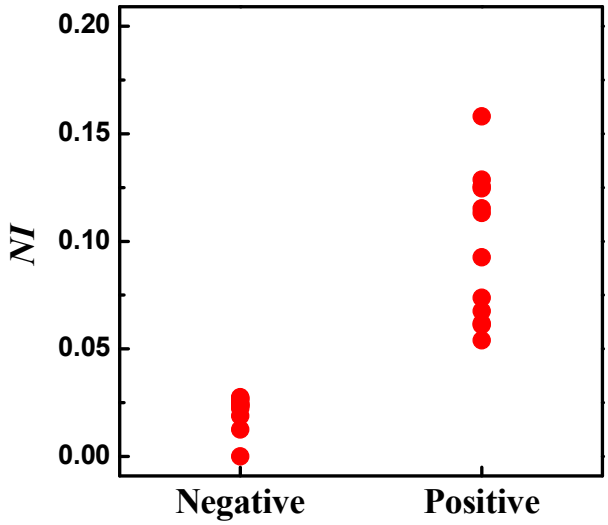

Figure 4.1: The signal response in normalized intensity generated by samples incorporating pooled throat swabs, divided into samples with (positive) and without (negative) strep cells added to the sample. The loading of the positive samples ranges from 24,000 to 1,600,000 CFU/swab. The normalized intensities are scaled by subtracting the lowest value to pin the lowest value to 0 NI.

For positive contrived samples, a known quantity of strep cells are added to the throat sample aliquots before lysis. For this validation study, the range of concentrations tested is from 24,000 CFU to 1,600,000 CFU per swab, with an effective dilution into 800mL (30,000-2,000,000 CFU/mL). This range is selected based upon the clinically relevant range established by previous

work using qPCR to quantify the concentration of strep cells found on throat swabs.[148] The range used for our validation study is from below the minimum concentration found by the qPCR (29,000 CFU/swab) to slightly above the average found by qPCR (1,100,000 CFU/swab). The highest likelihood for false negatives occurs at lower loading, as a result, we focus our attention on the lower half of the clinically relevant range.

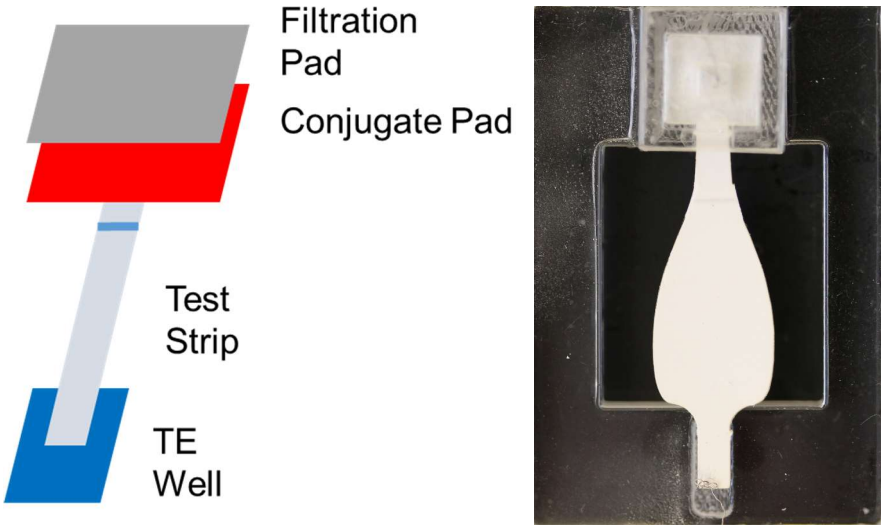

Figure 4.2: Schematic (left) and picture (right) of the design for a LID assay with in-line filtering.

The results shown in fig. 4.1 demonstrate no overlap in intensity values from positive and negative samples. Therefore, by setting the cutoff at 0.04 NI we obtain 100% sensitivity and 100% specificity in this validation trial. Pooled samples are used because they are less likely to introduce sample to sample variation, thus providing data more linked to the performance of the assay while incorporating the biological material. However, this information still lacks the single swab processing and in-line filtering that is required for operation as a point-of-care device. We will use the same elution from a swab process as the commercial lateral flow assay. This process involves submerging the swab in sodium nitrate and using a flexible plastic test tube to squeeze

the liquid out of the tip. For creating in-line filtering, we have designed a top down filtering setup that has shown success in preliminary testing, as shown in fig. 4.2. This system generates response from less than 100uL of sample solution and incorporates a conjugate pad.

In summary, we have validated the LID format in a clinically relevant format. The streptococcus pyogenes assay remains functional with the inclusion of pooled clinical samples, and is able to detect positive samples over the expected clinical loading range. We also have a design approach set forward for integrated filtering in LID assays.

Chapter 5. CONCLUSIONS AND RECOMMENDATIONS

5.1 Streptococcus pyogenes LID assay

In this work, we demonstrated that we can use ITP and a novel petal-shaped paper-based device to improve the LoD of a group A strep immunoassay by two-orders of magnitude over a commercially available lateral flow assay. This is the first time that ITP has been used to detect the presence of specific bacterium in a sandwich immunoassay, which has required optimization of solutions to lyse the target cells and provide favorable conditions for ITP stacking. We show that our petal-shaped lateral flow enhanced by isotachophoresis diagnostic (LID) devices result in five times lower LoD compared to straight LID devices because both devices use finite sample injection, and the increased volume of the target solution on the petal-shaped assay results in a larger target mass concentration being passed over the test line. We achieve an LoD of less than 2000 CFU/mL.

We develop a model based on antibody and operational parameters to assess when it is appropriate to use ITP to enhance a LF assay. From this, we have isolated the non-specific binding kinetics as the primary metric to investigate when evaluating antibody pairs. We also provide contrived clinical results demonstrating functionality over the expected clinical range in clinically relevant samples. The loading in these clinical samples is set based on results from clinical samples analyzed by quantitative PCR. The LID assay is able to successfully distinguish all positive samples from negative samples over this clinical range.

In the future, I recommend acquiring clinical samples that have been analyzed via qPCR or culture to test in the LID format to obtain true clinical sensitivity and specificity statistics. In addition, I recommend a full testing of integrated filtering into the LID assay for full point-of-care functionality.

5.2 Design of a LID assay around a fixed ITP chemistry

We screened 9 antibodies as potential components in a chlamydia trachomatis LID assay. To do so, we test the binding of the pairs in ELISA and lateral flow with a fixed LE binding chemistry. Unfortunately, none of the pairs tested were found to be promising candidates for the LID format.

For future design of LID assays with a fixed ITP chemistry, I recommend a process similar to the ELISA screening, followed by lateral flow screening, and final LID format testing. In the ELISA screening presented in this work, a fixed amount of detergent was included in the sample solution chemistry. For future testing, I recommend that the detergent be excluded from the ELISA screening, with an additional step after the lateral flow screening to determine the appropriate type and amount of non-ionic detergent.

Additionally, I recommend including additional testing of negative signal generation during the ELISA screening. This can be achieved by a second set of negative wells for each potential capture antibody to be tested with a different concentration of label antibody. If the negative signal generation is sensitive to the amount of label antibody, this is early indication that the pair may not be suitable for use in the LID format.

Lastly, I recommend that the testing of blank samples in the lateral flow screening be completed using a large excess of label (1 O.D. or more of conjugated gold). Any assays with an inverted signal under these conditions and functional positive signal generation is a prime candidate for the LID format.

5.3 Design of a LID assay using a given antibody pair

This thesis puts forth a method for investigating the effect of the parameters of pH and ionic strength (IS) on binding, as well as rules for utilizing the binding screening in the design of ITP. This method was used to design the streptococcus pyogenes assay as well as the 15174/MAV assay for chlamydia trachomatis. I recommend using this method in future assay development.

An overview of this method is to begin by investigating the effect of a range of IS on the specific and non-specific signal generation at a biological pH. The next step is to investigate the effect of pH on signal generation at a high-performing IS found in the first step. When analyzing these results, the non-specific signal generation is extremely important. I recommend testing high loading of label in negative lateral flow assays under the condition selected from the screenings. Depending on the lysis chemistry, there may be additional chemistry modifications required for incorporation into LID assays. The inclusion of a non-ionic detergent is likely a requirement for functionality with clinical samples. The effect of the non-ionic detergent on non-specific signal generation can be dramatic. I suggest that multiple detergents be investigated when progressing into using clinical samples.

My final recommendation is that any antibody pair/chemistry combination that shows any non-specific signal generation in the lateral flow format be removed from consideration for enhancement with ITP.

BIBLIOGRAPHY

1. Borysiak, M. D., Thompson, M. J. & Posner, J. D. Translating diagnostic assays from the laboratory to the clinic: analytical and clinical metrics for device development and evaluation. *Lab Chip* **16,** 1293–1313 (2016).
2. Lateral Flow Immunoassays - Cytodiagnostics. Available at: http://www.cytodiagnostics.com/store/pc/Lateral-Flow-Immunoassays-d6.htm. (Accessed: 8th August 2016)
3. High-Sensitivity Isotachophoretic Stacking CE Devices. Available at: https://microfluidics.stanford.edu/Projects/Archive/HighSensITP.html. (Accessed: 7th April 2017)
4. Yaghoubi Moghadam, B. Isotachophoresis in Paper-Based Microfluidic Devices. (2014).
5. Moghadam, B. Y., Connelly, K. T. & Posner, J. D. Isotachophoretic Preconcenetration on Paper-Based Microfluidic Devices. *Anal. Chem.* **86,** 5829–5837 (2014).
6. Garland Science - Book: Janeway's Immunobiology + 7. Available at: http://www.garlandscience.com/product/isbn/0815341237. (Accessed: 24th April 2017)
7. Thompson, M. & Van den Bruel, A. Screening Tests. in *Diagnostic Tests Toolkit* 66–74 (Wiley-Blackwell, 2011). doi:10.1002/9781119951827.ch9
8. NCCLS. Protocols for Determination of Limits of Detection and Limits of Quantification; Approved Guideline. (2004).
9. Currie, L. A. Nomenclature in evaluation of analytical methods including detection and quantification capabilities1: (IUPAC Recommendations 1995). *Anal. Chim. Acta* **391,** 105–126 (1999).
10. Wiley: Regulated Bioanalytical Laboratories: Technical and Regulatory Aspects from Global Perspectives - Michael Zhou. Available at: http://www.wiley.com/WileyCDA/WileyTitle/productCd-0470476591.html. (Accessed: 17th March 2017)
11. Burd, E. M. Validation of Laboratory-Developed Molecular Assays for Infectious Diseases. *Clin. Microbiol. Rev.* **23,** 550–576 (2010).
12. Pardue, H. L. Counterpoint The inseparable triad: analytical sensitivity, measurement uncertainty, and quantitative resolution. *Clin. Chem.* **43,** 1831–1837 (1997).
13. Bunk, D. M. Reference Materials and Reference Measurement Procedures: An Overview from a National Metrology Institute. *Clin. Biochem. Rev.* **28,** 131–137 (2007).
14. Dimeski, G. Interference testing. *Clin. Biochem. Rev.* **29 Suppl 1,** S43-48 (2008).
15. Detels, R. *et al.* The Incidence and Correlates of Symptomatic and Asymptomatic Chlamydia trachomatis and Neisseria gonorrhoeae Infections in Selected Populations in Five Countries. *Sex. Transm. Dis.* **38,** 503–509 (2011).
16. Wiley: Analytical Chemistry, 7th Edition - Gary D. Christian, Purnendu K. Dasgupta, Kevin A. Schug. Available at: http://www.wiley.com/WileyCDA/WileyTitle/productCd-EHEP002943.html. (Accessed: 17th March 2017)
17. Singer, J. M. & Plotz, C. M. The latex fixation test: I. Application to the serologic diagnosis of rheumatoid arthritis. *Am. J. Med.* **21,** 888–892 (1956).
18. Yalow, R. S. & Berson, S. A. IMMUNOASSAY OF ENDOGENOUS PLASMA INSULIN IN MAN. *J. Clin. Invest.* **39,** 1157–1175 (1960).
19. Product Classification. Available at: https://www.accessdata.fda.gov/scripts/cdrh/cfdocs/cfPCD/classification.cfm?ID=592. (Accessed: 19th April 2017)
20. Gubala, V., Harris, L. F., Ricco, A. J., Tan, M. X. & Williams, D. E. Point of Care Diagnostics: Status and Future. *Anal. Chem.* **84,** 487–515 (2012).
21. Yetisen, A. K., Akram, M. S. & Lowe, C. R. Paper-based microfluidic point-of-care diagnostic devices. *Lab. Chip* **13,** 2210–2251 (2013).

22. Sajid, M., Kawde, A.-N. & Daud, M. Designs, formats and applications of lateral flow assay: A literature review. *J. Saudi Chem. Soc.* **19,** 689–705 (2015).
23. Koczula, K. M. & Gallotta, A. Lateral flow assays. *Essays Biochem.* **60,** 111–120 (2016).
24. Fu, E. *et al.* Enhanced Sensitivity of Lateral Flow Tests Using a Two-Dimensional Paper Network Format. *Anal. Chem.* **83,** 7941–7946 (2011).
25. Linares, E. M., Kubota, L. T., Michaelis, J. & Thalhammer, S. Enhancement of the detection limit for lateral flow immunoassays: Evaluation and comparison of bioconjugates. *J. Immunol. Methods* **375,** 264–270 (2012).
26. Geertruida A Posthuma-Trumpie, J. K. Lateral flow (immuno)assay: its strengths, weaknesses, opportunities and threats. A literature survey. Anal Bioanal Chem. *Anal. Bioanal. Chem.* **393,** 569–82 (2008).
27. O'Keeffe, M. *et al.* Preliminary evaluation of a lateral flow immunoassay device for screening urine samples for the presence of sulphamethazine. *J. Immunol. Methods* **278,** 117–126 (2003).
28. Irina V. Safenkova, A. V. Z. Factors influencing the detection limit of the lateral-flow sandwich immunoassay: A case study with potato virus X. *Anal. Bioanal. Chem.* **403,** 1595–605 (2012).
29. Linares, E. M., Kubota, L. T., Michaelis, J. & Thalhammer, S. Enhancement of the detection limit for lateral flow immunoassays: evaluation and comparison of bioconjugates. *J. Immunol. Methods* **375,** 264–270 (2012).
30. Parolo, C., de la Escosura-Muñiz, A. & Merkoçi, A. Enhanced lateral flow immunoassay using gold nanoparticles loaded with enzymes. *Biosens. Bioelectron.* **40,** 412–416 (2013).
31. Chinnasamy, T., Segerink, L. I., Nystrand, M., Gantelius, J. & Svahn, H. A. A lateral flow paper microarray for rapid allergy point of care diagnostics. *Analyst* **139,** 2348–2354 (2014).
32. Shan, S., Lai, W., Xiong, Y., Wei, H. & Xu, H. Novel Strategies To Enhance Lateral Flow Immunoassay Sensitivity for Detecting Foodborne Pathogens. *J. Agric. Food Chem.* **63,** 745–753 (2015).
33. Fu, E. *et al.* Enhanced Sensitivity of Lateral Flow Tests Using a Two-Dimensional Paper Network Format. *Anal. Chem.* **83,** 7941–7946 (2011).
34. Rodríguez, M. O., Covián, L. B., García, A. C. & Blanco-López, M. C. Silver and gold enhancement methods for lateral flow immunoassays. *Talanta* **148,** 272–278 (2016).
35. Cui, X. *et al.* A remarkable sensitivity enhancement in a gold nanoparticle-based lateral flow immunoassay for the detection of Escherichia coli O157:H7. *RSC Adv* **5,** 45092–45097 (2015).
36. Wang, Y. *et al.* Study of superparamagnetic nanoparticles as labels in the quantitative lateral flow immunoassay. *Mater. Sci. Eng. C* **29,** 714–718 (2009).
37. Xie, Q.-Y. *et al.* Advantages of fluorescent microspheres compared with colloidal gold as a label in immunochromatographic lateral flow assays. *Biosens. Bioelectron.* **54,** 262–265 (2014).
38. Fridley, G. E., Le, H. & Yager, P. Highly Sensitive Immunoassay Based on Controlled Rehydration of Patterned Reagents in a 2-Dimensional Paper Network. *Anal. Chem.* **86,** 6447–6453 (2014).
39. Fu, E., Lutz, B., Kauffman, P. & Yager, P. Controlled Reagent Transport in Disposable 2D Paper Networks. *Lab. Chip* **10,** 918–920 (2010).
40. Govindarajan, A. V., Ramachandran, S., Vigil, G. D., Yager, P. & Böhringer, K. F. A low cost point-of-care viscous sample preparation device for molecular diagnosis in the developing world; an example of microfluidic origami. *Lab. Chip* **12,** 174–181 (2012).
41. Cui, X., Xiong, Q.-R., Xiong, Y.-H., Shan, S. & Lai, W.-H. Establishing of a Method Combined Immunomagnetic Separation with Colloidal Gold Lateral Flow Assay and Its Application in Rapid Detection ofEscherichia coliO157:H7. *Chin. J. Anal. Chem.* **41,** 1812–1816 (2013).
42. Li, P. *et al.* Current development of microfluidic immunosensing approaches for mycotoxin detection via capillary electromigration and lateral flow technology. *ELECTROPHORESIS* **33,** 2253–2265 (2012).
43. Eltzov, E. *et al.* Lateral Flow Immunoassays – from Paper Strip to Smartphone Technology. *Electroanalysis* **27,** 2116–2130 (2015).

44. Biosensors and biodetection; methods and protocols; v.2: Electrochemical and mechanical detectors, lateral flow and ligands for biosensors. *Scitech Book News* **33,** (2009).
45. Moghadam, B. Y., Connelly, K. T. & Posner, J. D. Two orders of magnitude improvement in detection limit of lateral flow assays using isotachophoresis. *Anal. Chem.* **87,** 1009–1017 (2015).
46. Tarín, A., Rosell, M. G. & Guardino, X. Use of high-performance liquid chromatography to assess airborne mycotoxins. *J. Chromatogr. A* **1047,** 235–240 (2004).
47. Marshall, L. A., Rogacs, A., Meinhart, C. D. & Santiago, J. G. An injection molded microchip for nucleic acid purification from 25 microliter samples using isotachophoresis. *J. Chromatogr. A* **1331,** 139–142 (2014).
48. Strychalski, E. A. *et al.* DNA purification from crude samples for human identification using gradient elution isotachophoresis. *Electrophoresis* **34,** 2522–2530 (2013).
49. Garcia-Schwarz, G., Rogacs, A., Bahga, S. S. & Santiago, J. G. On-chip Isotachophoresis for Separation of Ions and Purification of Nucleic Acids. *J. Vis. Exp. JoVE* (2012). doi:10.3791/3890
50. Cui, H., Dutta, P. & Ivory, C. F. Isotachophoresis of proteins in a networked microfluidic chip: Experiment and 2-D simulation. *ELECTROPHORESIS* **28,** 1138–1145 (2007).
51. Stowers, A. W., Spring, K. J. & Saul, A. Preparative scale purification of recombinant proteins to clinical grade by isotachophoresis. *Biotechnol. Nat. Publ. Co.* **13,** 1498–1503 (1995).
52. Bahga, S. S. & Santiago, J. G. Coupling isotachophoresis and capillary electrophoresis: a review and comparison of methods. *Analyst* **138,** 735–754 (2013).
53. Jung, B., Bharadwaj, R. & Santiago, J. G. On-chip millionfold sample stacking using transient isotachophoresis. *Anal. Chem.* **78,** 2319–2327 (2006).
54. Analytical Isotachophoresis [Electrophoresis Library] by Bocek, P.: VCH, Weinheim / New York. 9780895734778 Hardcover - Tiber Books. Available at: https://www.abebooks.com/Analytical-Isotachophoresis-Electrophoresis-Library-Bocek-P/3457265990/bd. (Accessed: 22nd March 2017)
55. Bahga - Ionic strength effects - Electrophoresis 2010.pdf.
56. Persat, A., Suss, M. E. & Santiago, J. G. Basic principles of electrolyte chemistry for microfluidic electrokinetics. Part II: Coupling between ion mobility, electrolysis, and acid–base equilibria. *Lab. Chip* **9,** 2454–2469 (2009).
57. Lukacs, K. D. & Jorgenson, J. W. Capillary zone electrophoresis: Effect of physical parameters on separation efficiency and quantitation. *J. High Resolut. Chromatogr.* **8,** 407–411 (1985).
58. Bahga, S. S., Bercovici, M. & Santiago, J. G. Ionic strength effects on electrophoretic focusing and separations. *Electrophoresis* **31,** 910–919 (2010).
59. Quirino, J. P. & Haddad, P. R. Online Sample Preconcentration in Capillary Electrophoresis using Analyte Focusing by Micelle Collapse. *Anal. Chem.* **80,** 6824–6829 (2008).
60. Yang, K. & Wu, J. Numerical study of in situ preconcentration for rapid and sensitive nanoparticle detection. *Biomicrofluidics* **4,** 034106 (2010).
61. Rosenfeld, T. & Bercovici, M. 1000-fold sample focusing on paper-based microfluidic devices. *Lab. Chip* **14,** 4465–4474 (2014).
62. Myers, J. K., Nick Pace, C. & Martin Scholtz, J. Denaturant m values and heat capacity changes: Relation to changes in accessible surface areas of protein unfolding. *Protein Sci.* **4,** 2138–2148 (1995).
63. Phosphate buffered saline P4417. *Sigma-Aldrich* Available at: http://www.sigmaaldrich.com/catalog/product/sigma/p4417. (Accessed: 13th June 2017)
64. Phosphate buffered saline. *Protocols Online* (2010).
65. Kirkwood, C. R. *et al.* The diagnostic content of family practice: 50 most common diagnoses recorded in the WAMI community practices. *J. Fam. Pract.* **15,** 485–492 (1982).
66. Danchin, M. H. *et al.* Burden of Acute Sore Throat and Group A Streptococcal Pharyngitis in School-aged Children and Their Families in Australia. *Pediatrics* **120,** 950–957 (2007).
67. Shaikh, N., Leonard, E. & Martin, J. M. Prevalence of Streptococcal Pharyngitis and Streptococcal Carriage in Children: A Meta-analysis. *Pediatrics* **126,** e557–e564 (2010).

68. Wormser, G. P. & Stratton, C. Manual of Clinical Microbiology, 9th Edition Edited by Patrick R. Murray, Ellen Jo Baron, James H. Jorgensen, Marie Louise Landry, and Michael A. Pfaller Washington, DC: ASM Press, 2007 2488 pp., illustrated. $209.95 (hardcover). *Clin. Infect. Dis.* **46,** 153–153 (2008).
69. CDC. Group A Streptococcal (GAS) Disease For Clinicians. (2014). Available at: http://www.cdc.gov/groupastrep/clinicians.html. (Accessed: 4th March 2016)
70. Murphy, T. K., Kurlan, R. & Leckman, J. The Immunobiology of Tourette's Disorder, Pediatric Autoimmune Neuropsychiatric Disorders Associated with Streptococcus, and Related Disorders: A Way Forward. *J. Child Adolesc. Psychopharmacol.* **20,** 317–331 (2010).
71. Swedo, S. E. *et al.* Sydenham's chorea: physical and psychological symptoms of St Vitus dance. *Pediatrics* **91,** 706–713 (1993).
72. Nakhoul, G. N. & Hickner, J. Management of adults with acute streptococcal pharyngitis: minimal value for backup strep testing and overuse of antibiotics. *J. Gen. Intern. Med.* **28,** 830–834 (2013).
73. Linder JA, Bates DW, Lee GM & Finkelstein JA. ANtibiotic treatment of children with sore throat. *JAMA* **294,** 2315–2322 (2005).
74. Lean, W. L., Arnup, S., Danchin, M. & Steer, A. C. Rapid Diagnostic Tests for Group A Streptococcal Pharyngitis: A Meta-analysis. *Pediatrics* peds.2014-1094 (2014). doi:10.1542/peds.2014-1094
75. Dingle, T. C., Abbott, A. N. & Fang, F. C. Reflexive culture in adolescents and adults with group a streptococcal pharyngitis. *Clin. Infect. Dis. Off. Publ. Infect. Dis. Soc. Am.* **59,** 643–650 (2014).
76. Stewart, E. H. *et al.* Rapid Antigen Group A Streptococcus Test to Diagnose Pharyngitis: A Systematic Review and Meta-Analysis. *PLOS ONE* **9,** e111727 (2014).
77. Shulman, S. T. *et al.* Clinical Practice Guideline for the Diagnosis and Management of Group A Streptococcal Pharyngitis: 2012 Update by the Infectious Diseases Society of America. *Clin. Infect. Dis.* cis629 (2012). doi:10.1093/cid/cis629
78. Participants, T. P. of I. G. A. S. I. W. Prevention of Invasive Group A Streptococcal Disease among Household Contacts of Case Patients and among Postpartum and Postsurgical Patients: Recommendations from the Centers for Disease Control and Prevention. *Clin. Infect. Dis.* **35,** 950–959 (2002).
79. Shapiro, D. J., Hicks, L. A., Pavia, A. T. & Hersh, A. L. Antibiotic prescribing for adults in ambulatory care in the USA, 2007-09. *J. Antimicrob. Chemother.* **69,** 234–240 (2014).
80. Hersh, A. L., Shapiro, D. J., Pavia, A. T. & Shah, S. S. Antibiotic prescribing in ambulatory pediatrics in the United States. *Pediatrics* **128,** 1053–1061 (2011).
81. Acon Strep A Rapid Test Strip. 510(k) Number: K010582. *Number: K010582* Available at: http://www.accessdata.fda.gov/scripts/cdrh/cfdocs/cfpmn/pmn.cfm?id=k010582. (Accessed: 26th October 2015)
82. Dunne, E. M. *et al.* Detection of group a streptococcal pharyngitis by quantitative PCR. *BMC Infect. Dis.* **13,** 312 (2013).
83. std-trends-508.pdf.
84. Chesson, H. W., Blandford, J. M., Gift, T. L., Tao, G. & Irwin, K. L. The estimated direct medical cost of sexually transmitted diseases among American youth, 2000. *Perspect. Sex. Reprod. Health* **36,** 11–19 (2004).
85. Detailed STD Facts - Chlamydia. Available at: https://www.cdc.gov/std/chlamydia/stdfact-chlamydia-detailed.htm#_ENREF_3. (Accessed: 15th March 2017)
86. O'Farrell, N. *et al.* Genital Ulcers and Concomitant Complaints in Men Attending a Sexually Transmitted Infections Clinic: Implications for Sexually Transmitted Infections Management: *Sex. Transm. Dis.* **35,** 545–549 (2008).
87. White, J. A. Manifestations and management of lymphogranuloma venereum: *Curr. Opin. Infect. Dis.* **22,** 57–66 (2009).
88. *Chlamydial Infections*. (Springer Berlin Heidelberg, 1987).

89. Farley, T. A., Cohen, D. A. & Elkins, W. Asymptomatic sexually transmitted diseases: the case for screening. *Prev. Med.* **36,** 502–509 (2003).
90. What proportion of episodes of gonorrhoea and chlamydia becomes symptomatic? *Int. J. STD AIDS* **13,** 91–101 (2002).
91. Price, M. J. *et al.* Risk of Pelvic Inflammatory Disease Following Chlamydia trachomatis Infection: Analysis of Prospective Studies With a Multistate Model. *Am. J. Epidemiol.* **178,** 484–492 (2013).
92. Zetola, N. M., Bernstein, K. T., Wong, E., Louie, B. & Klausner, J. D. Exploring the relationship between sexually transmitted diseases and HIV acquisition by using different study designs. *J. Acquir. Immune Defic. Syndr. 1999* **50,** 546–551 (2009).
93. Hosenfeld, C. B. *et al.* Repeat infection with Chlamydia and gonorrhea among females: a systematic review of the literature. *Sex. Transm. Dis.* **36,** 478–489 (2009).
94. Hillis, S. D., Owens, L. M., Marchbanks, P. A., Amsterdam, L. F. & Mac Kenzie, W. R. Recurrent chlamydial infections increase the risks of hospitalization for ectopic pregnancy and pelvic inflammatory disease. *Am. J. Obstet. Gynecol.* **176,** 103–107 (1997).
95. Bakken, I. J. & Ghaderi, S. Incidence of pelvic inflammatory disease in a large cohort of women tested for Chlamydia trachomatis: a historical follow-up study. *BMC Infect. Dis.* **9,** 130 (2009).
96. Chlamydial Infections - 2015 STD Treatment Guidelines. Available at: http://www.cdc.gov/std/tg2015/chlamydia.htm. (Accessed: 6th August 2016)
97. Black, C. M. *et al.* Head-to-head multicenter comparison of DNA probe and nucleic acid amplification tests for Chlamydia trachomatis infection in women performed with an improved reference standard. *J. Clin. Microbiol.* **40,** 3757–3763 (2002).
98. Gaydos, C. A., Theodore, M., Dalesio, N., Wood, B. J. & Quinn, T. C. Comparison of three nucleic acid amplification tests for detection of Chlamydia trachomatis in urine specimens. *J. Clin. Microbiol.* **42,** 3041–3045 (2004).
99. Johnson, R. E. *et al.* Evaluation of nucleic acid amplification tests as reference tests for Chlamydia trachomatis infections in asymptomatic men. *J. Clin. Microbiol.* **38,** 4382–4386 (2000).
100. Van Dyck, E., Ieven, M., Pattyn, S., Van Damme, L. & Laga, M. Detection of Chlamydia trachomatis and Neisseria gonorrhoeae by enzyme immunoassay, culture, and three nucleic acid amplification tests. *J. Clin. Microbiol.* **39,** 1751–1756 (2001).
101. Schachter, J., Chow, J. M., Howard, H., Bolan, G. & Moncada, J. Detection of Chlamydia trachomatis by Nucleic Acid Amplification Testing: Our Evaluation Suggests that CDC-Recommended Approaches for Confirmatory Testing Are Ill-Advised. *J. Clin. Microbiol.* **44,** 2512–2517 (2006).
102. Chlamydia & Gonorrhea Testing | Private MD Labs. Available at: https://www.privatemdlabs.com/lp/chlamydia-gonorrhea-testing.php. (Accessed: 17th June 2017)
103. Chlamydia and Gonorrhea NAAT Screening Method Endorsed by CDC. Available at: https://labtestsonline.org/news/140521naat/. (Accessed: 17th June 2017)
104. Geisler, W. M. *et al.* The Natural History of Untreated Chlamydia trachomatis Infection in the Interval Between Screening and Returning for Treatment: *Sex. Transm. Dis.* **35,** 119–123 (2008).
105. Schwebke, J. R., Sadler, R., Sutton, J. M. & Hook, E. W. Positive screening tests for gonorrhea and chlamydial infection fail to lead consistently to treatment of patients attending a sexually transmitted disease clinic. *Sex. Transm. Dis.* **24,** 181–184 (1997).
106. Recommendations for the Laboratory-Based Detection of Chlamydia trachomatis and Neisseria gonorrhoeae — 2014. Available at: https://www.cdc.gov/mmwr/preview/mmwrhtml/rr6302a1.htm. (Accessed: 15th March 2017)
107. Hislop, J. *et al. Systematic review of the clinical effectiveness and cost-effectiveness of rapid point-of-care tests for the detection of genital chlamydia infection in women and men*. (NIHR Journals Library, 2010).
108. Moncada, J., Schachter, J., Liska, S., Shayevich, C. & Klausner, J. D. Evaluation of self-collected glans and rectal swabs from men who have sex with men for detection of Chlamydia trachomatis

and Neisseria gonorrhoeae by use of nucleic acid amplification tests. *J. Clin. Microbiol.* **47,** 1657–1662 (2009).
109. Saison, F. *et al.* Prevalence of Chlamydia trachomatis Infection among Low- and High-Risk Filipino Women and Performance of Chlamydia Rapid Tests in Resource-Limited Settings. *J. Clin. Microbiol.* **45,** 4011–4017 (2007).
110. Wiggins, R., Graf, S., Low, N., Horner, P. J. & Chlamydia Screening Studies (ClaSS) Study Group. Real-time quantitative PCR to determine chlamydial load in men and women in a community setting. *J. Clin. Microbiol.* **47,** 1824–1829 (2009).
111. Michel, C.-E. C. *et al.* Chlamydia trachomatis Load at Matched Anatomic Sites: Implications for Screening Strategies. *J. Clin. Microbiol.* **45,** 1395–1402 (2007).
112. Helm, J. J. van der *et al.* Point-of-Care Test for Detection of Urogenital Chlamydia in Women Shows Low Sensitivity. A Performance Evaluation Study in Two Clinics in Suriname. *PLOS ONE* **7,** e32122 (2012).
113. Gift, T. L., Pate, M. S., Hook, E. W. & Kassler, W. J. The rapid test paradox: when fewer cases detected lead to more cases treated: a decision analysis of tests for Chlamydia trachomatis. *Sex. Transm. Dis.* **26,** 232–240 (1999).
114. Grossman, P. D. & Colburn, J. C. *Capillary Electrophoresis: Theory and Practice*. (Academic Press, 2012).
115. Spinola, S. M. & Cannon, J. G. Different blocking agents cause variation in the immunologic detection of proteins transferred to nitrocellulose membranes. *J. Immunol. Methods* **81,** 161–165 (1985).
116. Reverberi, R. & Reverberi, L. Factors affecting the antigen-antibody reaction. *Blood Transfus.* **5,** 227–240 (2007).
117. Sahin, E., Grillo, A. O., Perkins, M. D. & Roberts, C. J. Comparative effects of pH and ionic strength on protein–protein interactions, unfolding, and aggregation for IgG1 antibodies. *J. Pharm. Sci.* **99,** 4830–4848 (2010).
118. Safenkova, I., Zherdev, A. & Dzantiev, B. Factors influencing the detection limit of the lateral-flow sandwich immunoassay: a case study with potato virus X. *Anal. Bioanal. Chem.* **403,** 1595–1605 (2012).
119. Choi, J. R. *et al.* Sensitive biomolecule detection in lateral flow assay with a portable temperature–humidity control device. *Biosens. Bioelectron.* **79,** 98–107 (2016).
120. Persat, A., Chambers, R. D. & Santiago, J. G. Basic principles of electrolyte chemistry for microfluidic electrokinetics. Part I: Acid–base equilibria and pH buffers. *Lab. Chip* **9,** 2437–2453 (2009).
121. KD value: a quantitative measurement of antibody affinity | Abcam. Available at: http://www.abcam.com/primary-antibodies/kd-value-a-quantitive-measurement-of-antibody-affinity. (Accessed: 7th April 2017)
122. Kirby, B. J. & Hasselbrink, E. F. Zeta potential of microfluidic substrates: 1. Theory, experimental techniques, and effects on separations. *Electrophoresis* **25,** 187–202 (2004).
123. Gencoglu, A. & Minerick, A. Chemical and morphological changes on platinum microelectrode surfaces in AC and DC fields with biological buffer solutions. *Lab. Chip* **9,** 1866–1873 (2009).
124. Bahga, S. S., Bercovici, M. & Santiago, J. G. Robust and high-resolution simulations of nonlinear electrokinetic processes in variable cross-section channels. *ELECTROPHORESIS* **33,** 3036–3051 (2012).
125. Chemical Disruption Methods. *OPS Diagnostics LLC* Available at: http://www.opsdiagnostics.com/applications/samplehomogenization/homogenizationguidepart4.html. (Accessed: 19th March 2017)
126. Traditional Methods of Cell Lysis. Available at: https://www.thermofisher.com/us/en/home/life-science/protein-biology/protein-biology-learning-center/protein-biology-resource-library/pierce-protein-methods/traditional-methods-cell-lysis.html. (Accessed: 21st March 2017)

127. Cell lysis 101: 8 methods to break down cell walls. *Bitesize Bio* (2013). Available at: http://bitesizebio.com/13536/bringing-down-the-walls-part-ii-8-methods-to-break-down-cell-walls/. (Accessed: 21st March 2017)
128. Shechter, D. An Overview of Mechanical Methods of Cell Disruption. Available at: http://www.beei.com/blog/an-overview-of-mechanical-methods-of-cell-disruption. (Accessed: 31st May 2017)
129. Gram-positive vs Gram-negative Bacteria - Difference and Comparison | Diffen. Available at: http://www.diffen.com/difference/Gram-negative_Bacteria_vs_Gram-positive_Bacteria. (Accessed: 7th April 2017)
130. BD Chek Group A Strep Insert.
131. Park, J. Y. & Lee, Y. N. Solubility and decomposition kinetics of nitrous acid in aqueous solution. *J. Phys. Chem.* **92,** 6294–6302 (1988).
132. Pronovost, A. D., Mauck, J. C., Sullivan, S. S., Greer, C. E. & Gilbert, J. H. *High pH extraction composition and its use to determine a chlamydial, gonococcal or herpes antigen*. (Google Patents, 1992).
133. Zhang, Y. & Heller, A. Reduction of the nonspecific binding of a target antibody and of its enzyme-labeled detection probe enabling electrochemical immunoassay of an antibody through the 7 pg/ml-100 ng/mL (40 fM-400 pM) range. *Anal. Chem.* **77,** 7758–7762 (2005).
134. Non Specific Binding (NSB) in Antigen-Antibody Assays.
135. Buchwalow, I., Samoilova, V., Boecker, W. & Tiemann, M. Non-specific binding of antibodies in immunohistochemistry: fallacies and facts. *Sci. Rep.* **1,** (2011).
136. Jacobsen, C. & Steensgaard, J. Binding properties of monoclonal anti-IgG antibodies: analysis of binding curves in monoclonal antibody systems. *Immunology* **51,** 423–430 (1984).
137. Biacore. Kinetic & Affinity Analysis.
138. Molar Concentration of Gold Nanoparticles (Colloid) - Nanoparticles - Gold - Technical Support. Available at: https://www.bbisolutions.com/technical-support/gold/nanoparticles/molar-concentration-of-gold-nanoparticles-colloid.html. (Accessed: 12th April 2017)
139. QuickVue Chlamydia Test | Quidel. Available at: http://www.quidel.com/immunoassays/rapid-chlamydia-tests/quickvue-chlamydia-test. (Accessed: 31st May 2017)
140. O'Shannessy, D. J. Determination of kinetic rate and equilibrium binding constants for macromolecular interactions: a critique of the surface plasmon resonance literature. *Curr. Opin. Biotechnol.* **5,** 65–71 (1994).
141. Wassaf, D. *et al.* High-throughput affinity ranking of antibodies using surface plasmon resonance microarrays. *Anal. Biochem.* **351,** 241–253 (2006).
142. Wu, Y. *et al.* Expression and purification of a human anti-cyclin D1 single-chain variable fragment antibody AD5 and its characterization. *Int. J. Mol. Med.* **32,** 1451–1457 (2013).
143. Beatty, J. D., Beatty, B. G. & Vlahos, W. G. Measurement of monoclonal antibody affinity by non-competitive enzyme immunoassay. *J. Immunol. Methods* **100,** 173–179 (1987).
144. Hajighasemi, F., Shokri, F., Hajighasemi, F. & Shokri, F. Generation and Characterization of Mouse Hybridomas Secreting Monoclonal Antibodies Specific for Human IgG3. *Avicenna J. Med. Biotechnol.* **1,** 19–26 (2009).
145. Molecular Determinants for Antibody Binding on Group 1 House Dust Mite Allergens (PDF Download Available). Available at: https://www.researchgate.net/publication/51974080_Molecular_Determinants_for_Antibody_Binding_on_Group_1_House_Dust_Mite_Allergens. (Accessed: 18th June 2017)
146. Herr, A. E. *et al.* Electroosmotic Capillary Flow with Nonuniform Zeta Potential. *Anal. Chem.* **72,** 1053–1057 (2000).
147. Dommelen, L. van *et al.* Alarmingly poor performance in Chlamydia trachomatis point-of-care testing. *Sex. Transm. Infect.* **86,** 355–359 (2010).
148. Dunne, E. M. *et al.* Detection of group a streptococcal pharyngitis by quantitative PCR. *BMC Infect. Dis.* **13,** 312 (2013).

149. Graphical data selection tool - File Exchange - MATLAB Central. Available at: http://www.mathworks.com/matlabcentral/fileexchange/13857-graphical-data-selection-tool. (Accessed: 25th April 2017)

APPENDIX 1

MATLAB code used to determine normalized test-line intensity in LF assays using colloidal gold:

i. Function that takes a scanned image and averages across the test line to generate a plot that allows the user to select the test-line and background parts of the plot. Outputs the normalized intensity as described in the Experimental Methods section.

```
function [Value,Line,White,Grey]=AuQuant(filename)

x=0;
filename='1031_1.tif';
imcell=imread(filename);
imagesc(imcell)
title('Select Line Area')
cropVals=getrect;

newImage=double(imcrop(imcell,cropVals));
Profile(1,:)=((mean(newImage,2)));
Line=min(Profile);

imcell=imread(filename);
imagesc(imcell)
title('Select White Area')
cropVals=getrect;

newImage=double(imcrop(imcell,cropVals));
Profile2(1,:)=((mean(newImage,2)));
White=mean(Profile2);

imcell=imread(filename);
imagesc(imcell)
title('Select Grey Area')
cropVals=getrect;

newImage=double(imcrop(imcell,cropVals));
Profile3(1,:)=((mean(newImage,2)));
Grey=mean(Profile3);


Value=(White-Line)/(White-Grey);
close all

end
```

ii. Code that fits the input to a Gaussian function.

```
function [sigma,mu,A]=mygaussfit(x,y,h)

%
% [sigma,mu,A]=mygaussfit(x,y)
% [sigma,mu,A]=mygaussfit(x,y,h)
%
% this function is doing fit to the function
% y=A * exp( -(x-mu)^2 / (2*sigma^2) )
%
% the fitting is been done by a polyfit
% the lan of the data.
%
% h is the threshold which is the fraction
% from the maximum y height that the data
% is been taken from.
% h should be a number between 0-1.
% if h have not been taken it is set to be 0.2
% as default.
%


%% threshold
if nargin==2, h=0.2; end

%% cutting
ymax=max(y);
xnew=[];
ynew=[];
for n=1:length(x)
    if y(n)>ymax*h;
        xnew=[xnew,x(n)];
        ynew=[ynew,y(n)];
    end
end

%% fitting
ylog=log(ynew);
xlog=xnew;
p=polyfit(xlog,ylog,2);
A2=p(1);
A1=p(2);
A0=p(3);
sigma=sqrt(-1/(2*A2));
mu=A1*sigma^2;
A=exp(A0+mu^2/(2*sigma^2));
```

iii. Function that converts an image to MATLAB formatting

```
function [a] = mimread(direct,fname,st,k)
%  function [a] = mimread(direct,fname,st,k)


% hw=waitbar(0,['Reading Image Data File ', fname,'.tif']);
for frame=1:k
    % Read each frame into the appropriate frame in memory.
%     waitbar(frame/k);

    [a(:,:,1,frame),map] = imread([direct fname,'.tif'],[frame+st-1]);
    %f=Q(:,:,1,1);
    %Q(:,:,1,frame)=imadjust(Q(:,:,1,frame),[0.15 1],[0 .002],1);
end
% close(hw);
```

iv. "getrect" is a function of selectdata.m that was created by John D'Errico and obtained from a file exchange through the MathWorks website.[149]

APPENDIX 2

Anionic ITP buffer selection tables.

Buffer	pKa	Mobility at pH 6.4	Mobility at pH 7.26	Mobility at pH 8.1	Mobility at pH 9.3	Absolute Mobility (10^-9 m^2/V/s)	Notes
MES	6.21	16.29	24.79	26.46	26.73	26.8	May complex with
ACES	6.99	6.36	20.88	28.86	30.60	31.1	
MOPSO	7	5.34	17.72	24.64	26.17	26.6	
BES	7.26	3.24	13.96	23.33	25.92	26.7	
MOPS	7.31	2.67	12.06	21.00	23.60	24.4	
HEPES	7.66	1.14	6.62	15.99	20.26	21.8	
TAPSO	7.71	1.12	6.72	17.05	22.12	24	
Tricine	8.26	0.36	2.63	10.88	20.43	26.6	
TAPS	8.51	0.18	1.33	6.41	14.90	22.9	
Serine	9.33	0.04	0.32	1.91	7.54	34.3	Primary amine
Valine	9.71	0.01	0.11	0.68	2.99	28.4	Primary amine
L-Leucine	9.73	0.01	0.10	0.60	2.66	26.4	Primary amine
Glycine	9.78	0.02	0.12	0.77	3.40	37.4	pKa1 at 2.35
L-Alanine	9.86	0.01	0.09	0.55	2.47	32.2	Primary amine
Beta-Alanine	10.2	0.00	0.04	0.24	1.13	30.8	Primary amine

	Target Mobility			
pH	6.4	7.3	8.1	8.78
Mobility	3.5	6.327	7.07	9

Table generated for the selection of the trailing ion based on the calculated mobility at potential pH values. The mobility is calculated as $\mu = \frac{\mu_{Abs}}{1+10^{pKa-p}}$, where μ is the calculated mobility and μ_{Abs} is the absolute mobility.[4] These mobilities are compared to measured mobility values of the target at the pH values. Trailing ions that are expected to have lower mobility at the pH are highlighted in green.

Buffer	pKa	Low Functional pH	High Functional pH	Mobility (10^-9 m^2/V/s)	Notes
Creatinine	4.83	4.33	5.33	37.20	Primary amine
Bis-Tris	6.35	5.85	6.85	26.00	
Imidazole	7.15	6.65	7.65	52.00	Reactive and unstable
Triethanolamine (TEA)	7.76	7.26	8.26	40.00	
Tris	8.05	7.55	8.55	29.50	Primary amine
Ammediol	8.78	8.28	9.28	29.50	Primary amine
Bis-Tris Propane	9.00	8.50	9.50	21.60	pKa1 at 6.8
Ethanolamine	9.50	9.00	10.00	44.30	Primary amine

Table of anionic ITP compatible buffers. Selection of the buffer is based on the desired pH of the electrolyte. The pH ranges are suggestions generated by the pKa±0.5. This is an initial guide. It is recommended that the chemistry be simulated in Spresso or CurtiPot© to confirm the expected pH of the buffered system.

APPENDIX 3

Description of the process for conjugating Chlamydia antibodies to colloidal gold by adjusting the pH such that the electrostatic interactions are minimized and the protein sticks with van der Walls forces. This is not covalent bonding. This process is particular to these particles and antibodies and any changes in the reagents will require more research into the pH, concentrations, and other conditions to bind the antibodies to the gold and retain high affinity for the target.

Reagents:

- 26 ml of 40 nm unlabeled colloidal gold at OD540 = 1.66 by Arista Biologicals (CGUCG – 0000)
- Monoclonal Ab to Chlamydia species LPS at 5.19 mg/ml by Meridian Life Sciences (MAV07 – 347)

Protocol:

1. Thaw the Abs on crushed ice.
    a. For these Abs, conjugation works best at 4 ug/ml of Abs in AuNPs at OD = 1, pH of 9.9.
    b. To determine optimal conditions for different Abs and AuNPs, concentration and pH titrations should be performed (refer to Janssen protocol). This process was already completed by PATH and the optimal conditions are listed above.
2. Adjust pH of the AuNPs to 9.9 using phosphoric acid and potassium carbonate (0.2 M or less).

a. Do not use NaCl/NaOH to adjust the pH. It can induce coagulation of the particles.

b. If you overshoot the pH, use the original Au solution to re-adjust the pH. This will avoid addition of extra salt to the solution. In our case this was not possible because we were adding the potassium carbonate directly to the AuNP.

c. Use double-junction, gel filled electrode to measure the pH to prevent clogging of the electrodes. They typically use an electrode that is dedicated to AuNP. This is the probe near the hood on the west wall.

d. Put the AuNPs solution in a large container and mix using a stirring rod (the pH probe is an acceptable mixer) while measuring pH. In our case we had a small amount so we just vortexed it after adding small amounts of potassium carbonate.

e. Use disposable plastic containers if possible. Otherwise clean all the containers really well since AuNPs absorb contaminants really quickly (like oil from skin, proteins, etc).

f. Dedicate glassware to conjugation, acid-wash them using aqua regia acid, and rinse them with boiling water to remove any residue.

3. Make 4 ug/ml final concentration of Abs in AuNPs of OD = 1. Do this by first diluting Abs in 10% volume of the total AuNPs using 5 mM sodium tetraborate at pH = 9.9.

    a. For example: for 26 ml of AuNPs, we need to make 2.6 ml of Abs at 40 ug/ml. For stock Abs of 5.19 mg/ml, take 20 ul of Abs and increase the volume to 2.6 ml using 5 mM sodium tetraborate.

b. If your AuNPs are not at OD = 1, adjust the concentration of Abs accordingly. For example, for stock AuNP at OD = 1.66 we need Abs at 6.4 ug/ml.

c. Lightly centrifuge Abs before opening the container, to get all the solution from the cap, and vortex before pipetting them out.

4. Quickly add all of the Abs to the AuNPs solution while mixing the solution with a stirring rod. Use light vortex if stirring rod is not available.

    a. When all the Abs are added, vortex the solution for 5-10 minutes.

    b. You will see a shift in the peak absorption of the Au solution after adding the Abs, which is normal. Usually it's a good sign when the Au solution gets a bit darker in color.

5. Block the AuNp solution using 10% stock BSA (or PEG).

    a. Add BSA at 10% volume of the initial AuNps solution (2.6 ml for 26 ml of AuNPs) and mix (vortex for a couple minutes).